INVESTIGATING THE TARGETS AND BIOLOGICAL ROLES OF IRE1'S TWO ENZYMATIC ACTIVITIES

A DISSERTATION SUBMITTED TO
THE GRADUATE SCHOOL OF ENGINEERING AND SCIENCE
OF BILKENT UNIVERSITY
IN PARTIAL FULFILLMENT OF THE REQUIREMENTS FOR
THE DEGREE OF
DOCTOR OF PHILOSOPHY
IN
MOLECULAR BIOLOGY AND GENETICS

By
ASLI DİLBER YILDIRIM
JUNE 2022

INVESTIGATING THE TARGETS AND BIOLOGICAL ROLES OF IRE1'S TWO ENZYMATIC ACTIVITIES

By ASLI DİLBER YILDIRIM

JUNE 2022

We certify that we have read this dissertation and that in our opinion it is fully adequate, in scope and in quality, as a thesis for the degree of Doctor of Philosophy.

_____

Dr. Ebru Erbay

(Advisor)

_____

Prof Dr. Michelle Marie Adams

_____

Prof. Dr. Tayfun Özçelik

_____

Assoc. Dr. Çağdaş Devrim Son

_____

Prof. Dr. Erkan Yılmaz

Approved for the Graduate School of Engineering and Science

_____

Ezhan Karaşan

Director of the Graduate School of Engineering and Science

ABSTRACT

INVESTIGATING THE TARGETS AND BIOLOGICAL ROLES OF IRE1'S TWO ENZYMATIC ACTIVITIES

ASLI DİLBER YILDIRIM
Ph.D. in Molecular Biology and Genetics
Advisor: Ebru ERBAY
June 2022

The unfolded protein response (UPR) is composed of complex and intricate series of highly regulated pathways geared to resolve the accumulation of misfolded proteins and to maintain cellular homeostasis. Endoplasmic reticulum (ER) is an organelle that regulates the protein folding. Disregulation of the mechanisms underlying ER folding capacity can activate ER-related UPR pathways (UPR^{ER}). The inositol-requiring enzyme-1 (IRE1) is an ER stress sensor and proximal regulator of the UPR^{ER}. IRE1 harbors dual kinase and endoribonuclease (RNase) activities. IRE1 RNase activity initiates the transcriptional layer of the UPR^{ER}, but IRE1's kinase substrate(s) and their function are unknown. This study was undertaken with the objectives of (i) discovering novel IRE1 kinase targets and (ii) deciphering the pathways regulated by IRE1 during ER stress and related pathophysiological conditions, (iii) investigating the mechanisms underlying how bioactive lipids resolve saturated fatty acid-induced ER stress. For the first part, I found out that phosphorylation of sphingosine 1-phosphate (S1P) lyase (SPL), a S1P degrading enzyme, is induced upon IRE1 kinase activation and this phosphorylation leads to inhibition of SPL's enzymatic activity. Consequently, SPL inactivation by IRE1 results in the accumulation of cellular S1P levels.

Mitochondria is another important organelle and have their own UPR system (UPR^{mt}) to regain organelle proteostasis. However, the link between UPR^{ER} and UPR^{mt} is unclear. My experiments further showed that increased S1P levels potentiate UPR^{mt} signaling in an IRE1 kinase activity-dependent manner. As a result of these experiments, we present IRE1 kinase activity as an important regulator of sphingolipid metabolism linking UPR^{ER} to UPR^{mt}.

I also investigated the function of IRE1 in Kawasaki Disease (KD), a pathophysiological condition leads to coronary artery aneurysm. Upon analysis of publicly available transcriptome data sets from KD patients, I identified a significant increase in ER stress-related gene signatures that associated with KD progression. The single cell transcriptomics data from Lactobacillus casei cell wall extract (LCWE)- induced murine model of KD further confirmed the activation of ER stress in myeloid cells. Upon confirmation of ER stress activation, I used genetic or small molecule approaches to ablate IRE1 function in order to study IRE1's role in LCWE-induced KD progression. My data demonstrated significance decrease in caspase-1 induction and IL-1β secretion leading to inhibition of cardiovascular lesion formations that were dependent on IRE1's RNase activity. The data shows that ER stress plays a causal role in KD progression via IRE1 activity.

In last part, I studied how a bioactive lipid molecule, palmitoleate, acts on IRE1 in order to remodel ER membrane and to resolve lipid induced ER stress. My findings show that saturated lipids induce IRE1 oligomerization and activation while the monounsaturated fatty acid, palmitoleate, blocks this oligomerization.

The promosing results of our mice studies with IRE1 inhibition warrants future investigation to assess IRE1's therapeutic potential in metabolic and inflammatory human diseases.

ÖZET
IRE1'NİN İKİ FARKLI ENZİMATİK AKTİVİTELERİNİN BİYOLOJİK HEDEFLERİNİN VE ROLLERİNİN İNCELENMESİ

ASLI DİLBER YILDIRIM
Moleküler Biyoloji ve Genetik, Doktora
Tez Danışmanı: Ebru ERBAY
Haziran 2022

Katlanmamış protein yanıtı (KPY), yanlış katlanmış proteinlerin birikimini çözmek ve hücresel homeostazı sürdürmek için tasarlanmış karmaşık ve yüksek düzeyde düzenlenmiş yollardan oluşur. Endoplazmik retikulum (ER), protein katlanmasını düzenleyen bir organeldir. ER katlama kapasitesinin altında yatan mekanizmaların düzensizliği, ER ile ilgili KPY yollarını (KPY^{ER}) aktive edebilir. İnositol gerektiren enzim-1 (IRE1), bir ER stres sensörü ve KPY^{ER} 'in proksimal düzenleyicisidir. IRE1, ikili kinaz ve endoribonükleaz (RNaz) aktivitelerini barındırır. IRE1 RNase aktivitesi, KPY^{ER} 'in transkripsiyonel katmanını başlatır, ancak IRE1'in kinaz substratları ve işlevleri bilinmemektedir. Bu çalışma, (i) yeni IRE1 kinaz hedeflerini keşfetmek, (ii) ER stresi ve ilgili patofizyolojik koşullar sırasında IRE1 tarafından düzenlenen yolakları deşifre etmek, (iii) biyoaktif lipidlerin doymuş yağ asidi kaynaklı indüklenenleri nasıl çözdüğünün altında yatan mekanizmaları araştırmak amacıyla yapılmıştır. İlk bölümde, S1P degrade edici bir enzim olan sfingosin 1-fosfat (S1P) liyaz (SPL) fosforilasyonunun IRE1 kinaz aktivasyonu üzerine indüklendiğini ve bu fosforilasyonun SPL'nin enzimatik aktivitesinin inhibisyonuna yol açtığını öğrendim. Sonuç olarak, IRE1 tarafından SPL inaktivasyonu, hücresel S1P seviyelerinin birikmesine neden olur.Mitokondri başka bir önemli organeldir ve organel proteostazını yeniden kazanmak için kendi KPY sistemine (KPY^{mt}) sahiptir. Ancak, KPY^{ER} ve KPY^{mt} arasındaki bağlantı belirsizdir. Deneylerim ayrıca artan S1P seviyelerinin IRE1 kinaz aktivitesine bağlı bir şekilde KPY^{mt} sinyalini güçlendirdiğini gösterdi. Bu deneylerin bir sonucu olarak, KPY^{ER}'i KPY^{mt}'ye bağlayan sfingolipid metabolizmasının önemli bir düzenleyicisi olarak IRE1 kinaz aktivitesini sunuyoruz.

Ayrıca, koroner arter anevrizmasına yol açan patofizyolojik bir durum olan Kawasaki Hastalığında (KH) IRE1'in işlevini araştırdım. Kawasaki hastalarından alınan halka açık transkrioptom veri setlerinin analizi üzerine, KH ilerlemesi ile ER stresi ile ilişkili gen imzalarında önemli bir artış tespit ettim. Lactobacillus casei hücre duvarı özütü (LCHÖ) ile indüklenen murin KH modelinden elde edilen tek hücreli transkriptomik veriler ayrıca miyeloid hücrelerde ER stresinin aktivasyonunu doğruladı. ER stres aktivasyonunun onaylanmasından sonra, IRE1'in LCHÖ ile indüklenen KH ilerlemesindeki rolünü incelemek için IRE1 fonksiyonunu ortadan kaldıran genetik veya küçük molekül yaklaşımlarını kullandım. Verilerim, IRE1'in RNaz aktivitesine bağlı olan kardiyovasküler lezyon oluşumlarının inhibisyonuna yol açan kaspaz-1 indüksiyonunda ve IL-1β sekresyonunda anlamlı azalma olduğunu gösterdi. Veriler, ER stresinin IRE1 aktivitesi yoluyla KD ilerlemesinde nedensel bir rol oynadığını göstermektedir.

Son bölümde, biyoaktif bir lipid molekülü olan palmitoleatın ER zarını yeniden şekillendirmek ve lipid kaynaklı ER stresini çözmek için IRE1 üzerinde nasıl etki ettiğini inceledim. Bulgularım, doymuş lipidlerin IRE1 oligomerizasyonunu ve aktivasyonunu indüklediğini, tekli doymamış yağ asidi palmitoleatın ise bu oligomerizasyonu bloke ettiğini gösteriyor.

IRE1 inhibisyonu ile fare çalışmalarımızın teşvik edici sonuçları, IRE1'in metabolik ve inflamatuar insan hastalıklarındaki terapötik potansiyelini değerlendirmek için gelecekteki araştırmaları garanti eder.

Dedicated to Derin Leila,
My little sunshine

Acknowledgements

This project would not have been possible without the support of many people. First, I am very thankful to my supervisor Dr. Ebru Erbay for providing invaluable feedback on my analysis and guiding me throughout my Ph.D. degree. I am honored and grateful to study in both of her labs - at Bilkent University and Cedars Sinai Medical Center. With the guidance and mentorship of my supervisor Dr. Ebru Erbay, I was able to learn the scientific approach and publish my discoveries.

I appreciate the help and the remarkable insight of my thesis committee members Prof. Dr. Michelle Adams and Prof. Dr. Tayfun Özçelik. I also want to thank Assoc. Prof. Dr. Çagdaş Devrim Son and Prof. Dr. Erkan Yılmaz for their guidance during my dissertation and for their contributions as members of my thesis jury.

I am thankful to our collaborators Dr. Moshe Arditi, Dr. Roberta Gottlieb and Dr. Magali Noval Rivas. I am grateful for their guidance and contributions as well as their support during my PhD studies at Cedars Sinai Medical Center. They made me feel as a part of their lab and I know I could not manage without their support.

I would like to express my deepest appreciation to the brilliant minds both at Bilkent University and Cedars Sinai Medical Center for giving me the opportunity to do my Ph.D. degree in these amazing academic roofs. Thanks to them, I have improved not only in scientific knowledge but also in my personal skill.

I also want to thank for the funding that enabled me to complete my thesis; European Molecular biology Organization (EMBO) for Installation Grant and European Research Council (ERC) Starting Grant 336643.

I am very grateful to all my friends and colleagues who help me during my Ph.D. studies. Of course, I would like to give special thanks to some of them.

First, I want to thank Aslı Ekin Doğan for her friendship and great contribution to revision experiments. She performed greatly with every task that she was given, and she went above and beyond to help. Not only she is a great science colleague, but she is also a great friend.

I would like to thank Zehra Veli for her very good friendship and for helping me with the experiments. I learned to do kinase assay from her. She answered my questions tirelessly and showed me even the smallest details. Besides, she always stood by me with her sincere love.

I learned a lot from her I want to thank Umut İnci Onat for her friendship, guidance, and all the help she gave me especially while I was pregnant. She took care of every detail in my life. If İnci had not helped me, it would have been very difficult for me to get used to the laboratory and Ankara. Spending time with Zeynep, İnci's daughter, was very valuable to me.

I would like to thank my dear friend Buket Gültekin both for her scientific assistance while she was working in our laboratory and afterwards for being in my life with all her heart and always supporting me.

I would like to express my gratitude to Altay Koyaş. He became my family in Ankara when I returned from America to Ankara. I thank him so much for taking good care of me and my daughter. I can't find the words to describe how lucky I am to have him in my life.

Thank you very much to my friend Merve Kayhan. We have been apart for a very long time, but I have always felt her support and love. I hope the days when we will be together again are not too far away.

I would like to thank my family, who has the most special place in my life, for their trust in me and for their support under all circumstances. I can't even imagine what my life would be like without them. I would especially like to thank my brother Yağmur Alp Yıldırım and my sister Sıla Yıldırım. I felt with all my heart how important they were in my life, but after my daughter was born, I was once again grateful for their existence. I was able to entrust my daughter to them without any hesitation, and I would not have been able to complete my thesis without their support.

It is very difficult for me to describe how I feel for my dear husband Ali Can Savaş. First of all, I am grateful to my husband for being by my side on the path of life. Even though we have been apart for a very long time, I thank him for his support, understanding and love.

I want to give the most special thanks to my daughter Derin Leila Savaş. She has been my biggest motivation on this path. Even in my most unhappy and hopeless moments, looking into her eyes gives me peace of mind. During the two years we were separated from her father, I was grateful every day for her existence. I owe a debt of gratitude to the life that gifted me my daughter.

Table of Contents

List of Figures

List of Tables

Abbreviations

Δ2-HDE	Δ2-hexadecenal
3-KDS	3-ketosphinganine
5'UTR	5′ untranslated region
AIM2	Absent in Melanoma 2
AOM	Azoxymethane
APAP	Acetaminophen
APD	Ammonium persulfate
APOE	Apolipoportein E
ASC	Apoptosis-associated speck-like protein containing a CARD
ATF	Activating Transcription factor
ATF4	Activating transcription factor 4
ATF6	Activating transcription factor 6
ATF6f	Fragmented ATF6
ATFS-1	Activating transcription factor associated with stress
ATP	Adenosine-5'-triphospohate
BIP	Binding-immunoglobulin protein
BMDM	Bone marrow-derived macrophage
BSA	Bovine serume albumin
bZIP	Basic leucine zipper
C-EBP	CCAAT-enhancer binding proteins
C1P	Ceramide-1-phosphate
CAA	Coronary artery aneurysms
cDNA	Complementary DNA
CerK	Ceramide kinase
CerS	Ceramide synthase
CERT	Ceramide transfer protein
CHOP	C/EBP-homologous protein
CoA	Coenzyme A
DAMPs	Damage associated molecular patterns

DCs	Dendritic cells
DES	Dihydroceramide desaturase
DMEM	Dulbecco's modified eragle medium
DMSO	Dimethyl sulfoxide
DNA	Deoxyribonucleic acid
dPBS	Dulbecco’s phosphate buffered saline
dsRNA	Double-stranded RNA
DSS	Dextran sodium sulfate
DTT	Dithiothreitol
EDEM1	ER degradation-enhancing α-mannosidase-like protein 1
EDG	Endothelial differentiation gene
EDTA	Ethylenediaminetetraacetic acid
eIF2α	Eukaryotic translation initiation factor 2α
EP	Ethanolamine phosphate
ER	Endoplasmic reticulum
ERAD	Endoplasmic reticulum - associated degradation
ERK	Extracellular signal-regulated kinase
ERSE	ER stress response element
FA-CoA	Coenzyme A-linked fatty acid
FBS	Fetal bovine serum
GADD34	Growth arrest and DNA damage-34
GCN2	General control non-derepressible 2
GRP78	Glucose Regulated Protein 78
GRPEL1	GrpE-like 1
GRPEL2	GrpE-like 2
GTP	Guanosine-5'-triphosphate
HCAECs	Human coronary artery endothelial cell
HDAC	Histone deacetylase
HEK	Human embryonic kidney
HFD	High fat diet

HisRS	Histidyl-tRNA synthetase-related
HMGCR	3-Hydroxy-3-Methylglutaryl-CoA Reductase
HPLC	High-performance liquid chromatography
HRI	Heme-regulated eIF2α kinase
HRP	Horse radish peroxidase
HSAN1	Hereditary sensory and autonomic neuropathy
IFX	Infliximab
IKK	Inhibitor of NFκB kinase
IM	Inner membrane
IP3R	Inositol 1,4,5-triphosphate receptors
iPLA2β	Phospholipase A2 beta
IRE1	Inositol-requiring enzyme-1
ISR	Integrated stress response
IVIG	Intravenous immunoglobulin
IκB	Inhibitor of NF-κB
KB	Kinase buffer
KD	Kawasaki disease
KDSR	KDS reductase
LC-MS	Liquid chromatography–mass spectrometry
LC3B-II	Microtubule-associated protein 1A/1B-light chain 3 II
LCWE	Lactobacillus casei wall extract
LPA	Lysophosphatidate
LPS	Lipopolysaccharide
MAMs	Mitochondria associated membranes
MAPK	Mitogen activated protein kinase
MEF	Mouse embryonic fibroblast
MFN1	Mitofusin 1
MPP	Mitochondrial processing peptidase
MRM	Multiple Reaction Monitoring
MSF	Mitochondrial import stimulation factor

mtDNA	Mitochondrial DNA
MTS	Mitochondrial targeting signal
NLS	Nuclear localization sequence
NOX4	NADPH oxidase 4
NRF4	NF-κB repressing factor B
OCT	Optimal cutting temperature
OM	Outer membrane
OPA1	Mitochondrial dynamin-like GTPase
ORF	Open reading frame
ORMDL	ORM1-like protein
OTC	Ornithine transcarbamylase
PAM	Presequence translocase-associated motor
PAMPs	Pathogen associated molecular patterns
PBF	Presequence binding factor
PBS	Phosphate buffered saline
PDIA3	Protein disulfide-isomerase A3
PDIA6	Protein disulphide isomerase-associated 6
PEI	Polyethylamine
PERK	(PKR)-like ER kinase
PHB2	Prohibitin 2
PKR	Protein kinase RNA
PLB	Phospho Lysis Buffer
PLP	Pyridoxal 5′-phosphate
PMSF	Phenylmethylsulfonyl
PNBM	P-nitrobenzyl mesylate
PP1R15A	Protein phosphatase 1 regulatory subunit 15A
PPARγ	Peroxisome proliferator-activated receptor γ
PRRs	Pattern recognition receptors
PtdCho	Phosphatidylcholine
PtdEtn	Phosphatidylethanolamine

PtdSer	Phosphatidylserine
qRT-PCR	Quantitative real time polymerase chain reaction
RIDD	IRE1 dependent decay of mRNA
RNA	Ribonucleic acid
RNase	Endoribonuclease
ROS	Reactive oxygen species
RPMI	Roswell Park Memorial Institute
S/T	Serine/Threonine
S1P	Sphingosine 1-phosphate
SDS	Sodium dodecyl sulphate
SERCA	Sarcoplasmic Reticulum Ca^{2+} ATPase
SGPPase	S1P specific phosphatases
SM	Sphingomyelin
Smases	Sphingomyelinases
SPHK	Sphingosine kinase
SPL	Sphingosine 1 phosphate lyase
SPNS2	Spinster homolog 2
SPP	S1P specific phosphatases
SPT	Serine palmitoyl-CoA transferase
SRP	Signal Recognition Particle
STAT3	Signal transducer and activator of transcription 3
STZ	Streptozotocin
T1D	Type 1 diabetes
TBS	Tris-buffered saline
TbSpl	Trypanosoma brucei
TFs	Transcription factors
TG	Thapsigargin
THI	2-acetyl-4-(tetrahydroxybutyl)imidazole
TNF	Tumor-necrosis factor
TOM	Translocase of the outer membrane

TRAF2	TNF receptor associated factor 2
TRAF2	TNF receptor-associated factor 2
TUN	Tunicamycin
TXNIP	Thioredoxin – interacting protein
UPRE	Unfolded protein response element
UPR^{ER}	ER unfolded protein response
UPR^{mt}	Mitochondrial unfolded protein response
VSMCs	Vascular smooth muscle cells
WCL	Whole cell lysates
WT	Wild-Type
XBP1	X-box binding protein 1

Chapter 1

Introduction

1.1 The Endoplasmic Reticulum

Endoplasmic reticulum (ER) is the largest organelle spread through the cytoplasm of the cell. ER is surrounded by one continuous membrane bilayer. This membranous structure is composed of tubules and interspersed sheets forming a structural organization from nucleus to the plasma membrane (1, 2). Ribosome-associated ER regions are called as 'rough' ER and are the main site of synthesis, folding and maturation of secreted and transmembrane proteins. Matured proteins synthesized in ER are transported to Golgi apparatus by tubular ER structures. On the other hand, regions which are not associated with ribosomes namely 'smooth' ER maintain other functions such as communications with other organelles and plasma membrane (1). ER is closely interconnected with almost all membrane-bound organelles such as mitochondria, Golgi apparatus and lysosomes through physical contact sites (3). The most well-characterized organelle contact sites are those between the ER and mitochondria known as the Mitochondria Associated Membranes (MAMs). It has now become clear that MAMs synergize the functions of these two organelles and provide an opportunity to fulfill bidirectional trafficking of factors which are important for biological processes (4). Developing new strategies and techniques to discover the molecular mechanisms controlling ER dynamics is crucial to decipher how ER functions and collaborate with other organelles especially with mitochondria.

1.1.1 Function of Endoplasmic Reticulum

ER has four main functions in the cell: (i) protein synthesis, folding and maturation, (ii) degradation of misfolded/unfolded proteins, (iii) controlling calcium metabolism, (iv) synthesis of major lipid species.

1.1.1.1 Protein synthesis, folding and maturation

ER is the organelle where soluble and transmembrane proteins are folded (5). Protein folding is the most error prone steps in gene expression. Because of that, proper folding in ER occurs with the help of multiple factors reside in ER lumen. Binding of mRNAs to ribosome harboring to rough ER provides a state which unfolded nascent polypeptides enter ER lumen through an ER membrane spanning channel. Proteins are targeted to ER by N- terminal signal recognition

particle (SRP). This signaling sequence is cleaved by certain peptidase and nascent peptides are co-translationally entered into ER lumen (6). Numerous ER resident chaperones and oxidoreductases assist co-translationally and post-translationally protein folding. Unique oxidative features of ER lumen allow proper folding of translocated proteins by posttranslational modifications, including glycosylation, disulfide bond formation and lipidation. All these modifications play crucial roles for targeting properly folded proteins into their final cellular sub- compartments (5). If any of these steps in protein folding machinery fails, proteins cannot reach their final structures and stuck into ER lumen as insoluble aggregates. Thus activates another important ER dependent mechanism to decrease ER misfolded/unfolded protein load.

1.1.1.2 Degradation of misfolded/unfolded proteins

Endoplasmic Reticulum - Associated Degradation (ERAD) is a quality control system that selectively removes misfolded/unfolded proteins from ER lumen and targets them to highly controlled degradation machinery. Retranslocation of misfolded proteins to the cytosol activates ERAD pathways. Misfolded proteins undergo ubiquitination and degraded by proteasomes. This selective clearance pathway reduces immature protein load of ER and helps ER to work efficiently (7).

1.1.1.3 Calcium metabolism

ER also plays pivotal role for regulation of intracellular Ca^{2+} storage (8). Cytosolic and extracellular calcium concentrations are tightly regulated ~ 100 nM and ~ 2 mM respectively. Whereas, Ca^{2+} concentration in the ER lumen changes between ~100-800 uM (9). This huge difference in Ca^{2+} concentrations between cytosol and ER lumen clearly shows that ER is the main compartment in the cell for Ca^{2+}storage. Ca^{2+} storage within ER is required for pathways through Ca^{2+} signaling, post translational protein folding and maturation. ER chaperons, essential for proper folding, need sufficient supply of Ca^{2+} and Ca^{2+} depletion causes the accumulation of insoluble protein aggregates in ER lumen. The ER calcium concentration is regulated by calcium channels such as Sarcoplasmic Reticulum Ca^{2+} ATPase (SERCA) pump and inositol 1,4,5-triphosphate receptors (IP3R) on ER membrane and they are required for Ca^{2+} transfer from ER to cytosol or vice versa when it is needed (10).

1.1.1.4 Synthesis of major lipid species

Signals from inside and outside of the cell are sensed by ER resident enzymes. This allows ER mediated lipid synthesis to respond needs of the cells including proliferation, changes composition of lipid in membrane structures.

Synthesis of phospholipids happens at cytosolic side of ER membrane and requires addition of two fatty acids to glycerol phosphate backbone. Phopholipids such as phosphatidylcholine (PtdCho) and phosphatidylethanolamine (PtdEtn) are produced by ER localized enzymes and are mainly used as membrane building blocks. PtdCho is the most abundant phospholipid in mammalian cells and can be converted to phosphatidylserine (PtdSer) and PtdEtn on ER mitochondria contact sites (11).

In addition to its role in lipid bilayer composition and membrane building blocks, ER controls the activity of cholesterol synthesis. Since the cholesterol levels in ER membrane is particularly low, even small changes in cholesterol efficiently sense by ER and activates cholesterol related gene transcription (12, 13). SREBPs are ER localized transmembrane proteins. Under basal conditions SREBP is retained in ER via interactions with SCAP and Insig (14). Any changes in cholesterol composition of ER membrane influence SCAP conformation and block its binding to Insig. Thus allows SREBP/SCAP translocate from ER to Golgi. After processing and maturation in Golgi, SREBP translocates to nucleus where it activates the transcription of the cholesterol synthesis related genes such as 3-Hydroxy-3-

Methylglutaryl-CoA Reductase (HMGCR). HMGCR is a rate limiting enzyme for cholesterol production resides on ER membrane and sense the level of cholesterol in the cell (15)

ER also maintains a hub for sphingolipid synthesis, conversion and degradation pathways. Sphingolipids represents 10%–20% of cellular lipids (16). They are potent signaling molecules and have crucial roles as structural membrane components. Type and percentage of sphingolipids change fluidity and thickness of membranes and effect physical properties. Sphingolipids associate with trans- and peripheral-membrane proteins and thus association influences the activity of proteins. Serine palmitoyl- CoA transferase (SPT) is a transmembrane enzyme and its active site localizes on the cytoplasmic face of ER. This enzyme catalyzes the reaction between serine with a coenzyme A-linked fatty acid (FA-CoA).This reaction is the rate limiting step of *de novo* sphingolipid synthesis (17). Besides SPT, enzymes which are responsible for conversion of sphingolipid species into each other also locate in ER (18). Sphingolipid metabolism in ER and their role in cellular pathways deserve special emphasis and will be mentioned in a later section of this thesis.

1.1.2 ER stress and ER unfolded protein response (UPR^{ER})

One of the main functions of ER is create an environment to fold nascent polypeptides properly with the help of chaperons, foldases and cofactors localized in the ER lumen (5). If any dysfunctions occur in the activities of these enzymes, ER initiates ERAD pathway to remove insoluble/unfolded protein aggregates and decrease its own work load (7).

Physiological or environmental changes such as increased rate of protein synthesis, depletion of ATP, oxidative stress, alterations in Ca^{2+} level and exposure to excessive lipid species can lead to interruption of ER folding activities, causing unfolded protein accumulation in the ER lumen. Disruption the balance between the demand for protein folding and protein folding capacity of ER causes ER stress (19, 20). To cope with ER stress, an adaptive response mechanism is activated in ER, called as unfolded protein response (UPR^{ER}). ER resident transmembrane proteins sense the increased ER stress and initiate transcriptional and translational pathways (21, 22). There are three ER resident stress sensors in the ER membrane; inositol-requiring enzyme-1 (IRE1), the protein kinase RNA (PKR)-like ER kinase (PERK), and the activating transcription factor 6 (ATF6) (Figure 1.1). Under physiological conditions, Binding-immunoglobulin protein / Glucose Regulated Protein 78 (BIP/GRP78) binds to luminal domains of these three ER sensors and keep them in their inactive states. Under ER stress conditions, BIP disassociates from these effectors and binds to unfolded proteins in the ER lumen, initiating UPR^{ER} related pathways. The first aim of UPR^{ER} is to reduce ER protein load and to reestablish ER homeostasis by activating translational and transcriptional mechanisms. If ER stress is prolonged, ER sensors engage clearance cascades such as apoptosis to eliminate defected cells (22-25).

Figure 1. 1: Endoplasmic Reticulum Stress and Unfolded Protein Response

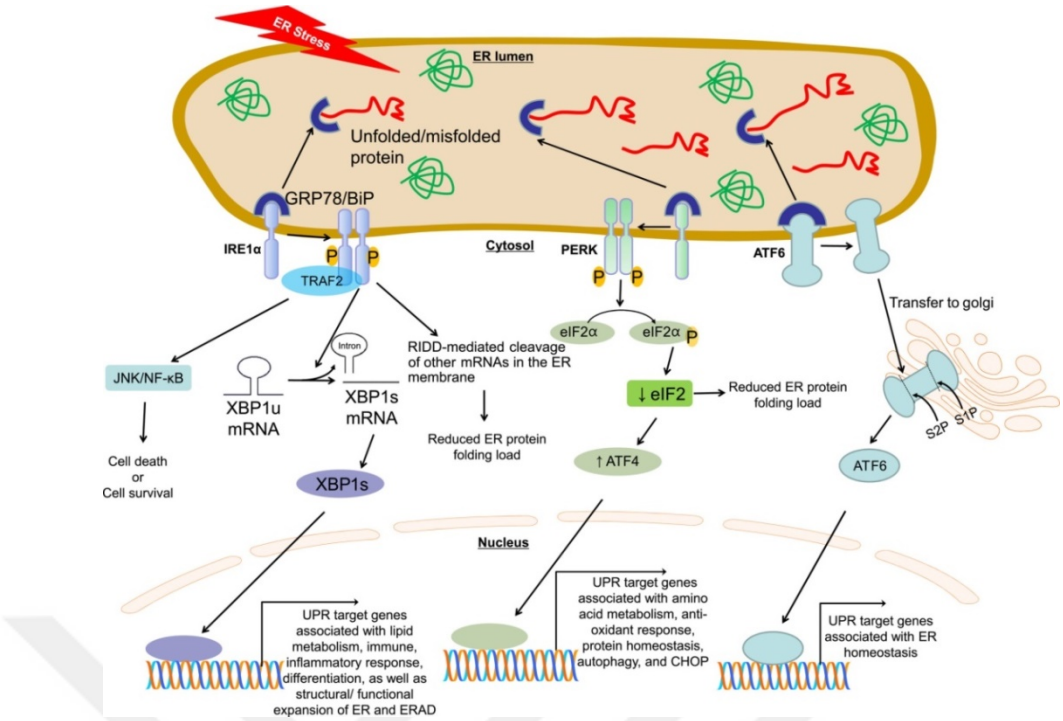

1.2 Unfolded protein response signaling in ER

Unfolded protein response is controlled by three ER resident signal transducers, IRE1, PERK and ATF6

1.2.1 IRE1

IRE1 is the first identified ER stress sensor located on ER membranes. Now it is clear that it is highly conserved from yeast to mammalian systems. There are two IRE1 homologs in mammalians IRE1α and IRE1β and they have diverse functions in the cell. ER stress is mainly mediated by IRE1α and the function of IRE1β is limited (26, 27). IRE1 protein contains three domains; a luminal domain, a transmembrane domain and a cytosolic domain. IRE1 has two different enzymatic activities; namely serine/threonine kinase and namely endoribonuclease (RNase). Disassociation of BIP from luminal domain promotes IRE1 to sense unfolded protein accumulation in ER lumen and this leads to activation by autophopsphotylation and higher-order assembly of IRE1. Activation of its kinase domain further activates its RNase domain. RNase domain of IRE1 has a unique feature and initiates the transcription of several ER stress related genes to reestablish ER homeostasis (28). Post-translational modifications on IRE1 are also important for IRE1 activity (29). IRE1 also associates with mitochondria through MAMs. IRE1 as a structural component of MAM is important for fine-tuning of bioenergetics between ER and mitochondria. Ablation of IRE1 leads to reduced calcium release and mitochondrial uptake. Also IRE1 serves a scaffold and controls the distribution of functional proteins through MAM under basal conditions (30).

In response to ER stress, IRE1 oligomerizes in ER lumen and activates its kinase and endoribonuclease functions. Endoribonuclease activity of IRE1 initiates specific splicing of X-box binding protein 1 (XBP1) mRNA through its RNase domain. RNase domain selectively cleaves a 26 nucleotide fragment from unspliced XBP1 mRNA and this in turn result in a frame shift in the XBP1 coding sequence. Spliced form of XBP1 is translated under ER stress conditions and acts as transcription factor. sXBP1 translocates to the nucleus and initiate transcription of UPR- and non-UPR related genes by binding unfolded protein response element (UPRE). It has been shown that uXBP1 can terminate UPR^{ER} response by directing

sXBP1 to proteosomal degradation in the cytosol (31). Recently it has been shown that IRE1 endoribonuclease function leads to unconventional maturation of miR-2137. Mature miR-2137 modulates ER to plasma membrane through PI(3,4,5)P3-dependent signaling pathway and determines growth decision in macrophages (32). Also, inhibition of IRE1 RNAse by its specific inhibitor, 4μ8c, alleviates inflammasome activation by reducing mitochondrial reactive oxygen species (ROS) (33). In addition to XBP1 mRNA splicing activity of IRE1, hyperactivated IRE1 is involved in IRE1 dependent decay of mRNA activity (RIDD). To reduce the protein load and lower the translational rate of ribosomes, IRE1 specifically targets mRNAs bound to ER associated ribosomes. Besides mRNAs, RIDD can also target rapid decay of specific microRNAs such as miRs-17 and 34 during ER stress to derepress proapoptotic Caspase-2 translation and inhibits cell death (34).

Kinase domain of IRE1 is important for its activation through autophosphorylation. Diverse ER stressors are sensed by its luminal domain and results in the conformational changes of IRE1 dimers from face-to-face to back-to-back. Thus allows IRE1 to autophosphotylate itself by its kinase domain and its activation (35). The kinase domain function of IRE1 is associated with inflammatory and apoptotic pathways. IRE1 activated JNK by binding adaptor protein TNF receptor associated factor 2 (TRAF2). Activated and phosphorylated IRE1 binds to TRAF2 and initiates the mitogen activated protein kinase (MAPK) pathway (36). Some small molecule inhibitors that target IRE1 kinase domain have been investigated. It has been shown that inhibition of IRE1 kinase domain by KIRA6 promotes cell survival under ER stress. KIRA6 systemically inhibits cell degeneration through increasing insulin and reducing hyperglycemia in diabetic mice (37).

Until now, the only reported kinase substrate of IRE1 is itself through autophosphorylation. IRE1 has been reported to be associated different proteins upon ER stress. Thus could increase the possibility of IRE1 to bind and phosphorylate other proteins to regulate different pathways to maintain cellular homeostasis (38).

1.2.2 PERK

PERK is another ER stress transducer located on ER membranes. Likewise IRE1, it contains 3 domains: luminal (stress sensing), transmembrane and cytoplasmic (kinase) domains. Under basal condition PERK binds BiP and is found in inactive state. Upon ER stress and BIP disassociation, PERK can autophosphorylate and oligomerize itself at threonine-980. Eukaryotic translation initiation factor 2α (eIF2α) is the best known PERK kinase substrate (39). Phosphorylation of eIF2α on serine 52 by PERK leads to general translational attenuation of capped mRNAs and blocks misfolded protein accumulation in ER lumen. However, translation of some selected mRNA through upstream alternative open reading frame (ORF) must be achieved to reestablish ER homeostasis. Activating transcription factor 4 (ATF4) is one of the preferentially translated mRNA during translational attenuation and it act as a transcription factor. ATF4 regulates the transcription of some set of genes involved in amino acid import, metabolism and resistance to oxidative stress. ATF4 axis of PERK signaling is important for cytoprotection at early stage of ER stress. However, under severe/prolonged ER stress condition ATF4 induces transcription of C/EBP-homologous protein (CHOP). CHOP is also another transcription factor controlled by PERK axis of UPR^{ER} and drives expression of cell death related genes (39, 40). Besides that, PERK phosphorylates NF-κB repressing factor B (NRF2) at Ser40, leading to NRF2 translocation to the nucleus and initiates transcription of antioxidant proteins (41). CHOP upregulates the expressions of protein phosphatase 1 regulatory subunit 15A (PP1R15A) or growth arrest and DNA damage-34 (GADD34) genes. These two proteins are responsible for dephosphorylating of eIF2α and reactivate the attenuated protein translation (42). Thus results in continuation of protein translation that necessary to regain protein homeostasis in ER lumen. Altogether, PERK fulfills opposing functions such as cytoprotection, apoptosis and anti-oxidative and thereby, can contribute to cellular homeostasis and determine cell fate.

1.2.3 ATF6

ATF6 is the third UPR sensor of unfolded protein response in ER. It has three domains; luminal (stress sensing), transmembrane and cytoplasmic domains. ATF6 isoforms are members of basic leucine zipper (bZIP) family of transcription factors. In mammalian cells, ATF6α and ATF6β homologous proteins reside on ER (43). ATF6α is a 90 kDa type II transmembrane glycoprotein and has two Golgi translocation signal sequences within its ER-luminal domain. Upon disassociation of BIP from ATF6 luminal domain, it gets activated (44, 45). Activated ATF6 isomers translocate to Golgi and are cleaved by two proteases, Site-1 protease and Site-2 protease . These two proteases remove the luminal domain and transmembrane anchor, 50 kDa fragmented ATF6 (ATF6f) protein enters into nucleus and acts as a transcription factor by binding ER stress response element (ERSE). ATF6a initiates transcription of chaperons and other ER stress related proteins such as BIP and XBP1 (46). Besides these, ER degradation-enhancing α-mannosidase-like protein 1 (EDEM1) and protein disulphide isomerase-associated 6 (PDIA6) are other known ATF6 targets which involve in ERAD pathway (47).

1.3 Integrated stress response

Integrated stress response (ISR) is an evolutionary conserved signaling response that activates an adaptive pathway to maintain cellular homeostasis. Changes in physiological and/or pathological conditions such as nutrition deprivation, viral infection, heme deficiency initiate ISR. Moreover, ER stress can also activate ISR. Phosphorylation of eif2α which leads reduction of global protein synthesis is the central event in this pathway and common player of both ISR and UPR^{ER}. This phosphorylation is catalyzed by one of the four serine/threonine (S/T) eIF2α kinases. PERK, double-stranded RNA-dependent protein kinase (PKR), heme-regulated eIF2α kinase (HRI), and general control non-derepressible 2 (GCN2) phosphorylate eIF2α on serine 51 depends on distinct stress stimuli (48). eIF2α kinases a have overlapping functions and can be activated cooperatively to maintain cellular homeostasis upon a wide variety of stressors.

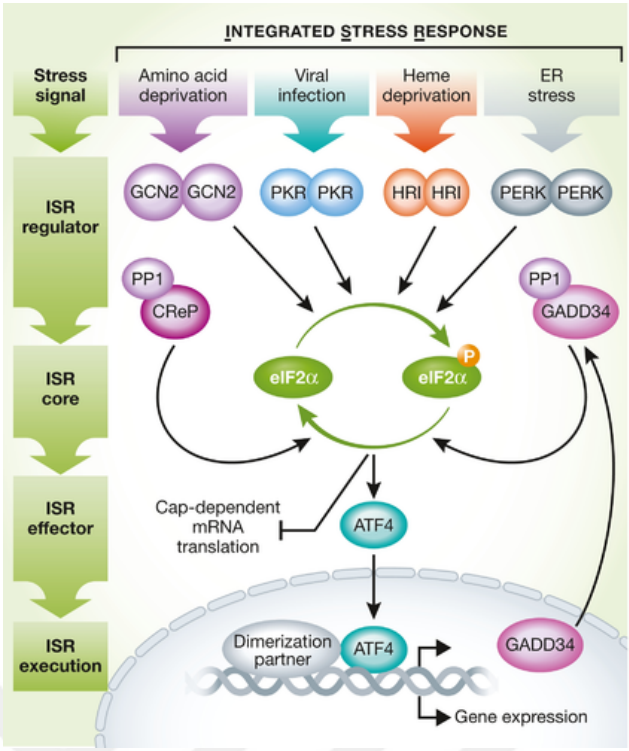

Figure 1. 2: Schematic Representation of ISR

PERK is the common stressor between ER stress and ISR. Activation of PERK upon cellular stressors leads to eIF2α phosphorylation which subsequently results in ATF4 and CHOP translation. These two transcription factor translocate to nucleus to activate ER stress related genes as well as other genes in a wide variety. PERK- ATF4 pathway recently has been implicated with regulation of metabolic pathways through mitochondria. PERK-regulated ISR has been shown to mediate mitochondrial clearance which is a vital role in cellular homeostasis (49).

The mammalian PKR is activated by double-stranded RNA (dsRNA) during viral infection and eIF2α phosphorylation by PKR results in subsequent inhibition of viral and host protein synthesis. Moreover, PKR can be stimulated by other stressor such as ER and oxidative stress, cytokines or growth factor deprivation as dsRNA independent manner. It has been shown that PKR activation is regulated by IRE1 and thus confirms ER stress is integrated with ISR to overcome stress in the cells by activating downstream pathways (50).

Other eIF2α kinase GCN2 can be activated by single amino acid deprivation. Uncharged tRNA molecules accumulate and bind to histidyl-tRNA synthetase-related (HisRS) domain of GCN2 upon decreased level of an amino acid. Subsequently, GCN2 phosphorylates eIF2α and leads to reducing amino acid supply by attenuating mRNA translation and protein synthesis (51).

Since other eIF2α kinases have a broad tissue distribution, HRI is mainly expressed in erythroid cells during erythropoiesis (52). HRI regulates the translation of globin mRNAs in the presence of heme for hemoglobin production and thus protects cells against aggregated toxin globin accumulation upon iron deficiency (52-54). Heme binds to heme binding domain of HRI. On the other hand, heme can also bind to the kinase insertion domain of HRI and thus leads to inhibition of HRI kinase activity. HRI is not only activated by heme. Other stresses such as oxidative stress, heat shock, osmotic stress and 26S proteasome inhibition can also induce HRI activity and leads to ISR activation through eIF2α phosphorylation (55). Moreover, increased mitochondrial protease OMA1 activation upon mitochondrial stress cleaves DELE1 protein. Cleaved- DELE1 fragments which are produced by OMA1 activity

bind to HRI in the cytosol, leading HRI activity. This adds another layer to communication between ISR and mitochondrial proteostasis (56, 57).

ISR leads to global translational attenuation through eif2α phosphorylation. As a result of this, concomitant translation of selected mRNAs that contain upstream uORF in their 5′ untranslated region (5′UTR) regions such as ATF4, ATF5, CHOP and GADD34 (58-60). ATF4, ATF5 and CHOP are regular proteins, acting as transcription factors. Indeed, GADD34 dephosphorylates eIF2α and provides a feedback loop that inhibits stress-induced gene expression (61). ATF4 is the central transcription factor in the ISR which is controlled by transcription, translation and several other post-translational modifications. ATF4 is one of the bZIP transcription factors that can form heterodimers with CCAAT-enhancer binding proteins / Activating Transcription factor (C-EBP/ATF) response elements to increase the complexity of transcriptional regulation (62). Dimerization partner of ATF4 is important for differentiation of the stress response such as survival vs. cell death. Transcription and translation of ATF4 under non-stress condition are very limited. The mouse ATF4 gene contains two ORFs and uORF2 which overlaps with coding sequence in an out-of-frame manner prevents ATF4 mRNA translation (63). However, ATF4 mRNA translation is initiated from ORF1 under stress condition and initiates some selected gene transcription with contribution of ATF5, CHOP and other bZIP transcription factors (40, 58, 62).

Transcriptional program initiated by the ISR varies across species and depends on stress types that trigger the ISR. Deregulation of ER- and mitochondria-related pathways most frequently initiates the ISR. Defects in mitochondrial protein synthesis and mtDNA maintenance are associated with ISR activation (64). In conclusion, ISR is a very important adaptation mechanisms which effect function of different organelles. This complex signaling in between ER-mitochondria is transferred to nucleus by ISR to encompass malfunctioning in the cell.

1.4 Mitochondria

Mitochondria are the power house which is the major energy- producing organelles in the cells. Besides energy conversion, they have other diverse functions such as calcium homeostasis, heme biogenesis, apoptosis and ROS production. Mitochondria serve as a scaffold to activate inflammasomes, resulting initiation of inflammasome related pathways. Due to these vital functions, these organelles maintain the balance between cell life and death. To sustain mitochondrial homeostasis, these organelles undergo dynamic interplay with their cellular environment. If there is any disruption in the environment, there organelles meet the metabolic needs and adopt the cells to internal and external changes (65).

1.4.1 Mitochondria structure

Mitochondria are enclosed by two membranes; inner membrane (IM) and outer membrane (OM). The structure and composition of these membranes are considerably different from each other to meet the metabolic need. OM provides a platform for proteins and transporters to initiate several signaling pathways related with various functions of mitochondria. It contains 8–10% of the total proteins of the organelle. All known proteins located on OM are encoded in nucleus and synthesized by ribosomes in cytosol. OM of mitochondria surrounds IM. IM contains high concentration of cardiolipin and protein to phospholipid ratio of this membrane is higher in comparison to OM. IM folds inwards to form cristae is packed with proteins involved in electron transport and ATP synthesis. IM surrounds mitochondria matrix (66, 67). IM serves as a functional barrier to transferring small molecules into matrix and fulfill the proton gradient required for ATP production by complexes located on IM. Mitochondrial membrane potential maintains a gradient to force hydrogen ions which is harnessed to make ATP (68).

Mitochondria have another unique feature which is having its own genome in mitochondria matrix. Mitochondrial DNA (mtDNA) exists in several copies per cell and many human

disease linked dysfunction and alteration of the number and/or the integrity of mtDNA. Vast majority of mitochondrial proteins are encoded by nucleus and folded in the cytoplasm and import into mitochondria to maintain mitochondrial proteostasis. Besides, 13 mitochondria-resident proteins are encoded by mtDNA. Mitochondrial gene- encoded proteins join into protein complexes of oxidative phosphorylation system (69, 70).

1.4.2 Mitochondrial Proteostasis and mitochondrial unfolded protein response (UPR^{mt})

Such as endoplasmic reticulum, balanced functional protein load of mitochondria is critical for mitochondrial function. Mitochondria fulfill its key functions such as energy homeostasis and metabolism by maintaining a functional proteome. To cope with proteomic challenges, mitochondrial proteostasis mechanisms activate and initiate protein quality control pathways through mitochondria localized translocases involved in protein import machinery, chaperones and proteases (71). Also there is a retrograde signal between mitochondria and nucleus to control the transcription rate of nuclear encoded mitochondrial proteins.

1.4.2.1 Protein import into mitochondria

Nuclear-encoded mitochondrial proteins are transported to cytosol and translated here by cytoplasmic ribosomes. Mitochondrial precursor proteins contain mitochondrial targeting signal (MTS) peptide that are recognized by receptors on the OM and targeted to their functional sub-compartments in the mitochondria. There are two main groups of targeting signals. The first group includes precursor proteins which have amino terminal extension presequences at N-termini of preproteins and these presequences are proteolytically cleaved after import into mitochondria. Second, many precursor proteins do not have removable extensions. These proteins contain internal signals that remain part of mature protein (72, 73).

General chaperones such as HSP70 and HSP90 and other specific components in cytosol bind to mitochondrial precursor proteins and target them to the surface of mitochondria. These chaperons also bind to the receptor Tom70 and this association ensures a direct interaction of precursor proteins to mitochondrial import machinery (74). Surface receptors on OM sense and bind to mitochondrial target presequences. These receptors are part of translocase complexes, called as translocase of the outer membrane (TOM) complex. The central component of TOM complex is Tom40. Tom40 engaged with three preprotein receptors, Tom20, Tom22 and Tom70 and other several small TOM components. Two receptor proteins of TOM complex, Tom20 and Tom 22, initiate the recognition of presequences. Tom22 recognizes the positively charged surface of presequences on mitochondrial surface whereas Tom20 binds hydrophobic sites. β-barrel protein Tom40, similar to porin proteins in bacteria, forms import channel for preprotein translocation into inner membrane space of mitochondria (75, 76). TIM23, another translocase complex, resides on IM and comprises Tim23, Tim17 and Tim50 and other additional Tim proteins in yeast. TIM23 complex structure and function differ depending on the type of the Tim proteins in the complex. $TIM23^{SORT}$ contains Tim21 and is responsible for the lateral release of preproteins into IM. The other form is TIM23-presequence translocase-associated motor (PAM) complex and this complex maintains translocation of preproteins into the matrix (77, 78). After precursor proteins reach to matrix of mitochondria, mitochondrial processing peptidase (MPP), a heterodimeric enzyme, proteolytically removes presequence. To generate more stable proteins, cleaved preproteins are processed by a second protease, either Oct1 or Icp55 according to N-end rule (79, 80). Cleavage of preproteins causes the generation of short peptides which need to be cleared by further degradation through other protease. Although yeast TIM23 complex has similarities with its mammalian orthologous, it is more complex and has unidentified components in mammalian translocase complex since it is involved in a variety of elaborate functions. There are three distinct TIM23 complexes, respectively A, B1, and B2 in humans. These translocase complexes are formed by different Tim subunits and additional J- proteins. B1 and B2 complexes fulfill basic translocase function and compose of Tim17b isoform along with DnaJC19. Complex B has normal import rate and are important for maintaining constitutive

mitochondrial functions whereas complex A is nonessential and has lower import rate. Complex A imports oncoproteins lacking presequences and this indicates its role in oncogenesis (81).

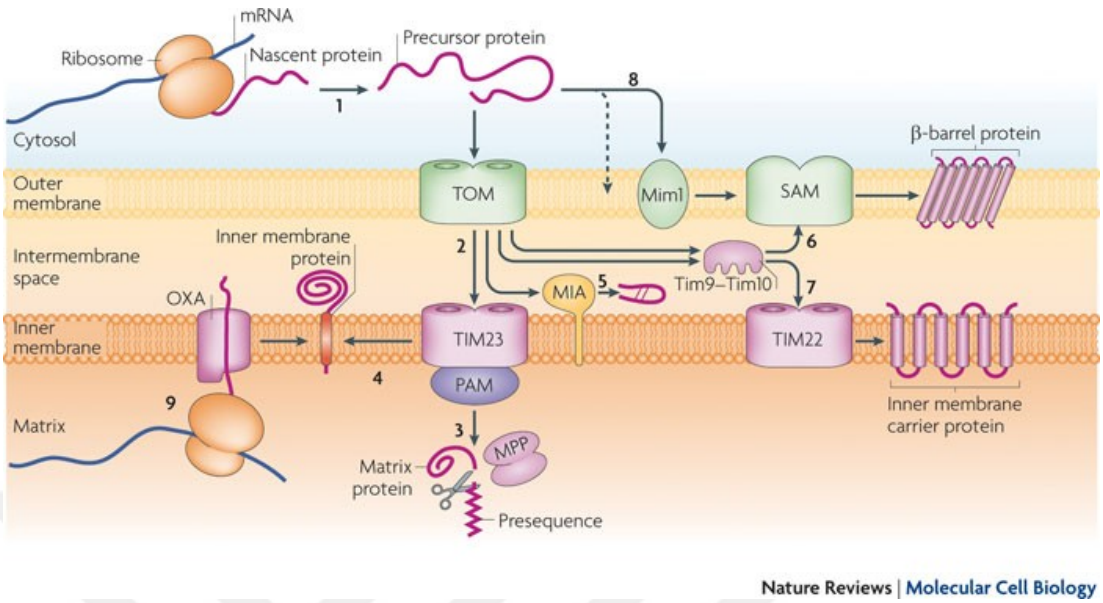

Figure 1. 3: Biogenesis pathways of mitochondrial proteins

1.4.2.2 Protein folding and degradation in mitochondria

Most of the mitochondrial proteins are encoded by nucleus and transported into mitochondria as described above. Around 1000 in yeast and around 1500 mitochondrial precursor proteins are produced on cytosolic ribosomes (82, 83). Only 13 mitochondrial proteins are encoded by mitochondrial genome. These mitochondrial encoded proteins such as core subunits of respiratory chain and ATP synthase are very hydrophobic and translated by ribosomes in the mitochondria (70). Therefore, balanced and coordinated translation between mitochondria and cytosol is crucial for maintaining functional mitochondria. Several chaperons and cytosolic factors such as mitochondrial import stimulation factor (MSF) and presequence binding factor (PBF) in cytosol are involved in post translational protein transfer in cytosol. HSP70 and HSP90 cytosolic chaperones are involved mitochondrial protein folding through their post translational targeting abilities (74). Post translational targeting by cytosolic chaperones encompasses several mechanisms, they keep precursor proteins unfolded. These cytosolic chaperones direct precursor proteins to mitochondrial surface receptors; in particular to Tom70. Beyond their general role in precursor targeting, their substrate specificity is unclear (84).

Accumulation of unfolded precursor proteins is prevented by mitochondrial chaperones in mitochondria. mtHsp70 (Mortalin, Ssc1 in *Saccharomyces cerevisiae*) is a member of heat shock protein family and mediates mitochondrial protein import as an ATP dependent manner (85). ATP-bound mtHSP70 is in open form which allows rapid binding of its substrates. After ATP hydrolysis, it turns to its ADP-bound close form. GrpE-like 1 (GRPEL1) and GRPEL2, nucleotide exchange factors, assists the exchange of ADP with new ATP molecule and thus allows mtHSP70 binding to a new preprotein (86).

Once precursor protein are imported to matrix, they are processed by MPP to remove MTSs. mtHSP70 has a dual import functions ; (i) at import channels and (ii) in the matrix. Interactions of mtHSP70 with different co-chaperones determine its role in protein import and protein folding. Thus attributes the existence of two different complexes (87). First, membrane bound mtHSP70 interacts with peripheral side of the presequence translocase TIM23. With the help

of its peptide binding domain, mtHSP70 tightly binds to unfolded polypeptide chain in the matrix. Second, after import and proteolytic processing, soluble form of mtHSP70 fulfills its chaperoning activity. mtHSP70 with the help of HSP60-HSP10 chaperoning complex mediate folding of imported preproteins and prevent misfolded or aggregated protein accumulation in the matrix (77).

The coordinated import and folding of preproteins reduces the accumulation of non-functional protein aggregates and ensures efficient assembly of protein complexes in mitochondria.

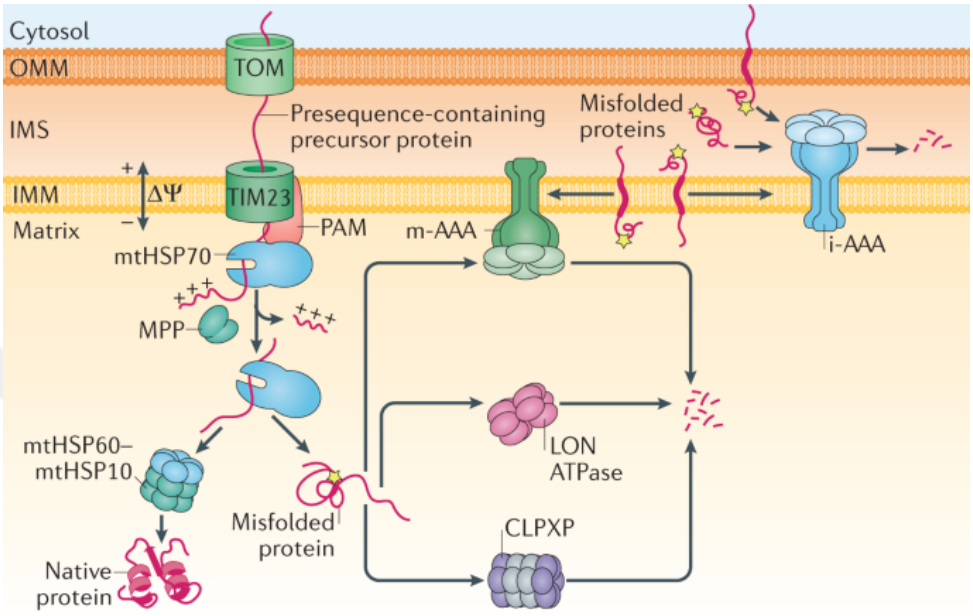

Figure 1. 4: Protein quality control in inner mitochondrial compartments.

Besides import and folding machineries, degradation of denatured or misfolded protein is an additional step responsible for maintaining mitochondrial proteostasis. Balanced protein import and degradation is important for mitochondrial protein quality control. Different compartments of human mitochondria harbor independent proteolytic systems which comprise at least 45 proteases. Some of mitochondrial localized proteases do not have catalytic activity, called as pseudomitoproteases. 18 intrinsic mitoproteases can be classified as ATP-dependent peptidases, processing peptidases, oligo peptidases, and other mitochondrial peptidases (88, 89).

ATP dependent proteases localize in different subcompartments of mitochondria. Two ATP-dependent serine proteases, LON protease (LONP1) and ClpXP (ClpP protease and its regulatory subunit ClpX), localize to the mitochondrial matrix, whereas the homologous i-AAA (catalytic site faces to IMS) and m-AAA (catalytic site faces to matrix) proteases localize to the inner mitochondrial membrane (90-92). These four proteases establish chambered protease complexes to degrade proteins with broad specificity.

LONP1 plays a central role for mitochondrial proteostasis. After cytosolic translation of its mRNA, LONP1 is directed to mitochondria through its N- terminal MTS. LONP1 polypeptide is folded by mitochondrial chaperones to assemble into active enzyme conformation in mitochondrial matrix. Proteolysis properties and substrate specificities of LONP1 have been extensively studied in yeast and now it is clear that mammalian LONP1 also exhibits practically identical with its yeast ortholog (93). LONP1 has 3 major roles in mitochondrial proteostasis: (i) degrading aggregated proteins in matrix, (ii) reinforcing mitochondrial gene expression, (iii) involving in mitochondrial clearance under some pathological condition. All

these tasks are coordinated with each other to maintain protein quality control of mitochondria (94).

ClpP and its regulatory subunit ClpX are encoded by nucleus and are directed to mitochondrial matrix by N- terminal MTS. They form multimeric complex in mammalian cells. Substrate of ClpXP complex recognized and unfolded by ClpX as an ATP dependent manner. These unfolded proteins enter into proteolytic domain of ClpP and are fragmented into small peptides (95, 96). Several ClpXP substrates are identified including proteins involved in electron transport chain, fatty acid metabolism and amino acid metabolism (97).

In conclusion; multiple pathways involved in mitochondrial proteostasis are tightly controlled and balanced to maintain cellular homeostasis. Disruptions in any of these pathways lead to dysfunction in mitochondria. Malfunctioning in mitochondria can be sensed by other organelles and thus results in several metabolic diseases beyond mitochondrial-related ones.

1.4.2.3 Mitochondrial unfolded protein response (UPR^{mt})

Mitochondrial unfolded protein response (UPR^{mt}) is an adaptive stress response and conceptually similar to UPR^{ER}. UPR^{mt} has been reported 15 years ago in non-degradable misfolded protein overexpressed mammalian cells (98). Chemical inhibitors, disruption in OXPHOS activity, accumulation of unfolded proteins within mitochondria and genotoxic stress cause mitochondrial dysfunction. Mitochondrial dysfunction activates ensemble of genes and cellular activities related with UPR^{mt}. Reduction of mitochondrial membrane potential has been shown to induce UPR^{mt} (99). Since UPR^{mt} activates transcription of some set of genes required for cell homeostasis. UPR^{mt} is a retrograde signaling process and it requires a balanced communication network in between mitochondria and nucleus. Factors required for optimal UPRmt activation have been identified in *C. elegans* by using transcriptional reporter assays (100-103).However, mechanisms which regulate mammalian UPR^{mt} is more complicated and still need to be clarified.

Activating transcription factor associated with stress (ATFS-1) is the most studied transcription factor required for UPR^{mt} activation in warms (100). ATFS-1 has two localization signals, (i) a nuclear localization sequence (NLS; common to all bZIP transcription factors and (ii) N-terminal MTS. In basal/normal conditions, ATFS-1 is imported into mitochondria and degraded by the matrix-localized LONP1. If mitochondrial dysfunction occurs ATFS-1 directed to nucleus by NLS and activates transcription (104). Compartmentalization and import of ATFS-1 into mitochondria is important for its transcriptional activity and this suggest that its mitochondrial import is a key component for UPR^{mt} regulation. Since mitochondrial import machinery is crucial for mitochondrial proteostasis, it is clear that any perturbation in this machinery leads to UPR^{mt}. It has been shown that many mitochondrial proteins mislocalize to the cytosol when mitochondrial proteostasis and protein import are impaired in *S. cerevisiae.* These mislocalized proteins are very toxic and needed to be degraded immediately by cytosolic proteasomes (105, 106).

ATF5 is shown as mammalian orthologue of ATFS-1. ATF5 has high structural homology within bZIP domain to ATFS-1. ATF5 localizes both in nucleus and mitochondria in Bortezomib treated cultured mammalian cells. Several mitochondrial stressors such as paraquat, doxycycline and expression of mitochondrial protein ornithine transcarbamylase (OTC) lacking 84 amino acids rendering it unable to fold (ΔOTC) induce transcription UPR^{mt} related genes as an ATF5 dependent manner (107).

Transcriptional response activated by mitochondrial dysfunction share similarities in mammals and worms; however regulation is probably more complicated. In recent years, mammalian UPR^{mt} and its regulatory pathways became clearer. In mammalian, UPR^{mt} is regulated by three bZIP transcriptional factors, CHOP, ATF4 and ATF5 which are associated with ISR (55, 62).

CHOP and ATF4 are the shared transcription factors in UPR^{ER}, ISR and UPR^{mt}. As in CHOP and ATF4 activation, it has been shown that ATF5 also requires eIF2α phosphorylation. Besides ER stress sensor PERK, eIF2α can be phosphorylated by other three kinases responsive to diverse cellular stresses as it is discussed in section 1.3. Upon eIF2α phosphorylation, global protein synthesis reduces and preferentially mRNAs with ORF in their 5´ UTR are translated, such as those encoding CHOP, ATF4 and ATF5 (40, 108, 109). Several studies have shown that diverse forms of mitochondrial stress induce transcription of CHOP, ATF4 and ATF5 as well as genes involved in mitochondrial proteostasis and metabolic restoring (89, 110, 111). However, it is not clear how each these transcription factors is regulated to fulfill a specific mitochondrial stress response upon variety of stress conditions such as endoplasmic reticulum stress, amino acid depletion and viral infection,(40, 108, 112)

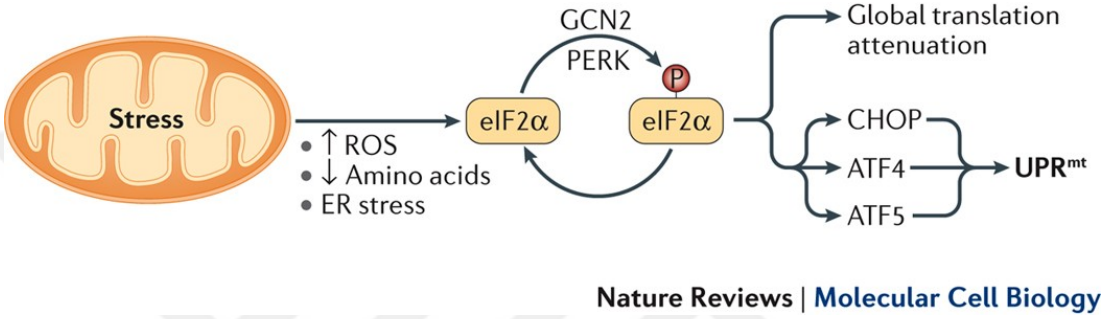

Figure 1. 5: Signaling the mammalian mitochondrial unfolded protein response.

Mitochondrial proteostasis is a complicated mechanism which needs perfect balance between translation of both nuclear- and mitochondrial- encoded mitochondrial proteins. There is a tight regulation in import, folding and degradation of those proteins into the mitochondria. Any disruption of one of these steps initiates a retrograde UPR^{mt} signaling in-between nucleus and mitochondria to activate the transcription of genes to regain organelle homeostasis. Several studies demonstrate that cells demand tightly regulated crosstalk and cooperation of these pathways to maintain healthy mitochondrial network.

During UPR^{mt}, mitochondrial import efficiency impairs and allows levels of ATFS-1 to rise in the cytosol. Elevated ATFS-1 translocates into nucleus and activates transcription of genes involved in mitochondrial import machinery (104). It has been reported that Tim17A subunit of TIM23 subunit is induced by stress regulated signaling. Translational attenuation after eif2α phosphorylation decreases Tim17A protein levels through activation of mitochondrial protease. Degradation of Tim17A by mitochondrial proteases attenuates TIM23 dependent mitochondrial protein import and initiates the increase of UPR^{mt} related proteostasis genes in *C. elegans* and mammalian cells (113). More recently, it has been demonstrated that lipid composition of mitochondrial membranes which surrounds the protein translocases in the mitochondrial import machinery changes upon early stage of UPR^{mt} (114).

Also defects in mitochondrial proteolytic system through mitochondrial proteases induce UPR^{mt}. LONP1 is induced by phosphorylation of eif2a through PERK-ATF4 arm of ISR (49). Several mitochondria stressors increase the transcription level of LONP1 as an ATF5 dependent manner (107). Ablation of LONP1 results in impaired ribosome function which causes a complete suppression of mitochondrial translation. Prolonged depletion of LONP1 causes aggregation of massive matrix proteins and initiates ISR (115). LONP1 has been shown to be the master regulator of degradation of unfolded, however it cannot remove aggregated proteins in mitochondrial matrix (116).To do this, LONP1 collaborates with mtHSP70 chaperoning system (117).

Besides LONP1, ClpXP also activates UPR^{mt} by degrading unfolded proteins in the mitochondrial matrix under several stress conditions in *C. elegans*. Then, small peptides produced by ClpXP are exported into cytoplasm by the HAF-1 transporter. It is proposed that peptides generated by the enzymatic activity of ClpXP induces the expression of mitochondrial chaperones and proteases by directing ATFS-1 into the nucleus to maintain mitochondrial quality control and restore proteostasis (100, 101). The role of ClpPX in UPR^{mt} is studied extensively in *C. elegans* and a similar pathway is likely to present in higher organisms.

Controlling the activities of mitochondrial chaperones and proteases in response to stress conditions maintains mitochondrial homeostasis. Sensing the changes in mitochondria and transferring this information to nucleus to activate related transcriptional machineries is crucial for cell fate.

1.5 Sphingolipids

Sphingolipids are ubiquitous structural components of eukaryotic cell membranes and preserve crucial roles in maintaining barrier function and fluidity (118).The neurochemist t J. L. W. Thudichum discovered them in brain extracts in the 1800s and named 'sphingosine' after Sphinx, a Greek mythical structure, due to their enigmatic chemical structure. Despite their long history, the roles sphingosine and its relatives in biology are beginning to be understood (119). Indeed, besides their roles in cellular membranes, they are now recognized as critical bioactive molecules that have key roles in regulation many physiological progresses.

1.5.1 Sphingolipid metabolism

The biochemical pathways involved in synthesis and degradation of sphingolipids are regulated by several enzymes and fluxes of different metabolites. Until now, around 40 enzymes related to sphingolipid metabolism in mammals have been identified (120). Alternative splice variants and post translational modifications can affect the activity of these enzymes and change the biological response in the cell.

Sphingolipid in mammalians are characterized by an amino-alcohol sphingosine backbone which contains 18 carbon atoms. Attachment of charged, neutral, phosphorylated, or glycosylated moieties to sphingosine backbone gives the structural diversity and complexity (121).

De novo sphingolipid pathway starts with the action of SPT enzyme in ER (122). SPT is the rate limiting enzyme of this pathway and catalyze condensation reaction of serine and palmitoyl coenzyme A (CoA) which forms 3-ketosphinganine (3-KDS). Mutations of SPT subunits (SPTLC1 and SPTLC2) change the substrate preference of enzyme from serine to alanine or glycine and lead to production of toxic deoxysphingolipids. Thus is the main cause of human hereditary sensory and autonomic neuropathy (HSAN1) disease (123). SPT activity is negatively regulated by ORMDL proteins to limit the level of sphingolipid intermediates (124). Produced 3-KDS by SPT then reduced by KDS reductase (KDSR) to sphinganine (dihydrosphingosine) that is then *N*-acylated by one of six ceramide synthases (CerS1–CerS6) (125). These CerS enzymes use specific acyl chains and forms dihydroceramides that are subsequently dehydrogenated to ceramides by dihydroceramide desaturase (DES) (126). Ceramide is produced at the cytosolic surface of the ER and transferred to *trans*-Golgi regions by ceramide transfer protein (CERT) via non vesicular mechanism (127) where it converted to sphingomyelin by sphingomyelin synthase (SM synthase) (128). Ceramide is also produced by sphingomyelinases (SMases) which hydrolyses sphingomyelin into phosphocholine and ceramide. Ceramide can be converted to glucosylceramide for the synthesis of higher glycosphingolipids in the cis-Golgi regions. Ceramide can be phosphorylated by ceramide kinase (CerK) into ceramide-1-phosphate (C1P) in trans-Golgi and plasma membrane which has crucial roles in cell survival and proliferation (121). Since ceramide is involved in all these

conversion pathways, it is considered as one of the central bioactive molecules in regulation of sphingolipid metabolism.

Ceramide catabolized by ceramidases causes deacylation of it and forms sphingosine. This is the only known pathway to generate sphingosine. Recycle between ceramide and sphingosine has a significant role in sphingolipid homeostasis (118). Sphingosine can be phosphorylated by sphingosine kinases (SPHK1 and SPHK2) as an ATP dependent manner to form sphingosine 1-phosphate (S1P). ER resident S1P specific phosphatases (SPPs) dephosphorylate S1P and generate sphingosine. On the other hand, S1P can be irreversibly degraded by sphingosine 1 phosphate lyase (SPL) to phosphoethanolamine and hexadecenal and this reaction named as the exit point of sphingolipid metabolism. The end products produced by SPL are subsequently reincorporated into glycerolipid metabolic pathways (129).

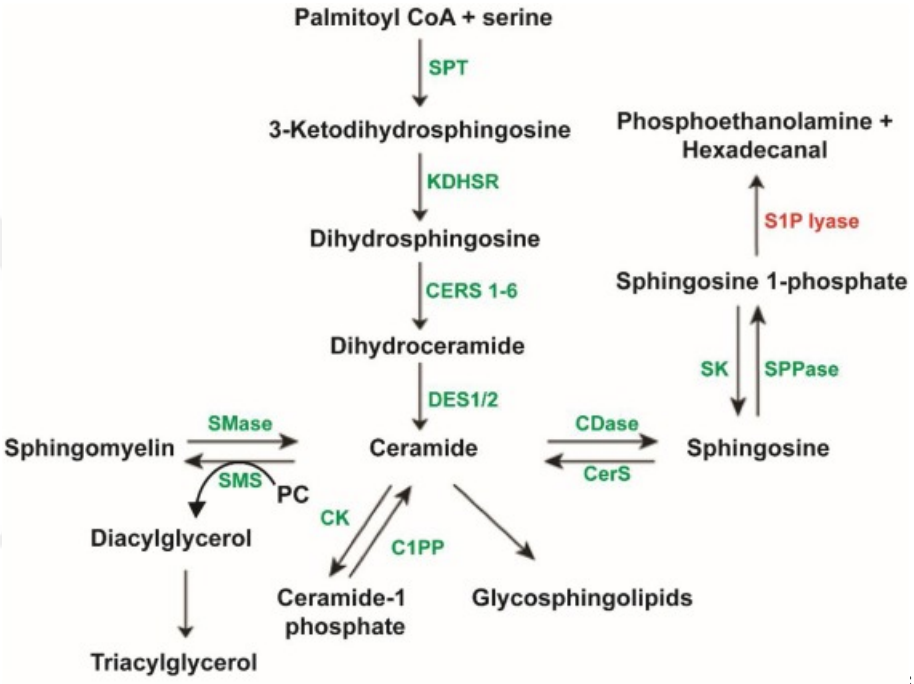

Figure 1. 6. Sphingolipids metabolism pathways, including the enzymes and molecules related to ceramides and S1P levels.

1.5.2 S1P metabolizing enzymes

As it mentioned before, there are several bioactive molecules through sphingolipid pathway including ceramide, C1P and S1P. Those bioactive molecules are involved in regulation of several cellular processes important for health and disease condition. S1P is one of the most important bioactive molecules in this pathway.S1P is a bioactive signaling molecule. The balance between production and degradation of S1P is crucial for cell fate determination. Besides, S1P also has roles in regulation of cell migration and vascularity such as cell motility and invasion, angiogenesis and vascular maturation. Diversity of pathways regulated by S1P makes its role more obvious in pathophysiological processes such as cancer, allergy, and atherosclerosis, evoking such diverse biological functions of S1P (130).

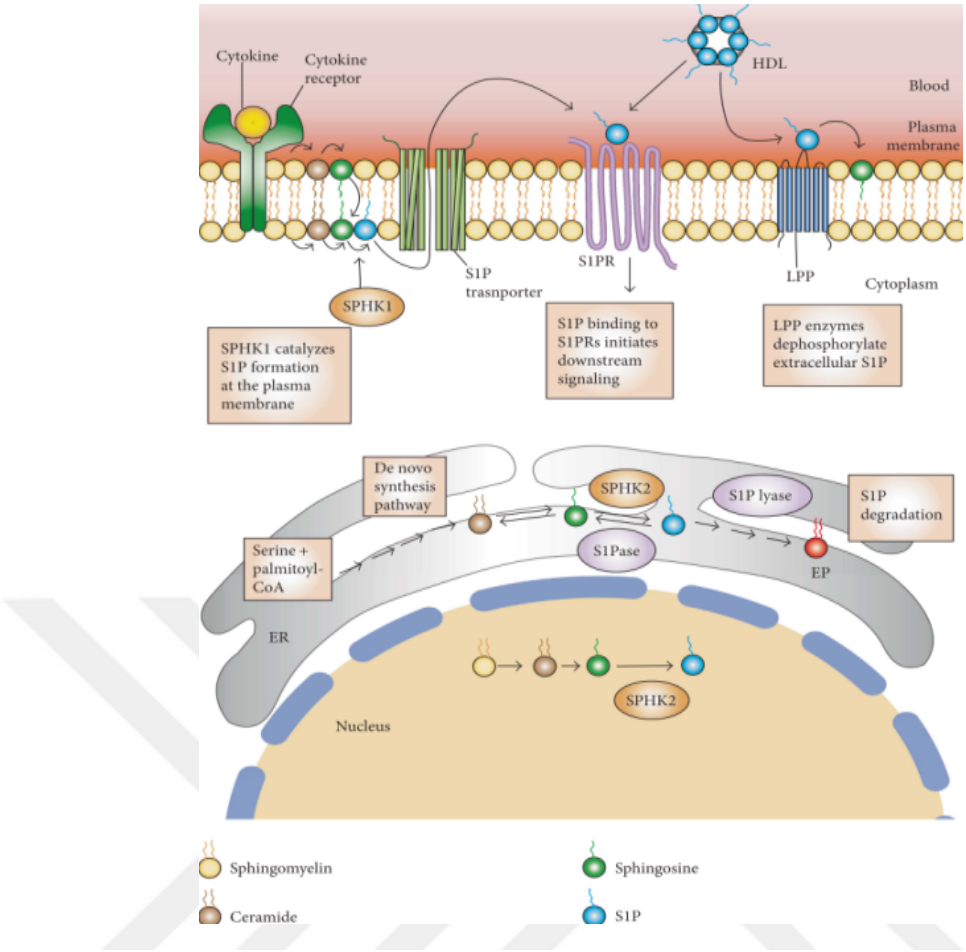

Figure 1. 7: S1P metabolism, synthesis, and inside-out signaling.

1.5.2.1 S1P receptors

S1P acts extracellularly through S1P specific cell surface receptors in an autocrine and/or paracrine manner. There are five S1P specific-G-protein-coupled receptors on cell surface, termed S1PR1–5. S1P receptors are composed of seven-transmembrane helix arranged in a structurally conserved form Each member of this family has different tissue-specific pattern. For example, S1PR1 activation generally promotes T cell egress, whereas S1PR5 is specifically expressed on the surface of natural killer T cells and mainly regulates the distribution of NK cells (131).

Since extracellular S1P binds to its receptors with high affinity to initiate its downstream signaling pathways, there have been concerted efforts to identify specific compounds with therapeutic potentials. The immunosuppressant FTY720 (fingolimod) was the first identified compound targets S1P receptors. FTY720 is a sphingosine analogue and can be phosphorylated by specific sphingosine kinases *in vivo* (132, 133). Phosphorylated FTY720 acts as S1P mimetic and agonist for all S1P receptors except S1PR2. Binding of FTY720-P to S1PR1 leads to its downregulation and subsequent degradation which prevents lymphocytes from sensing the S1P gradient. FTY720 also downregulates other S1PRs. Thus induces the retention of lymphocytes in lymphoid organs, termed lymphopenia (134). FTY720 is approved by the FDA and is used in the clinic for the treatment of multiple sclerosis (135).

1.5.2.2 Sphingosine Kinases

S1P is produced by two sphingosine kinase isozymes, SphK1 and SphK2, which phosphorylate sphingosine. They are expressed in human, mice, yeast and plants (136).

Dimerization properties and variety in subcellular localization of SPHKs maintain the diversity of SPHK functions. They are predominantly located in cytosol. In recent years, it has been clear that these isozymes can be found in different sub-compartments of the cell including plasma membrane, ER, mitochondria and nucleus to fulfill a variety of actions (137). There are numerous factors activate SPHK isozymes including growth factors, hormones, angiogenic factors, lipopolysaccharide, ligation of the IgE and IgG receptors (138).

SPHK1—SPHK1 function is more characterized in comparison to SPHK2. SPHK1 is predominantly found in cytosol. Phosphorylation of SPHK1 at serine 225 by extracellular signal-regulated kinase (ERK) causes SPHK1 translocation from the cytosol to the plasma membrane. Interaction of SPHK1 with other proteins induces its translocation to plasma membrane. For example, binding of SPHK1 to integrin-binding protein 1 in a calcium-dependent manner causes its translocation (139). Moreover, recently it has been shown that C1P also induces the translocation of SPHK1 to the plasma membrane without changing ERK signaling (140). S1P produced by SPHK1 at plasma membrane directly binds to tumor-necrosis factor (TNF) receptor-associated factor 2 (TRAF2) and induces phosphorylation of inhibitor of NFκB kinase (IKK). Thus results in degradation of inhibitor of NF-κB (IκB) and therefore activates NFκB signaling (141). S1P generated by SPHK1 also directly interacts with peroxisome proliferator-activated receptor γ (PPARγ) and induces the transcription of PPARγ target genes related to neo-angiogenesis (142).

SPHK2-- While SPHK1 localizes on cytosol and plasma membrane (under certain stimulus), SPHK2 is found in nucleus, ER and mitochondria. SPHK2 produces S1P by phosphorylating sphingosine. SPHK2, but not SPHK1, can also phosphorylates several cellular and synthetic lipids such as d,l-threo-dihydrosphingosine and phytosphingosine (143). Diversity of its substrates gives more advantage to SPHK2 to effect various downstream effectors. As it mentioned above, SPHK2 is the primary kinase responsible for FTY720 phosphorylation (132, 133).

SPHK2 commutes between cytosol and nucleus since it has a nuclear localization signal and a nuclear export signal (144). SPHK2 phosphorylation by PKC is induced by *Pseudomonas aeruginosa* infection in lung epithelium and drives its nuclear localization. This translocation enhances acetylation of histone H3 and H4, which are important for pro-inflammatory cytokines secretion (145). In addition, nuclear S1P generated by SPHK2 binds to and inhibits HDAC1 and HDAC2, resulting changes in gene expression (146). Moreover, FTY720 administered *wild type* mice shows higher histone acetylation and expression of genes related to learning and memory in comparison to *SphK2* $^{-/-}$ mice (147). Recently, it has been shown that *Sphk2* deletion regulates the expression of NADPH oxidase 4 (NOX4) gene and mediates nuclear ROS generation, HDAC1/2 oxidation, and chromatin remodeling (148)..SPHK2 found in mitochondria increases mitochondrial S1P levels. S1P interacts with prohibitin 2 (PHB2) in the mitochondrial inner membrane and regulates mitochondrial respiration through complex IV assembly (149). Intracellular S1P produced by activation of sphingosine kinases can be secreted by specific sphingolipid transporter, named protein spinster homolog 2 (SPNS2) or promiscuous ABC transporters (150).

1.5.2.3 Sphingosine 1 phosphate phosphatases

S1P produced by sphingosine kinases is reversible converted to sphingosine by S1P specific phosphatases (SGPPase) or by lipid phosphatases with a broader specifity (LPPs) (151). There are two SGPPases, SGPP1 and SGPP2, located in the ER and dephosphorylate S1P. SPPases regulates the flux of sphingolipids towards different metabolic pathways. SGPP1 has been shown to regulate ceramide levels in the ER. (152). *Sgpp1* deletion enhanced expression of proinflammatory cytokines and immune cell infiltration into the colon (153).

SGPP2 also located in the ER is implicated in cytokine mediated inflammatory responses. It has been shown that SGPP2 expression is controlled by NFκB. Deletion of *Sgpp2* in

endothelial cells results in significant reduction of TNF-α-induced proinflammatory cytokine production(154). *Sgpp2* deletion profoundly reduced extran sodium sulfate (DSS)–induced colitis severity. This suggests that SGPP2 expression contributes to the pathogenesis of colitis by promoting disruption of the mucosal barrier function (153).

1.5.3 Sphingosine 1-Phosphate Lyase

Dephosphorylation of S1P by SGPPs convert S1P to sphingosine and reduces the cellular S1P levels. S1P is degraded by Sphingosine 1- Phosphate lyase (SPL). SPL is encoded by *Sgpl1* gene in mammalians and catalyzes the irreversible cleavage of S1P to produce a long-chain aldehyde, Δ2-hexadecenal (Δ2-HDE), and ethanolamine phosphate (EP). Since this is an irreversible reaction, SPL is accepted as the exit point of sphingosine metabolism. SPL is necessary for a dynamic balance between ceramide and S1P which influences cellular outcome in response to stress.

SPL is an ER resident enzyme and located on the ER membrane. It is a pyridoxal 5′-phosphate (PLP)-dependent enzyme and its catalytic site faces to the cytosol (129). Since sphingolipids are evolutionary conserved, the first Sgpl1 gene, dpl1, is found from a genetic screen for sphingosine resistance in *S. cerevisiae*. This study is followed by recognition of many biological functions SPL which is now clear to be encoded by a single gene in every genome. Besides significant increase in sphingosine related metabolites, *dpl1*Δ was resistant to heat shock and nutrient deprivation suggesting a protective role of DPL1 (155, 156).

Global disruption of *Sgpl1* causes early lethality. *Sgpl1* KO mice accumulate a variety of lipid metabolites including sphingolipids, triglycerides, and cholesteryl esters (157). Since *Sgpl1* deficiency involves in lymphopenia, thymic atrophy, neutrophilia, anemia, nephrosis (excessive protein loss in the urine), *Sgpl1* KO mice exhibits severe pathological disorders (157-159). Conditional *Sgpl1* KO mice live much longer and allow much deeper investigation of SPL function. Intestinal epithelium-specific *Sgpl1* KO *(*$Sgpl1^{Gut}$KO*)* mice exhibits increased colon shortening, cytokine levels, S1P accumulation in comparison to control mice. The level of circulating and colon specific cytokines are higher in azoxymethane/dextran sodium sulfate (AOM/DSS) treated $Sgpl1^{Gut}$KO mice in comparison to control mice. $Sgpl1^{Gut}$KO promotes susceptibility to AOM/DSS-induced colitis-associated cancer, tumor formation, and crypt cell proliferation (160). Also conditional loss of neural specific *Sgpl1* shows grater sphingolipid accumulation in mice brain and exhibit spatial learning and motor function deficiencies via an ubiquitin- proteasome mediated mechanism (161).

Partial loss of SPL activity also affects its immune functions. FTY720 treatment inhibits SPL activity without effecting its gene expression and protein levels *in vitro* and *in vivo*. This suggests SPL may be a potential target for immunomodulatory therapy. Also, chemical inhibition of SPL by the food colorant 2-acetyl-4-(tetrahydroxybutyl) imidazole (THI) blocks lymphocyte egress from the thymus and secondary lymphoid organs. These data indicate SPL has specific roles in mediating immunomodulatory responses (162).

Localization of SPL--Mammalian SPL primarily localizes at the ER membrane. Biochemical characterization and structural remodeling approaches show that SPL has transmembrane segment close to the N-terminus. The catalytic domain of SPL enzyme faces the cytosol which allows SPL to catalyze S1P through its active site (163). 20- amino acid stretch in SPL ,amino acids 344–364, contains several conserved lysine residues and these residues are important for pyridoxal 5′-phosphate binding (164). SPL in protozoan parasite *Trypanosoma brucei* (TbSpl) also has been shown to be located on mitochondria. Depletion of TBSpl has no alteration in mitochondrial structure or mitochondrial membrane potential. Whereas, ablation in TbSpl causes aggregation of acidocalcisomes (165).Also LegS2 (the *Legionella* homolog of eukaryotic SPL) has been found at the host cell mitochondria, rather than the ER (166). These results allow speculating that EP produced by SPL in mitochondria could contribute the formation of phosphatidylethanolamine which is enriched in the mitochondrial inner

membrane. More recently, nuclear localization of SPL has been identified. Δ2-HDE produced by nuclear SPL in the nucleus acts as a modulator of HDAC activity and histone acetylation in lung epithelial cells (167). These varieties of SPL localization in cells raise interesting questions regarding the potential participation of SPL functions in unique mechanisms.

1.5.5 Regulation of ER stress by sphingolipids

Since *de novo* sphingolipid synthetic pathway starts in ER, ER is a central hub for sphingolipids. There are bi-directional mechanisms between UPR and sphingolipids and thus is related with a diverse range of diseases such as cancer, diabetes and liver disease.

Regulation of ER stress by sphingolipids – ER stress is not only activated by accumulation of unfolded/misfolded protein in ER lumen but also changes in cellular lipid composition can induce ER stress. Sphingolipids contain N-linked, long chain, unsaturated acyl chains and it is known that they can also change membrane properties. Studies have been shown that exposure of fatty acids such as palmitate (PA), a building block in sphingolipid synthesis, can activate UPR via alteration of membrane lipid composition which affects protein trafficking from the ER to the Golgi and results in UPR^{ER}. Also altering the activity of sphingolipid metabolism related-enzyme via depletion or activation induces UPR activation by changing cellular level of main sphingolipid species.

The link between sphingolipids and ER stress has also been observed in many different tissues both *in vitro* and *in vivo*. Genetically and pharmacologically inhibition of SPHK2 has been found to induce UPR activation in myeloma cells. Bortezomib, a proteasome inhibitor, induces ER stress and SPHK2 inhibition synergistically enhances the effect of bortezomib, as evidence induction of apoptotic cell death via IRE1 activation and its downstream kinases related to apoptosis such as JNK and p38MAPK (168). It has been shown that deficiency of SPHK1 alleviates drug induced acute liver failure by decreasing ER stress and impairing the transcription of inflammatory genes in hepatocytes. *Sphk1*$^{-/-}$ mice exhibited reduced IRE1 and PERK- eIF2α activation upon Acetaminophen (APAP) administration, a drug which causes induced liver injury (169). These mice exhibited reduced hepatotoxicity and much higher survival rate than WT littermates treated with APAP. Mice lacking *Sgpp2* gene have increased level of ER stress associated chaperones within their β-cells upon high fat diet administration. These cells exhibit less proliferative behavior upon the exposure to β-cell toxin Streptozotocin. However, the link between low proliferation rate in *Sgpp2* deficient mice and ER stress needs to be investigated in more detail (170).

1.5.5.1 Regulation of Sphingolipids by ER stress

Even though research mainly focuses on the effect of sphingolipid metabolism on UPR activation, there are number of studies that show this is a bi-directional regulation and activation of the ER stress is in turn able to affect sphingolipid metabolism.

In insulinoma cells, the activation of UPR by dithiothreitol (DTT) induces ceramide levels due to increase CerS6 expression (171). In another study also using insulinoma cells, activation of UPR by Thapsigargin (TG), an ER toxin, increases in neutral sphingomyelinase levels and as a result of this, cellular sphingomyelin and ceramide levels increased. In same study, it has been shown that inhibition of sphingomyelinase promotes cell death by increasing level of apoptotic sphingolipid species upon ER stress. In human keratinocytes, TG- induced ER stress exhibits elevated cellular ceramide, sphingosine and S1P. Thus results in increased level of cathelicidin antimicrobial peptide (CAMP) which is a player of innate immunity response to external pathogen infection. In parallel to this, induction of CAMP by TG is blocked in *Sphk1*$^{-/-}$mice. Increased S1P levels in response to ER stress specifically interacts with UPR related chaperones such as HSP90 andGRP94. S1P- chaperone units form a complex with IRE1 and TRAF2, stimulates of CAMP production through to NF-KB activation (172).

Administration of Tunicamycin (TUN),another ER toxin, to mice induces expression of both ER stress related genes and also sphingolipid related genes such as CerS3, Sphk2, Acer2 and Acer3 in *WT* mice and also elevates protein level of SPHK2. However, hepatic *Sphk2* gene expression is found to be down regulated in liver of mice fed with HFD compared to control mice. In the same study, it has been exhibited that Sphk2 expression is transcriptionally regulated by ATF4. ATF4 mediated Sphk2 upregulation in response to inflammatory ER stress leads to reduction of lipid droplets by increased fatty acid oxidation and shows improved insulin signaling under pathophysiological condition (173). Cell death driven by ER stress is one of the main reasons in progression of type 1 diabetes (T1D) development, a chronic autoimmune disease, since chronic ER stress results in dysfunction of β-cells. ER stress induces activation of the Ca^{2+}-independent phospholipase A2 beta (iPLA2β). ER stress induced iPLA2β activation promotes generation of pro-apoptotic sphingolipids such as ceramides and decrease pro-survival ones in β-cells (174).

Addressing the question how UPR and sphingolipid metabolism influence each other is important for understanding the mechanisms underlying disease progression and to develop preventing approaches.

1.5.5 Sphingolipids in mitochondria

Since sphingolipids have been related to metabolic disease progression, it is not surprising that they have also serious implication in mitochondrial homeostasis. Especially effects of ceramide and S1P on mitochondrial dynamics have been intensively studied.

Degradation of cytoplasmic components in lysosome is a conserved catabolic process in the cells and termed as 'autophagy'. 'Mitophagy' is an organelle specific autophagy which targets mitochondrial membranes to autophagosomes for degradation of superfluous and damaged mitochondria. Ceramide produced by CerS1 locates on OMM and binds to hydrophilic residues of an adaptor protein, microtubule-associated protein 1A/1B-light chain 3 II (LC3B-II). This lipid –protein interaction between LC3B-II and ceramide suggests a novel role for ceramide as an anchoring molecule for autophagosomes, leading to mitophagy in head and neck squamous cell carcinoma (175).

S1P is also implicated to have important functions in mitochondrial pathways. S1P-produced by mitochondrial SPHK2 binds to prohibitin 2 (PHB2), a mitochondrial inner membrane protein. Interaction between S1P and PHB2 is important for respiratory chain complex assembly and mitochondrial respiration (149). Moreover, inhibition of SPHKs by inhibitor results in reduces S1P and leads to decreased protein level of mitochondrial dynamin-like GTPase (OPA1) and mitofusin 1 (MFN1), which are regulatory factors in mitochondrial fusion and fission (176). S1P produced by SPHK1 has been shown to regulate UPR^{mt} activation in *C. elegans*. SPHK1 localization on mitochondrial results in subsequent induction of S1P levels which leads to elevated level of UPR^{mt}-related gene transcription. In the same study, it has been shown that RNAi-targeted knock down of SPL leads to UPR^{mt} upon mitochondrial stress (177). SPL is mainly found in ER membranes. Recently, mitochondrial localization of SPL has been shown in *Trypanosoma brucei.* Depletion of SLP has no effect on mitochondrial morphology however it results in acidocalcisomes aggregation (165). Indeed, SPL is mainly found in ER membranes. Recently, mitochondrial localization of SPL has been shown in Trypanosoma brucei. There are other studies which speculate SPL is found on MAMs. All these evidences suggest that S1P produced by SPL is critical for mitochondrial bioenergetics. SPL deficiency leads to reduction in total mitochondrial volume. Also, in same the same study, protein of oxidative phosphorylation components also reduced when SPL is deficient.

1.6 ER stress- associated inflammation and metabolic disease

Since stress is associated with cellular abnormalities, cellular hemostasis is sustained by initiation of multifactorial and independent transcriptional and signaling pathways through

UPR and ISR to resolve the stress signal. Thus mainly serves to control tissue damage and aim to repair tissues. However, under certain conditions, ER stress activates multiple proinflammatory responses and eventually lead to cell death through activation of several pro-apoptotic pathways. Consequently, ER stress has been implicated in chronic disease such as atherosclerosis, vasculitis and diabetes (22, 27).

ER stress-related inflammation results in production of many proinflammatory molecules. ER resident ER stress sensors, IRE1, PERK and ATF6, mediate proinflammatory transcriptional programs by transcription factors such as NF-κB and AP-1 which are the central players in proinflammatory pathways. Under non-stress conditions, NF-κB activation is prevented by its inhibitors, IκB proteins, in cytoplasm and its nuclear translocation is inhibited. Different branch of mammalian UPR activates NF-κB pathways by activating different machinery. For example, IRE1 branch of UPR initiates degradation of IkB by activating IκB kinase (IκK). Degradation of IκB frees NF-κB and activates NF-κB related proinflammatory gene transcription. On the other hand, PERK-eif2α arm activates global translational attenuation and causes decreased level of IKB protein. Translational inhibition of IκB by PERK-eif2α arm results in accumulation of free NF-κB to translocate into nucleus and consequently leads to initiation proinflammatory gene transcription controlled by NF-κB. Recruitment of NF-κB into nucleus leads to transcription of IL-1β and NLRP3 proteins, crucial molecules for inflammatory response (178).

Pattern recognition receptors (PRRs) are expressed in immune cells such as macrophages and dendritic cells as wells as in epithelial cells. PRRs can recognize pathogen associated molecular patterns (PAMPs) upon infection and damage associated molecular patterns (DAMPs) upon cell damage. Thus leads to assembly and activation of cytoplasmic complexes called as 'inflammasomes' (179). Inflammasomes are multimeric protein complexes and have fundamental differences depends on stress stimuli. Based on different core PRRs, inflammasomes are divided into 5 different subtypes: NLRP1, NLRP3, NLRC4, Pyrin, and Absent in Melanoma 2 (AIM2). Upon activation of cell surface receptors that are transfer stress stimuli into the cell, inflammasome serves as a scaffold to recruit inflammasome related components such as PRRs, the adaptor protein called ASC (Apoptosis-associated speck-like protein containing a CARD), and the effector protein, pro-caspase-1. Oligomerization of inactive zymogen pro-caspase protein within the other proteins in inflammasome leads to autoproteolytic cleavage into active caspase1. Active caspase-1 act as a cysteine dependent protease and cleaves the precursor of cytokines such as Il1beta and IL-18 respectively, generating active form of these proinflammatory cytokines (179, 180).

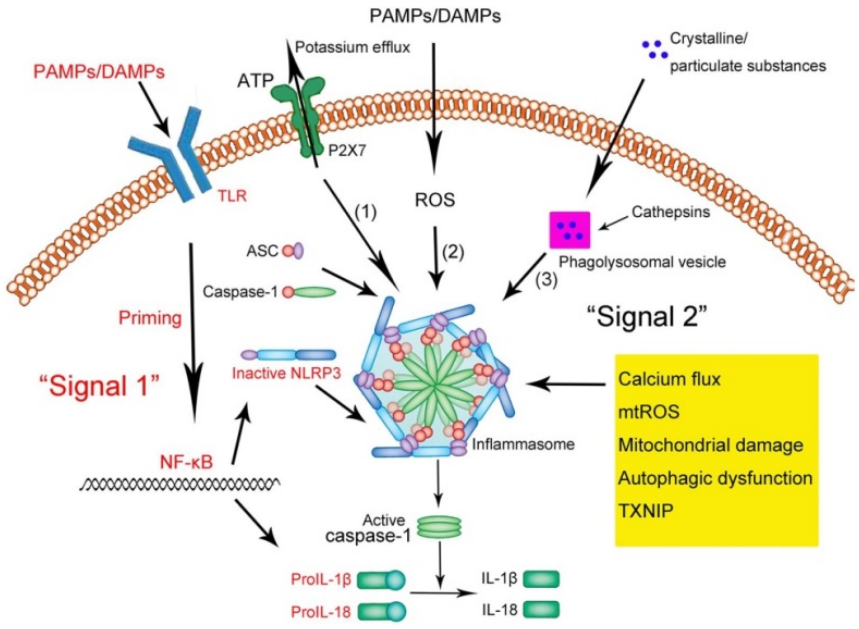

Figure 1. 8: Schematic illustration of the NLRP3 inflammasome activation.

In several disease pathogenesis, ER stress has been shown to provoke inflammatory response through NLRP3 activation. ER stress sensor IRE1 has been shown to induce Thioredoxin – interacting protein (TXNIP) by degrading pre-miR17, which is an inhibitor of TXNIP expression. In turn, elevated level of TXINP protein activates NLRP3 inflammasome, elevating proinflammatory response through increased cleaved caspase-1 and mature IL-1β (181). In another study, it has been shown that IRE1 activation increases mitochondrial ROS levels and leads to NLRP3 association with mitochondria. Activation of IRE1-sXBP1 axis by lipid stress in lipopolysaccharide (LPS) - induced macrophage cells initiate NLRP3 inflammasome activation. Pharmacological inhibition of IRE1 RNase domain by 4μ8c leads to reduced lipid stress- induced mitochondrial ROS and inhibited NLRP3 inflammation activation. Effect of 4μ8c in NLRP3 inflammation inhibition consequently results in reduced transcription of proinflammatory cytokines such as IL-1β and CCL2 in lipid loaded macrophages. In the same study, reduced proinflammatory response by inhibition of IRE1 RNase domain led to a significant decreased in hyperlipidemia induced atherosclerosis plaque size without altering lipid profiles *in vivo* (33). As well as IRE1, inhibition of other ER stress sensor PERK decreases mitochondrial ROS and induces mitochondria-specific clearance pathways such as mitophagy. PERK inhibition leads to reduced lipid-induced inflammasome activation and pro-inflammatory cytokine secretion such as IL-1β and IL-18 through increased mitophagy. In same study, inhibition of PERK effectively reduces hyperlipidemia-induced inflammasome activation and prevents atherosclerosis progression (49)**.**

ER stress was demonstrated to have roles in endothelial cell inflammation in diabetes associated vascular disease. Increased in the demand for insulin leads to ER stress and causes inflammatory response in obesity –related disease onset. It has been demonstrated signal transducer and activator of transcription 3 (STAT3) is activated by ATF4 is responsible for vascular endothelial damage and inflammation in streptozotocin (STZ)-induced type 1 diabetes *in vivo*. Furthermore, STZ-induced proinflammatory gene expression and vascular permeability is ameliorated in *ATF4-/-*mice (182).

ER stress has been implicated in Kawasaki disease (KD). KD is an acute systemic vasculitis that occurs in young children (183-185). Although several factors such as environmental factors, pathogen infection and genetic background seem to be causative for KD progression, its etiology is still unknown. Patients with KD develop coronary artery aneurysms (CAA) which leads to sudden cardiac arrest ad hearth failure (186). KD patients can be treated with oral aspirin or TNF-α blockers, such as infliximab (IFX). Gold-standard treatment for KD patient is intravenous immunoglobulin (IVIG) that can block CAA formation however about 20% of patients is resistant to IVIG administration (184, 187). KD has been implicated with high level of mitochondrial ROS accumulation and proinflammatory cytokine production through NLRP3 inflammasome activation in myeloid cells infiltrating in inflamed vascular tissues (188-190). It has been shown that human coronary artery endothelial cell (HCAECs) exhibited elevated level of intracellular ROS and ER stress activation upon serum stimulation isolated from KD patients (191). ER stress markers also induced in *Lactobacillus casei* wall extract (LCWE)- induced KD rat model (192). However, which arm of UPR regulates inflammasome activation and proinflammatory cytokine secretion related to KD progression is unknown.

1.7 Hypothesis and study aims

Maintaining cellular protein homeostasis, proteostasis, requires tight control of protein synthesis, folding, proper subcellular localization and degradation. A complex and adaptive proteostasis is maintained by cooperatively functioning of organelle. Activation of unfolded

stress response in different organelles leads to activation of transcriptional pathways related to cellular homeostasis. Indeed, molecular chaperons in different classes and organelle-specific proteases are also crucial for balancing protein synthesis and degradation. Any disruption in cellular proteostasis leads to disease progression such as atherosclerosis, diabetes, neurodegenerative disorders. From this end, in this current study, I deciphered different roles of ER resident ER stress sensor IRE1 in different concepts.

In first part of my thesis, I sought to understand the stress signaling and transferring in between ER and mitochondria. ER and mitochondria associates through MAMs and disruption in one of these organelles can be sensed by the other. This bidirectional signaling network alters the function of both organelles **(4)**. Towards this goal, I first analyzed the impact of ER stress on UPR^{ER} and UPR^{mt} related gene expression by using ER stress toxins. Keeping in mind the effect of PERK arm of UPR^{ER} and UPR^{mt} through eIF2α phosphorylation, I would like to validate the effect of other UPR arm, IRE1, on mitochondrial proteostasis. To achieve this, I used either $IRE1^{-/-}$ MEF cells or specific IRE1 inhibitors targeting its enzymatic activities. I first analyzed the expression level of UPR^{ER} and UPR^{mt} related genes. Then I assessed the mitochondrial protein level of UPR^{mt} related proteases and chaperone under ER stress conditions.

IRE1 activation occurs by auto phosphorylation through its kinase domain and the only kinase target of IRE1 is itself. Recently, IRE1 interactome study has been reported. SPL, S1P degrading enzyme, is one of the candidates which may interact with IRE1. To validate this interaction, we performed immunoprecipitation assay. To further validate the relationship between IRE1-SPL, I performed *in vitro* and 'cell based' kinase assays and demonstrated potential phosphorylation of SPL by IRE1. I validated these phosphorylation sites on SPL by using phospho mass spectrometry.

SPL is an enzyme which degrades S1P and this reaction is referred as exit point of sphingolipid metabolic pathways **(162)**. I investigated the effect of ER stress on SPL activity by using fluorogenic SPL activity assay. Furthermore, I first used specific inhibitors of IRE1 and validated the changes in SPL activity upon ER stress. Alteration in SPL activity upon knocking down or inhibition has been reported to lead changes in sphingolipids in the cells. To test this, we measured level of sphingolipid derivatives when IRE1 is either inhibited or ablated under ER stress condition.

I sought to investigate the effect of SPL on UPR^{mt} by either inhibiting SPL by using its specific inhibitor THI or overexpressing SPL-WT in MEF cells. To connect effect of IRE1 on SPL under ER stress condition to mitochondrial proteostasis, I also validated the impact of SPL when it is mutant that prevents its phosphorylation by IRE1.

Since eIF2α phosphorylation is the common event shared by UPR^{ER} and UPR^{mt} through ISR, I sought to decipher the connection of IRE1-SPL axis with ISR. I analyzed ER stress induced ISR activation by (i) knocking down IRE1, (ii) inhibiting SPL by THI, (iii) overexpression SPL in WT MEF cells. Also, I tested ER stress induced UPR^{mt} related gene expression in PKR-, PERK- and eif2α phospho- deficient MEF cells when SPL is inhibited by using THI. To further confirm my hyphothesis, I also validated the effect of mutant SPL on UPR^{mt} in eif2α phospho- deficient MEF cells.

In the second part of my thesis, I sought to investigate the role of ER stress on KD progression. First, I analyzed publicly available human transcriptomics datasets obtained from whole blood of KD patients and determined the genes differentially expressed compared to healthy controls. Then, I analyzed the same genes in another transcriptomics dataset obtained from IVIG-treated KD patients in comparison to acute KD patients.

After validating differentially expressed ER stress signature genes in KD progression from human datasets, I also mimicked KD in murine model by injecting LCWE and assessed cell

specific expression level of these signature genes by analyzing single cell RNA sequencing data. Since inflammation is the driven source of abdominal aorta aneurysms in KD progression, I assessed the effect of IRE1 inhibition on LCWE-induced inflammation by using IRE1 specific inhibitors in mouse macrophages. I also tested LCWE –induced inflammation activation in macrophages isolated from myeloid restricted Ern1 knockout mice (*LysM*$^{Cre+}$*Ern1*$^{\Delta/\Delta}$).

In vivo, I investigated the consequences of IRE1 inhibition on LCWE-induced KD progression. I used LCWE-injected LysMCre+Ern1$^{\Delta/\Delta}$ mice to validate the impact of IRE1 and also I administered specific IRE1 RNase domain inhibitor to assess the effect of IRE1 RNase domain in KD progression. I assessed KD progression by (i) determining hearth vessel inflammation, (ii) measuring maximum diameter of aorta and (iii) measuring caspase-1 activity in hearth tissue.

In the third and last part of my thesis studies, I sought to investigate how different lipid types impact ER- membrane remodeling and its biological outcomes. To do this, I treated cells with either saturated or unsaturated fatty acids and examine their effect on activation of inflammatory pathways. To further investigate the mechanistic behind their actions, I sought to decipher the lipidomic remodeling of ER membranes in macrophages by high-resolution quantitative lipidomics. Since lipid composition of ER membranes is crucial for occurrence of UPR^{ER}, we validated the effect of different lipids on activation of IRE1 by using confocal imager.

Overall, in this study we aimed to understand the biological functions and behaviors of IRE1 arm of UPR^{ER} and how IRE1 maintains organelle proteostasis and cellular homeostasis under different pathological stress conditions.

Chapter 2

Materials and Methods

2.1 Materials

2.1.1 Reagents

General laboratory reagents and chemicals are listed in Table 2.1.

Table 1: Chemicals and reagents that are used in laboratory generally

Product	**Company**	**Catalog No.**
β-Mercaptoethanol	AppliChem	A1108,0100
Acrylamide %40 Solution (Acrylamidebisacrylamide)	Fisher scientific	BP1408-1
Amersham ECL Prime Western Blotting Detection Reagen	GE Healthcare	RPN2236
Amersham ECL Select Western Blotting Detection Reagen	GE Healthcare	RPN2232
Chloroform	Sigma –Aldrich	24216
Ethanol Absolute	Sigma –Aldrich	32221
Ethylenediaminetetraacetic Acid (EDTA)	Thermo Fisher Scientific	R1021
Formalin Solution 10 %	Sigma-Aldrich	HT501128-4L

Glycine	Glentham	GM2385
HEPES Buffer, 1M Stock in Normal Saline	Lonza	17-737F
Ampicillin Sodium Salt	Cayman	69-52-3
Fatty acid free BSA	GoldBio	A-421-10
DC Protein Assay Reagents	Biorad	5000116
NucleoBond Xtra Midi	Macherey Nagel	740410100
Page Ruler Prestained Protein Ladder	Thermo Fisher Scientific	26620
Protease Inhibitor Cocktail EDTA Free	Sigma	P8340-5ML
Phosphatase Inhibitor Cocktail 3	Sigma	P0044
PVDF Transfer Membrane	Pierce–Thermo Scientific	88518
Nitrocellulose Transfer Membrane	VWR	27377-000
Ponceau S solution	Sigma	P7170-1L
Roche LightCyler 480 SYBR Green Master Mix	Roche	4887352001
Tris Base	Sigma	T1503
Triton X-100	AppliChem	A1388,0500
Trisure	Bioline	Bio 38033
ProLong™ Gold Antifade Mountant with DAPI	Invitrogen	P36931
O.C.T. Compound	VWR	25608-930
HEPES Buffer, 1M Stock in Normal Saline	Lonza	17-757F
Methanol	Sigma-Aldrich	32213
Sodium orthovanadate	Sigma	S6508
PMSF	Ambresco	M145-5G
Ammonium Persulfate (APS)	Sigma	A3678
ATP-gamma-S, Kinase substrate	Abcam	ab138911
P-nitrobenzyl mesylate	Abcam	ab138910
N6-Fu-ATP-gS	Biolog Life Science	F008
ATP	Santa Cruz Biotechnology	sc-20240A

Digitonin	Sigma Aldrich	D141
Sucrose	Sigma	S0389
Protein G Magnetic Beads	Biorad	1614023

2.1.2 Cell Culture Reagents

Reagents used in cell culture are listed in Table 2.2.

Table 2: Reagents, chemicals and kits used in cell culture

Product	**Company**	**Catalog No**.
DMEM 4.5g/H Glucose w/U1	Lonza	BE12-604F/U1/12
RPMI	Gibco	21875091
BSA-Fatty Acid Free	Sigma	A7030-500G
Dulbecco's Phosphate Buffered Saline (dPBS)	Biowest	L0625
DMSO	Sigma	472301
Sodium pyruvate solution	Sigma-Aldrich	S8636
Neon™ Transfection System 100 µL Kit	Thermo Scientific	MPK10096
Fetal bovine serum (FBS)	Gibco	10270-106
Trypsin-Edta (0,25%) phenol red	Gibco/ Thermo Fisher	25200-056
Polyethylamine	PolySciences	33966
Penicillin-Streptomycin (10,000 U/mL)	Gibco	15-140-122
L-Glutamine (200 mM)	Gibco	25-030-081

2.1.3 Antibodies

Antibodies used in Immunofluorescence and Western blot are listed in Table 2.3**.**

Table 3: Antibodies used in all procedures

Western Blot Antibody	**Provider**	**Catalog Number**
IRE1 phospho-S724	Abcam	ab48187
IRE1α	Cell Signaling	3294

FLAG M2	Sigma	F1804
SGPL1	R&D System	AF5535
Thiophosphate ester antibody [51-8]	Abcam	ab133473
Mortalin/GRP75 (N52A/42)	Antibodies Incorporated	75-127
CLPP	Sigma	WH0008192M1 -100 UG
LONP1/Lon	Abcam	ab103809
PERK (C33E10)	Cell Signaling	3192S
Recombinant Anti-PKR (phospho T446)	Abcam	ab32036
PKR (B-10)	Santa Cruz Biotecnolog	sc-6282
eIF2 alpha (phospho Ser51)	GeneTex	GTX24837
eIF2α	Cell Signaling	9722
Anti-SQSTM1 / p62 antibody	Abcam	ab56416
Parkin (Prk8)	Cell Signaling	4211
Anti-IL-1 beta antibody	Abcam	9722
Anti-pro Caspase1	Abcam	179515
ERp57	Santa Cruz	sc-23886
β-Actin	Santa Cruz	sc-47778
normal Rabbit IgG	Cell Signaling	2729S
normal mouse IgG	Santa Cruz Biotecnology	sc-2025;
Secondary Antibodies		
Anti-Mouse -HRP	Seracare Life Sciences Inc.	5450-0011
Anti-Rabbit-HRP	Seracare Life Sciences Inc.	5220- 0337
Mouse Anti-Goat IgG-HRP	Santa Cruz	sc-2354

2.1.4 Study Specific Reagents and Kits

Study specific chemicals, reagents and kits are listed in table 2.4.

Table 4: Study Specific Reagents, Chemicals and Kits

Product	**Company**	**Catalog No.**

IRE1 kinase inhibitor, KIRA6	Cayman	19151
IRE1 kinase inhibitor, AMG 18 hydrochloride	Tocris	6166
IRE1 RNase inhibitor, 4μ8c	Calbiochem	412512
SPL inhibitor (2-Acetyl-5-tetrahydroxybutyl Imidazole, THI	Cayman	13222
SPL Fluorogenic Substrate	Cayman	13238
PERK Inhibitor I	Calbiochem	516535
Thapsigargin	Santa Cruz Biotecnology	sc-24017,
Tunicamycin	Santa Cruz Biotecnology	sc-3506
PKR Inhibitor	Santa Cruz Biotecnology	sc-204200
Doxycycline monohydrate	Sigma	D1822
IRE1 siRNA	Qiagen	SI00605248
SGPL1 siRNA	Qiagen	SI00057631
scrambled siRNA	Qiagen	1027281;
MitoTracker Red CMXRos kit	Invitrogen Thermo Scientific	M7512
Rhod-2, AM, cell permeant	Thermo Scienific	R1244
Lactobacillus casei	ATCC	11578
Hematoxylin and Eosin Stain Kit	Vector Labs	H-3502
V-PLEX Mouse IL-1β Kit	Meso Scale Diagnostics	K152QPD-1
Palmitoleic acid	Sigma	76169
Palmitic acid	Sigma	P0500
FAM-FLICATM Caspase-1 Assay kit	Immunochemistry Technologies	98

2.1.5 Solutions

Solutions used in this study are listed in table 2.5.

Table 5: Solutions used in this study

Solution	**Ingredient**
Phospho Lysis Buffer (PLB)	50 mM HEPES (pH: 7.9)

	100 mM NaCl 4 mM Na4P2O7 10 mM EDTA 10 mM NaF 1% Triton Just prior using add: 2 mM Sodium orthovanadate (Na3VO4) 1 mM phenylmethanesulfonylfluoride (PMSF) 1X Phosphatase Inhibitor Cocktail 3 (100X) 1X Protease Inhibitor Cocktail (100X)
Homogenizing buffer (for mitochondria isolation)	250 mM sucrose 1 mM EDTA 10 mM HEPES; pH 7.4
Kinase buffer (KB);	20 mM HEPES pH 7.4, 50 mM KoAC 1 mM MnCL2 1 mM MgCl2 1 mM Na2Mao4 2 mM NaF
5X SDS Loading Dye	10% SDS 50% glycerol 25% 2-mercaptoethanol 0.02% bromophenol blue 0.3125 M Tris HCl, pH: 6,8
0.5 M Tris-HCl (pH: 6.8)	12 g Tris Base is dissolved in 60 ml ddH2O pH is adjusted to 6.8 with 1 N HCl Complete to 100ml with ddH2O. It is stored at 4 °C
1.5 M Tris-HCl (pH: 8.8)	54.45 g Tris Base (Trizma) is dissolved in 150 ml ddH2O, pH is adjusted to 8.8 with 1 N HCl and complete volume to 300 ml with ddH2O. It is stored at 4 °C.
10% Resolving Gel	2,5 ml 40% Acrylamide mix

	2,5 ml 1.5 M Tris-HCl (pH: 8.8) 100 ul 10% SDS 100 ul 10% Ammonium persulfate ;4 ul 0.08% TEMED Complete to 10 ml with ddH2O
12% Resolving Gel	3 ml 40% Acrylamide mix 2,5 ml 1.5 M Tris-HCl (pH: 8.8) 100 ul 10% SDS 100 ul 10% Ammonium persulfate ;4 ul 0.08% TEMED Complete to 10 ml with ddH2O
5 % Stacking Gel	620 ul 40% Acrylamide mix 630 ul 0.5 mM Tris-HCl (pH: 6.8) 50 ul 10% SDS 50 ul 20% Ammonium persulfate ; 5 ul 0.1% TEMED Complete to 5 ml with ddH2O
10X SDS Running Buffer	30g Tris-Base 144g Glycine 10gr SDS Complete volume to 1L with ddH2O
10X Transfer Buffer	30g Tris-Base 144g Glycine Complete volume to 1L with ddH2O
10X TBS	1,5 M NaCl 100 mM Trizma Base adjust pH 7,8 with 1N HCl complete volume to 1L with ddH_2O
1X TBS-T	900 ml ddH2O 100 ml 10x TBS 1 ml Tween
10X PBS	80 g NaCl

	2 g KCl 15,2 g Na2HPO4.2H2O adjust to 1L dH2O, pH to 7,4

2.1.6 Plasmids

Plasmid encoding SPLyase (HsCD00378787) was purchased from Harvard plasmid bank and FLAG-CMV14 was purchased from Addgene.

IRE_WT, IRE_KD and IRE1_ASKA and pcDNA5-IRE1-3F6HGFP-frt plasmids were a kind gift from Dr. Peter Walter (University of California, San Francisco).

2.1.7 Cell lines and Their Growth Conditions

Mouse embryonic fibroblasts (MEFs) from Wild type (WT), IRE1$^{-/-}$, PERK$^{-/-}$, and PKR$^{-/-}$ mice were a kind gift from Dr. Gokhan Hotamisligil (Harvard University, T.H. Chan School of Public Health, Boston). MEFs from eif2 S/S (WT) and eif2 A/A (phospho mutant) mice were a kind gift from from Dr. Mauro Costa Mattioli, (Baylor College of Medicine, Houston)

HEK293T cells were purchased from ATCC.

Bone marrow derived macrophages (BMDM) isolated from mice used in this study.

IRE1-3F6HGFP stable HEK293T cell lines were made with pcDNA5-IRE1-3F6HGFP-frt.

2.1.8 Transgenic Mice Used

Apoe^{tm1Unc} (*Apoe*$^{-/-}$) mice were obtained from Jackson Laboratory (Bar Harbor, ME) and used in UPR^{mt} studies.

C57BL/6 wild type (WT) mice and *LysM*^{cre} (004781) mice were obtained from Jackson laboratory (Bar Harbor, ME). IRE1 conditional knock out (*Ern1*$^{fl/fl}$) mice were a kind gift from Dr. Takao Iwawaki (Kanazawa Medical University, Japan) and characterized previously (193). *Ern1*$^{fl/fl}$ mice were crossed from with LysMcre mice to generate myeloid-specific IRE1 gene deletion (*LysMCre*+ *Ern1*$^{\Delta/\Delta}$). WT, *Ern1*$^{fl/fl}$ and *LysMCre*+ *Ern1*$^{\Delta/\Delta}$ mice were used for isolation of BMDM and in LCWE-induced KD studies.

2.1.9 Diet Used in UPR^{mt} studies

Western Type Diet (Catalog: TD.88137 #E15721); high cholesterol/high fat (0.21% cholesterol and 21% butter fat) was purchased from Ssniff Spezialdiaten, Germany.

2.2 Methods

2.2.1 Cell Culture and Treatments

MEF and HEK293 cells were cultured in DMEM medium containing 10% FBS and 1% L-Glutamine in a humidified, 5% CO2 at 37°C incubator. Cells were treated with indicated inhibitors for indicated times and collected for further analysis.

BMDM isolation Mouse femur and tibiae were dissected and cleaned out from surrounding tissues and kepst in sterile PBS. Bone marrows were flushed with 23G needle with RMPI and collected into RPMI supplemented with 1% Penicillin/streptomycin (P/S). Collected bone marrows passed through a cell strainer (BD, 352350) and centrifuged at 400 x g for 5 minutes

at 4°C. Pelleted cells were cultured in RPMI1640 medium containing 1% Penicillin/streptomycin (P/S) cocktail with 15% L929 conditioned medium and 10% FBS in a humidified, 5% CO^2 at 37°C incubator until differentiation into macrophages for 7 days.

Inflammasome activation Differentiated BMDM cells were pretreated with indicated concentration of IRE1 inhibitors for 1 hour and the stimulated with indicated concentration of LCWE for 16 hours for Kawasaki Disease studies.

Inflammasome activation Differentiated BMDM cells were pretreated with PAO (1000 μM/ml) for 1 hour then stimulated with 200 ng/ml ultrapure Lipopolysaccharide (LPS) for 3 hours. Then cells were treated with palmitate- BSA (1000 μM/ml). for 20 hours.

2.2.2 Plasmid Transfection and siRNA Electrophorations

Transfection of indicated plasmids was performed when MEF and HEK293 reached 60–80% confluency. 2ug DNA was used for every $4.5x10^5$ and PEI was used in 1:3 ratios. HEK293 cells were electroporated with 50 nM siRNA against *IRE1* (SI00605248; Qiagen), 50 nM siRNA against *SGPL1* (SI00057631; Qiagen) or scrambled siRNA (1027281; Qiagen) for 48h prior to treatments. Neon Electroporator (Invitrogen, MPK10096) was used according to the manufacturer's protocol.

2.2.3 Western Blot Analysis

Cells were lysed by using phospho-lysis buffer (PLB) (50 mM HEPES (pH 7.9), 100 mM sodium chloride, 10 mM EDTA, 10 mM sodium fluoride, 4 mM tetrasodium diphosphate, 1% Triton X-100, 2 mM sodium orthovanadate, 1 mM PMSF (phenylmethylsulfonyl), 1× phosphatase inhibitor mixture, 1× protease inhibitor mixture). Lysates were cleared from cellular debris by centrifugation and protein concentrations were measured DC assay (Biorad). Equalized lysates were boiled with 5X sodium dodecyl sulphate (SDS) loading dye and proteins were subjected to SDS/PAGE separation. For the detection of inflammatory cytokine (IL1-β and caspase-1) in the cell medium, Cell culture supernatants were collected and centrifuged to clear from cell debris. Supernatants were boiled with 5X SDS loading buffer for 5 minutes at 95°C and subjected to SDS/PAGE separation. Separated proteins were transferred to PVDF membrane and membranes were blocked with 5% milk. Blocked membranes incubated with primary and secondary antibodies prepared in in Tris-buffered saline (TBS) containing 0.1% (vol/vol) Tween-20 and 1% (wt/vol) dry milk or BSA. Membranes were developed with ECL (Amersham™) and analyzed using the BioRAD chemiluminescence imager.

2.2.4 Immunoprecipitation

Protein G Magnetic Beads (1614023; Bio-Rad) were first blocked by incubating in 2% fatty acid free BSA (A-421-10; GoldBio) on a rotator and conjugated with indicated antibodies overnight at 4°C. Conjugated beads were washed with PLB 3 times. Antibody conjugated-beads were incubated with lysates obtained from either HEK293T cell lysate or Abdominal aortas from vehicle of LCWE injected C57BL6 mice overnight on a rotator. Antibody-cell lysates conjugated beads were washed with PLB and boiled upon adding 5X SDS loading buffer for 5 minutes at 95°C. Proteins were then subjected to SDS/PAGE separation and fallowing experimental procedures.

2.2.5 In vitro and cell based kinase assays

In vitro kinase assay - Antibody-cell lysates conjugated beads were washed with PLB buffer three times and kinase buffer (KB; 20 mM HEPES pH 7.4, 50 mM KoAC, 1 mM MnCL2, 1

mM MgCl2, 1 mM Na2Mao4, 2 mM NaF) once, followed by incubation in KB containing ATP-gamma-S for 30 minutes at 30°C. EDTA was used to stop reaction. P-nitrobenzyl mesylate (PNBM) was added and incubated for 45 minutes at 25°C to generate thiophosphate esters on the thiophosphorylated substrates in the in vitro kinase assay, as previously described (194). Antibody-cell lysates conjugated beads were washed with PLB and boiled upon adding 5X SDS loading buffer for 5 minutes at 95°C. Proteins were then subjected to SDS/PAGE separation and fallowing experimental procedures.

Cell based kinase assay – HEK293T cells were transfected with indicated plasmids and were treated with 300nM TG treatment for 1 hour. Cells were collected, washed with PBS and centrifuged at 1000 rpm for 5 mins. Cell pellets were incubated with KB containing 30 µg/ml digitonin and rotated for 10 minutes at 30°C and then centrifuged. Cell pellets were incubated with KB containing 250 µM N6-Fu-ATP-gS 100 uM ATP and 1 mM GTP for 1 hour at 30°C. PLB containing 20 mM EDTA was used to stop kinase reaction. Cells were lysed by quick vortexing (5 second intervals) for 10 minutes and centrifuged at highest speed for 15 minutes. PNBM (12.5 mM, (final concentration) was added to the supernatants. Supernatants were filtered with PD-10 columns and washed with PLB to get rid of PNBM. Eluted supernatants were incubated antibody-conjugated beads and rotated at 4°C overnight. Antibody-cell lysates conjugated beads were washed with PLB and boiled upon adding 5X SDS loading buffer for 5 minutes at 95°C. Proteins were then subjected to SDS/PAGE separation and fallowing experimental procedures.

2.2.6 RNA Isolation and qRT-PCR

Total RNA from cells was isolated by using Trisure (Bioline) and RevertAid First Strand cDNA Synthesis Kit (Thermo Scientific) was used for reverse-transcription of RNA into cDNA according to the manufacturer's protocols.

cDNAs were amplified (Biorad instrument) and qRT-PCR reactions were prepared with LightCyler 480 SYBR Green Master Mix (Roche). Analysis was done in the Rotor Gene (Qiagen) or CFX96 Touch Real-Time PCR Detection System (Biorad). Quantifications were performed using the ΔΔCt (threshold cycle) method using the following formula: (primer efficiency) −ΔΔCt, where ΔΔCt means ΔCt (target gene) − ΔCt (reference gene). Gene expression levels were normalized relative to Gapdh transcript levels.

The primers used for mRNA analysis in q-RT PCR experiments are listed in Table 2.6.

Table 6: q-RT PCR Primers used in the study

Gene	**Forward**	**Reverse**
hGAPDH	GACCACAGTCCATGCCATCACT	TCCACCACCCTGTTGCTGTAG
hXBP1	TGCTGAGTCCGCAGCAGGTG	GCTGGCAGGCTCTGGGGAAG
hHSPA9	TGGTGAGCGACTTGTTGGAAT	ATTGGAGGCACGGACAATTTT

hHSPE1	ATGGCAGGACAAGCGTTTAGA	CCGATCCAACAGCGACTAC T
hATF5	AGGGGACCGCAAGCAAAAG	GCCTTGTAAACCTCGATGA GC
hLONP1	GACGATCCCCGATGTGTTTCC	GGGCGAGACGAACTTTCCT T
hATF4	CCCTTCACCTTCTTACAACCTC	TGCCCAGCTCTAAACTAAA GGA
mmGAPDH	GTGAAGGTCGGTGTGAACG	GGTCGTTGATGGCAACAAT CTC
mmXbp1	TGAGAACCAGGAGTTAAGAACACGC	CCTGCACCTGCTGCGGAC
mmHspa9	ATGGCTGGAATGGCCTTAGC	ACCCAAATCAATACCAACC ACTG
mmHspe1	AGTTTCTTCCGCTCTTTGACAG	TGCCACCTTTGGTTACAGT TTC
mmAtf5	TGGGCTGGCTCGTAGACTAT	GTCATCCAATCAGAGAAG CCG
mmClpp	GCCTTGCCGTGCATTTCTC	CTCCACCACTATGGGGATG A
mmLonp1	CTCATGGTGGAGGTTGAGAATG	CAGAGGGTTCAAGGCGAT GATA
mmAtf4	TCGATGCTCTGTTTCGAATG	AGAATGTAAAGGGGGCAA CC
mmDdit3	CCTAGCTTGGCTGACAGAGG	CTGCTCCTTCTCCTTCATGC
mmIl1β	CAACCAACAAGTGATATTCTCCAT	GATCCACACTCTCCAGCTG CA
mmTnfα	CATCTTCTCAAAATTCGAGTGACAA	TGGGAGTAGACAAGGTAC AACCC;
mmIl6	GAGGATACCACTCCCAACAGACC	AAGTGCATCATCGTTGTTC ATACA

2.2.7 Proteomics

Sample preparation – in-gel digestion: Samples were separated by SDS-PAGE and stained with Coomassie blue. The bands were cut from the gel and subjected to in-gel digestion with trypsin (PMID: 25278616). Peptides were extracted from the gel pieces by sonication for 15 minutes, followed by centrifugation and supernatant collection. Second extraction was performed with 50:50 water: acetonitrile, 1% formic acid (2 x the volume of the gel pieces) solution. The samples were again sonicated for 15 minutes, centrifuged and the supernatant

pooled with the first extract. Using speed vacuum centrifugation was used to process the pooled supernatants. 10 µL of reconstitution buffer (96:4 water: acetonitrile, 1% formic acid was used to dissolve samples and analyzed by Liquid Chromatography with tandem Mass Spectrometry (LC-MS/MS).

LC-MS/MS: For peptide separation, the UltiMate 3000 RSLC nano LC system (Dionex) fitted with a trapping cartridge (µ-Precolumn C18 PepMap 100, 5 µm, 300 µm i.d. x 5 mm, 100 Å, ThermoFisher) and an analytical column (Acclaim PepMap 100 75 µm × 50 cm C18, 3 µm, 100 Å, ThermoFisher) was used. QExactive plus (ThermoFisher) was coupled directly to the outlet of the analytical column using the nanoFlex source in positive ion mode. The peptides were introduced into the mass spectrometer (QExactive plus, ThermoFisher) via a Pico-Tip Emitter 360 µm OD x 20 µm ID; 10 µm tip (New Objective) and a spray voltage of 2.3 kV was applied. The capillary temperature was set at 320 °C. Full scan MS spectra with mass range 350-1400 m/z were acquired in profile mode in the FT with resolution of 70,000. The filling time was set at maximum of 30 ms with a limitation of 3x106 ions. DDA was performed with the resolution of the Orbitrap set to 35000, with a fill time of 105 ms and a limitation of 2x105 ions. Normalized collision energy of 26 was used. The peptide match algorithm was set to 'preferred' and charge exclusion 'unassigned', charge states 1, 5 - 8 were excluded.

Data processing: IsobarQuant (PMID: 26379230), as search engine Mascot (v2.2.07) was used to process acquired data. Common contaminants, reversed sequences and the sequences of the proteins of interest containing data was searched against Uniprot Homo sapiens proteome database (UP000005640). The following modifications: Carbamidomethyl (C; fixed modification), Acetyl (N-term), Phospho (STY) and Oxidation (M) (variable modifications) were searched in the data. The mass error tolerance for the full scan MS spectra was set to 10 ppm and for the MS/MS spectra to 0.02 Da. A maximum of two missed cleavages was allowed. For protein identification a minimum of 2 unique peptides with a peptide length of at least seven amino acids and a false discovery rate below 0.01 were required on the peptide and protein level.

2.2.8 Lipidomics Analysis

Lipidomics specific chemicals and reagents are listed in table 2.7.

Table 7:Lipidomics specific chemicals and reagents

Product	**Company**	**Catalog No.**
Cer/Sph Mixture I	Avanti Polar Lipids	LM6002-1EA
DNA LoBind® Tubes	Eppendorf	0030108078
Methanol suitable for HPLC	Millipore	65541
Chloroform suitable for HPLC	Sigma-Aldrich	650498
Dichloromethane suitable for HPLC	Sigma-Aldrich	34856
Acetonitrile	Sigma-Aldrich	34998

Sample preparation- Whole cells were pelleted in 2 mL microfuge tubes at 4 °C. 10 µL of the internal standards from Cer/Sph Mixture I was added to each tube. 726 µL of chloroform:

methanol:12.1 N HCl (40:80:1) solution used for initiation of lipid extraction, fallowed vortexing samples in an Eppendorf Thermomixer at full speed at 4°C for 15 minutes. Then, 720 µL of chloroform was added, and samples were vortexed for another 5 min. Finally, 354 microliters of 1 N hydrochloric acid (HCl) was added and samples were vortexed for 2 minutes. Samples were centrifuged for 5 minutes at 1,000 x g at 4°C and the lower phases were collected in a fresh 2 mL tube. An additional 1098 µL chloroform: methanol: 1.185 N HCl (86:14:1, v:v:v) was added to the upper phase followed by vortexing and centrifugation at 1,000 x g for an additional 5 minutes. Previously collected lower phase was combined with the resultant. Collected lower phase was dried using a refrigerated Labconco Centrivap at -4 °C under full vacuum. The dried samples were analyzed via liquid chromatography tandem mass spectrometry. Samples were re-suspended in 100% methanol (LC-MS Optima grade, Fisher) prior to chromatographic separation at ambient temperature on a C8 column (Thermo Hypersil Gold C8 2.1 x 50; 1.9 µm). 10 mM Formic Acid in water (A) and 10 mM formic acid in acetonitrile/methanol (50:50 v/v) (B) were used to initiation of a gradient and delivered at a flow rate of 0.3 mL/min by a Waters Acquity UPLC. The gradient progressed from 37 to 100% B from 2 to 10 min following injection. A Waters ACQUITY FTN autosampler set at room T injected 1–5 uL of sample extract. For quantitative analysis the effluent was monitored by a Waters XEVO TQ-S MS/MS via Multiple Reaction Monitoring (MRM) in positive ion mode. Protonated sphingolipid metabolites were detected in positive ion mode using a cone voltage of 55 and collision energy of 18. Lipid levels were calculated from peak areas normalized to internal standards. A further normalization was applied based on total protein quantification of the samples.

2.2.9 Mitochondrial Fractionation

Cells were homogenized in ice cold mitochondrial isolation buffer (250mM sucrose, 1mM EDTA, 10mM HEPES, pH 7.4) containing protease and phosphate inhibitor cocktails. Homogenates were run through 27.5 g needle four times and spinned at 600 g for 5 min at 4°C to eliminate nuclear and unbroken membranes. Supernatants were transferred to another tube and small portions of them kept as whole cell lysates (wcl). The rest was centrifuged at 7,000 g for 10 min at 4°C and supernatant kept as cytosolic fraction. Pellets were re-suspended with homogenizing buffer and spinned at 7,000 g for 5 min at 4°C and supernatant were carefully removed. Mitochondria enriched pellet dissolved with PLB with inhibitors. Equalized wcl, cytocolic and mitochondrial fractions were boiled with 5x SDS buffer and subjected to SDS/PAGE separation and transferred onto nitrocellulose membranes. Membranes are then stained with Ponceau S. solution (Sigma-Aldrich, P7170-1L), washed with distilled water and imaged, as equal loading control.

2.2.10 Sphingosine-1-Phosphate Lyase Fluorogenic Substrate assay

Sphingosine-1-Phosphate Lyase Fluorogenic Substrate assay was performed according to manufacturer protocol (195). Cell lysates were incubated with Sphingosine-1-Phosphate Lyase Fluorogenic Substrate which is converted to aldehyde by SPLyase in the presence of 0,25 mM pyrodoxal 5 phosphate. Mixtures were kept for six hours at 37°C and aldehyde was converted to umbelliferone after beta elimination at neutral ph. Fluorescent signal was measured at plate reader (Excitation=325 nm and Emission =452). Cell lysates without substrate were used as blank.

2.2.11 Mitochondria Ca2+ measurements

WT MEF cells were treated with 100 nM TG for indicated time points. 1 µM RHOD-2 AM (cell-permeable fluorescent calcium indicator) (Thermo Scientific) was used for mitochondria-specific calcium measurement according to previously published protocols (196).

2.2.12 Mice Studies and Treatments

UPRmt studies-Apolipoprotein E-deficient (Apoe -/-) mice were purchased from Jackson laboratory. (Bar Harbor, ME) and used in UPRmt studies. Male mice fed with high-cholesterol/high-fat mouse diet (0.21% cholesterol and 21% butter fat), obtained from Ssniff Spezialdiaten, Germany (corresponding to TD.88137 diet; catalog number: E15721) starting from age of 8–10 weeks. Then, Apoe -/- mice injected twice a day with either 30 mg/kg AMG18 or DMSO with vehicle (20% vol/vol cremophor-EL (Sigma) prepared with saline solution) for 4 weeks by intraperitoneal method.

LCWE-induced KD vasculitis murine model- Lactobacillus casei (ATCC 11578) cell wall extract (LCWE) was used to induce KD vasculitis murine model as described previously (188). In brief, 5-week old male mice were injected with a single dose of 500 ug LCWE of PBS by intraperitoneal method. Mice euthanized one or two weeks after injection depending on experimental purpose. Related tissues were collected embedded with Optimal Cutting Temperature (OCT) for further experimental analysis.

Pharmacological inhibition of IRE1- Mice were injected with either 10 mg/kg 4μ8c or DMSO with vehicle (20% vol/vol cremophor-EL (Sigma) prepared with saline solution) for 1 week by intraperitoneal method. 4μ8c injection was performed daily and started 2 days prior to LCWE injection. Related tissues were collected and embedded with OCT for further experimental analysis

Mice were housed under specific pathogen-free conditions. All animal experiments were performed according to protocols approved Cedars-Sinai Medical Center institutional committee.

2.2.13 ELISA.

Serum IL-1β levels were measured with the V-PLEX Mouse IL-1β Kit (Meso Scale Diagnostics according to manufacturer's instructions. EMasurements were done with MSD QuickPlex SQ120 instrumentation and analyzed with Workbench 4.0 Software (Meso Scale Diagnostics).

2.2.14 Imaging and Staining of Cryosections

Collected abdominal aortas were photographed prior to embedding with OCT. The area and maximal diameter were quantified from the infrarenal part located between the left renal artery and common iliac branches. 5 different areas in indicated part of abdominal aorta were measured with ImageJ.

Immunohistochemical staining -Embedded and frozen hearth and abdominal aorta tissues in OCT were cut in 7μm thickness and stained with Hematoxylin & Eosin (H&E). Histopathological scoring of H&E-stained tissue sections carried out as blind analysis.

Immunofluorescent staining- Heath tissue cryosections were stained with FAM-FLICATM Caspase-1 Assay kit to assess Caspase-1 and NLRP3 inflammasome activation according to the manufacturer's protocol. Hearth tissue section were stained with mouse anti ERP57 for 1 hour at room temperature. After wash, the sections were incubated with Alexa Fluor 594-conjugated anti-Mouse mAb. Protein block serum free (Dako co. CA, US) was used for blocking, and ProLong Gold Antifade Reagent with DAPI (Invitrogen, NY, US) for DAPI counter staining.

The data were obtained by fluorescent microscope (BZ-9000E, KEYENCE). Signal quantification was performed by calculating the corrected total cell fluorescence (CTCF) by using ImageJ.

2.2.15 Abdominal Aorta Single-Cell RNA sequencing

A publicly available scRNA-seq data set generated from the abdominal aortas of PBS (pool of n=9) and LCWE-injected (pool of n=7) mice (GSE178765) (197) was analyzed and ER-stress-related gene expression profiles were assessed. Uniform Manifold Approximation and Projection (UMAP) projections were performed using the R package umap v0.2.2.0 (198). Seurat V3 and SingleR were used for cell clustering and clusters annotations (190).

2.2.16 Analysis of murine abdominal aorta gene expression dataset.

Murine RNA-seq dataset generated from abdominal aorta of PBS (n=5) and LCWE-injected (n=5) mice (GSE141072) was analyzed and ER stress signature gene expression profiles were assessed. edgeR and Limma-voom packages in R were used for gene expression data normalization and analysis, as previously described (199). Differentially expressed ER stress signature genes cut off adjusted to p-value <0.05 and FC ≥ 1.5. "ComplexHeatmap" package in R was used to generate heatmaps showing the expression relative to the mean of selected genes.

2.2.17 Analysis of human gene expression datasets

Publicly available gene expression datasets GSE68004 (200), GSE73461 (201) and GSE63881 (202) were obtained from NCBI Gene expression Omnibus (**https://www.ncbi.nlm.nih.gov/geo/**). GEO2R software as part of the GEO database was used to analyze transcriptomics data and limma topTable function used to generate summary statistics. ER stress signature genes were narrowed and fallowing genes were selected: ATF4, ATF6, CEBPB, DDIT3, DNAJB11, DNAJC3, EDEM1, EDEM2, EIF2A, EIF2AK2, EIF2AK3, ERN1, ERP29, ERP44, HSPA5, OS9, PDIA3, PDIA4, PDIA6, RTN3, S100P, SEL1L, SOD2, SSR1, TRIB1, TRIB3, WFS1, WIPI1, XBP1. Expression levels of these genes were analyzed in whole blood of acute KD patients and HC (n=37 HC and n=76 acute KD patients for GSE68004 (200); n=55 HC and n=78 acute KD patients for GSE73461 (201)). Differentially expressed ER stress signature genes cut off adjusted to p-value <0.05 and FC ≥ 1.5 (Benjamini-Hochberg) in these two datasets (GSE68004 and GSE73461). The expression of these ER stress signature genes were subsequently analyzed in the whole blood of acute KD patients (n=146) and IVIGtreated convalescent KD patients (n=145) (adjusted p-value <0.05) (GSE63881) (202).

2.2.18 Statistical analysis

Data were analyzed with Prism software (GraphPad) and are presented as mean ± SEM. Unpaired Student's t test, with Welch's correction was used for 2 group comparisons of normally distributed data. The Mann-Whitney test was used for nonparametric data. Significance was evaluated by 2-way ANOVA with Tukey's post hoc test analysis for multiple-comparison testing. A p-value <0.05 was considered significant.

Chapter 3

The role of IRE1 in intraorganelle crosstalk

3.1 Regulation of UPR^{mt} by ER stress through IRE1

ER is closely interconnected with mitochondria through MAMs and changes in ER functions by ER stress can be reflecting in mitochondria as mitochondrial dysfunction, resulting abolished mitochondrial proteostasis. ER sensor IRE1 has been shown to located on MAM and its deficiency leads to metabolic stress by changing mitochondria-related degradation pathways (30). From this end, we hypothesized IRE1 may affect UPR^{mt}. To investigate the role of IRE1 in mitochondrial proteostasis, we used mouse embryonic fibroblast (MEF) and treated them with Thapsigargin (TG), a non-competitive inhibitor that inhibits SERCA and activates ER stress (20). We observed that TG-induced ER stress is associated with elevated expression of both UPR^{mt} and UPR^{ER} related transcription factors (TFs) such as ATF5, ATF4 and CHOP (are encoded by Atf4, Ddit3 and Atf5, respectively) in wild type (WT or IRE $^{+/+}$). However, the effect of TG on transcription of these TFs was reversed in IRE1 $^{-/-}$ MEF cells, as an evidence of ER stress sensor IRE1 is responsible for this induction (Fig 3.1. A-C). During mitochondrial proteostasis, accumulation of unfolded protein in mitochondrial matrix increases the level of mitochondrial chaperons to overcome with protein in mitochondrial matrix (100). We also checked expression level of UPR^{mt} related mitochondrial chaperones mtHSP70 and HSP10 (are encoded by Hspa9 and Hspe1, respectively). Their expression also induced by TG- induced ER stress in WT MEF and block when IRE1 is abolished (Fig 3.1. D-E).

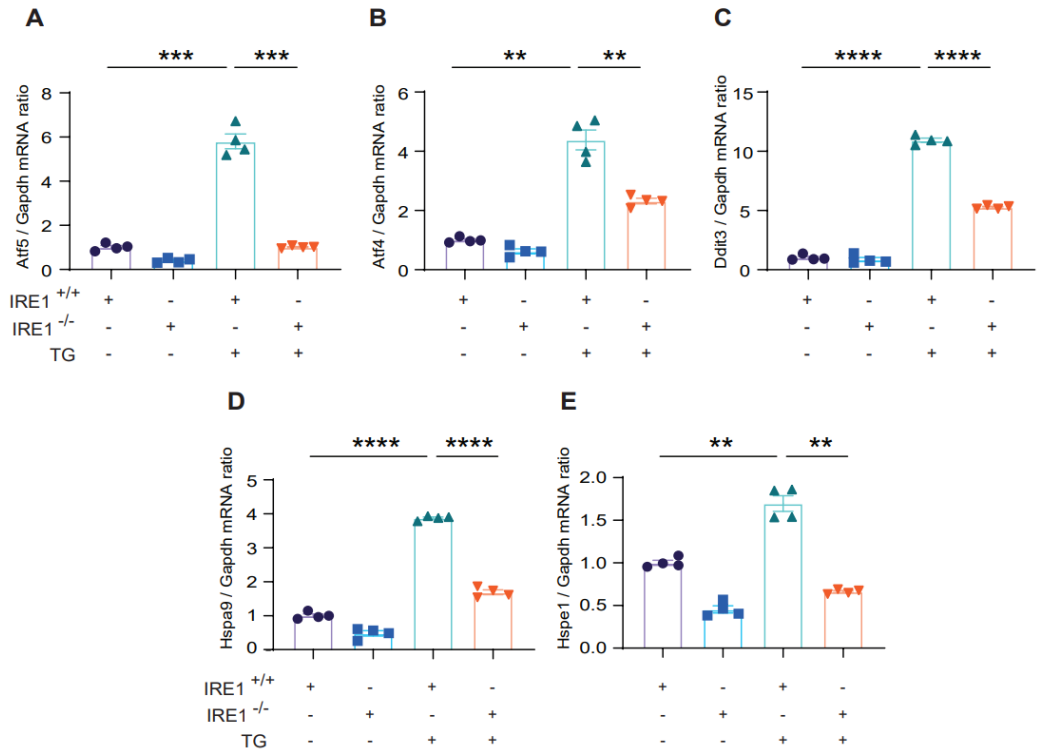

Figure 3. 1: IRE1-deficiency blocks expression of both UPRmt and UPR ER related transcription factors during ER stress. (A-E) IRE1$^{+/+}$ and IRE1$^{-/-}$ MEFs were treated with TG (100 nM; 12 hours), and total RNA was analyzed by qRT-PCR for Atf5, Atf4, Ddit3, Hspa9, Hspe1 and Gapdh mRNA (n=4 biological replicates). Data information: All data are mean ± SEM; (n = 4). Unpaired t-test with Welch's correction. * P ≤ 0.05, ** P ≤ 0.01, *** P ≤0.001, **** P ≤0.0001

We have also checked the protein level of mitochondrial proteases LONP1 and CLPP1 and mitochondrial chaperone mtHSP70 in mitochondria. To do this, WT (IRE1$^{+/+}$) and IRE1 deficient (IRE1$^{-/-}$) MEF cells treated with TG and mitochondrial protein levels were assessed. ER stress induction by TG increases the mitochondrial protein levels of LONP1, CLPP1 and mtHSP70 in WT MEFs and IRE1 deficiency reverses TG induced level of these proteins (Fig 3.2.). Collectively, these findings demonstrate that ER stressor can induce UPRmt signaling in an IRE1-dependent manner.

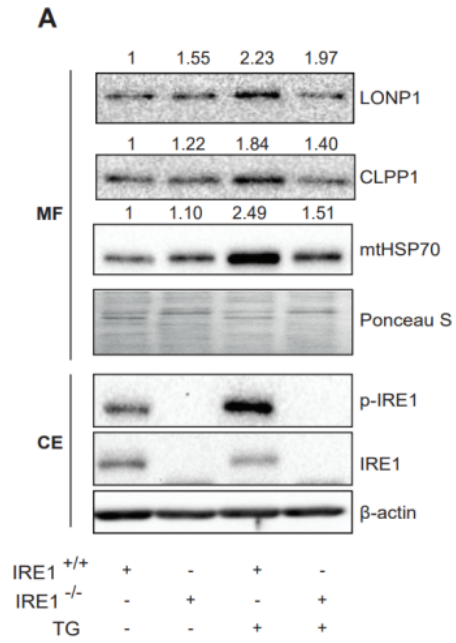

Figure 3. 2: IRE1-deficiency decreases UPR^{mt} related protein levels in mitochondria and elevates mitochondrial membrane potential. (A) IRE1$^{+/+}$ and IRE1$^{-/-}$ MEFs were treated with TG (100 nM; 4 hours) and mitochondrial fraction (MF) and total cellular extract (CE) protein lysates were analyzed by Western blotting using specific antibodies for LONP1, mtHSP70, CLPP1 (for MF) and p-IRE1, IRE1 and β-actin (for CE). The membrane was stained by Ponceau S (n=3 biological replicates; a representative blot is shown).

3.2 ER stress induces UPR^{mt} in MEF and HEK293 cells.

We would like to decipher UPR^{mt} induction have seen in MEF cells specific to TG or another ER toxin can also elevate the transcription of UPR^{mt} related genes. To decipher this, we used Tunicamycin (TUN) that leads to ER stress by inhibiting protein glycosylation. TUN also led to robust induction of both UPR^{ER} and UPR^{mt} in WT MEFs (Fig 3.3.).

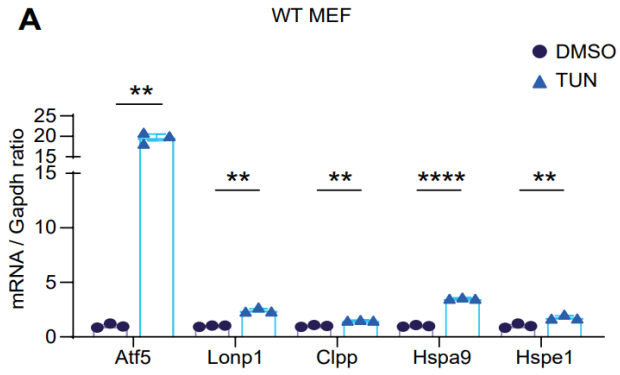

Figure 3. 3: TUN induces UPR^{mt} in MEF cells. WT MEFs were treated with TUN for (2.5 µg/ml; 12 hours) and total RNA was analyzed by qRT-PCR for Atf5, Lonp1, Clpp, Hspa9, Hspe1 and Gapdh mRNA (n=3 biological replicates). Data information: All data are mean ± SEM; (n = 3). Unpaired t-test with Welch's correction. * P ≤ 0.05, ** P ≤ 0.01, *** P ≤0.001, **** P ≤0.0001

We also tested effect of ER stressors on UPR^{mt} in human cells (human embryonic kidney (HEK) 293T (HEK293T)). Both ER toxins induce the expression level of ATF5, LONP1 and HSPA9 (Fig 3.4. A-B). Over all these results concludes ER stress induces UPRmt in UPRmt in both mouse and human cells.

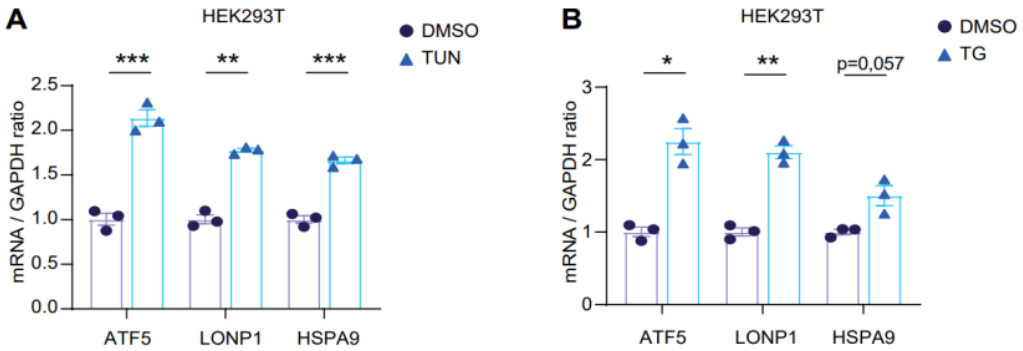

Figure 3. 4: Different ER toxins induce UPR^{mt} in HEK293T cells. (A-B) HEK293T cells were treated with either (A) TUN (2.5 µg/ml; 12 hours) or (B) TG (100 nM; 12 hours) and total RNA was analyzed by qRT-PCR for ATF5, LONP1, HSPA9 and GAPDH mRNA (n=4 biological replicates). Data information: All data are mean ± SEM; (n = 3). Unpaired t-test with Welch's correction. * P ≤ 0.05, ** P ≤ 0.01, *** P ≤0.001, **** P ≤0.0001

3.3 Regulation of UPR^{mt} by IRE1 kinase domain

ER sensor IRE1 localizes on ER membrane and 3 functional domains: luminal domain, transmembrane domain and cytosolic domain. Cytosolic domain of IRE1 encompasses 2 catalytic activities. Endoribonuclease activity of IRE1 splices XBP1 RNA and sXBP1 acts as a transcription factor to modulate ER stress related gene transcription(203). IRE1 kinase domain is important for its activation through autophosphorylation. To decipher which catalytic activity of IRE1 is responsible for UPR^{mt} regulation, we used specific IRE1 kinase inhibitor, KIRA6, and checked the UPR^{mt} markers under ER stress condition. We found that blocking of IRE1 kinase domain by KIRA6 inhibits ER stress induced UPR^{mt} related gene expression in WT MEFs (Figure 3.5. A-E).

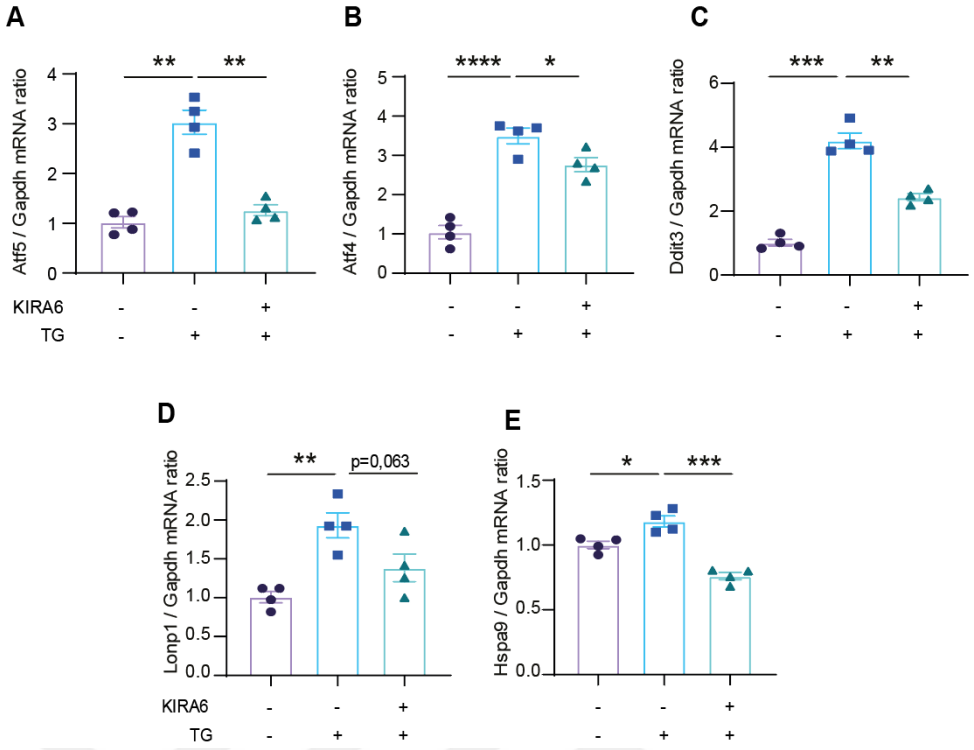

Figure 3. 5 Specific IRE1 inhibitor, KIRA6, blocks TG induced UPR^{mt} upregulation. (A-E) Wild type (WT) MEFs were treated with KIRA6 (5 mm) and TG (100 nM) for 12 hours, and total RNA was analyzed by qRT-PCR for Atf5, Atf4, Ddit3, Lonp1, Hspa9 and Gapdh mRNA (n=4 biological replicates). Data information: All data are mean ± SEM; (n = 4). Unpaired t-test with Welch's correction. * P ≤ 0.05, ** P ≤ 0.01, *** P ≤0.001, **** P ≤0.0001

We also investigate the effect of KIRA6 on mitochondrial level of UPR^{mt} proteins in mitochondria. KIRA6 treatment alleviates TG induced LONP1, CLPP1 and mtHSP70 protein levels (Fig 3.6).

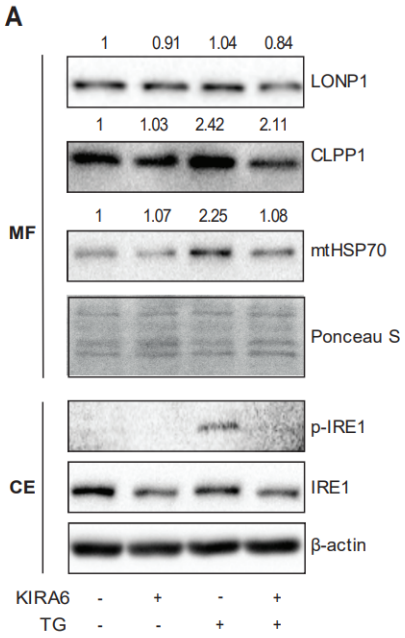

Figure 3. 6: Inhibition of IRE1 kinase activity decreases UPR^{mt} related protein levels in mitochondria. (A) WT MEFs were treated with TG (100 nM; 4 hours) and mitochondrial fraction (MF) and total cellular extract (CE) protein lysates were analyzed by Western blotting using specific antibodies for LONP1, mtHSP70, CLPP1 (for MF) and p-IRE1, IRE1 and β-actin (for CE). The membrane was stained by Ponceau S (n=3 biological replicates; a representative blot is shown).

We further confirmed the gene expression results by performing the same experiments by using a different IRE1 kinase inhibitor, AMG18, in WT MEF cells (Fig 3.7 A-E).

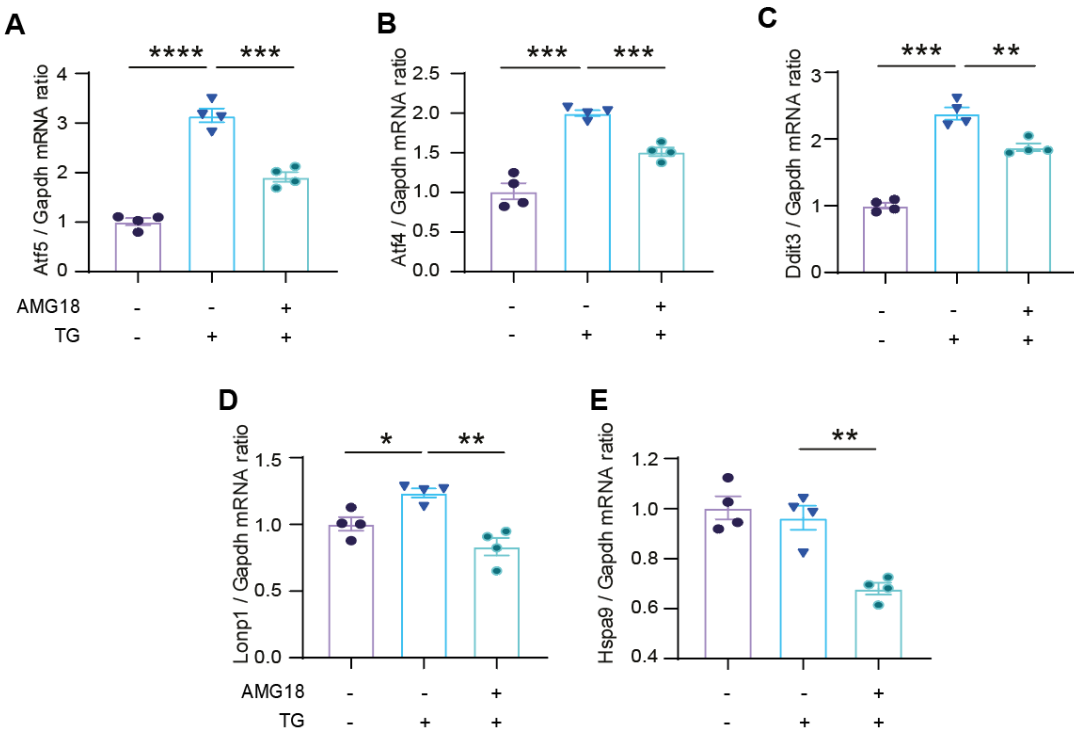

Figure 3. 7: Confirmation of UPR^{mt} gene expressions by IRE1 in AMG18 treated WT MEFs. (A-E) WT MEFs were treated with 2 µM AMG18 and 100 nM TG for 12 hours, and total RNA was analyzed by qRT-PCR for Atf5, Atf4, Ddit3, Lonp1, Hspa9 and Gapdh mRNA (n=4, biological replicates). Data information: All data are mean ± SEM; (n = 4). Unpaired t-test with Welch's correction. * P ≤ 0.05, ** P ≤ 0.01, *** P ≤0.001, **** P ≤0.0001

3.4 The impact of IRE1 kinase activity inhibition on TG- Induced UPR^{mt} in vivo

After observing the regulation of UPR^{mt} related gene expression by IRE1 kinase inhibitors *in vitro*, we next sought to confirm this is also applicable *in vivo*. For this, we used the apolipoprotein E-deficient (*Apoe* $^{-/-}$) mice and fed them with high fat diet (HFD) to induced lipotoxic ER stress. We analyzed liver tissues that were obtained from AMG18- and DMSO (control)- treated high fat diet applied *Apoe* $^{-/-}$ mice. We see a significant reduction in expression level of UPR^{mt} relates genes such as LONP1 and mtHSP70 (Fig 3.8 A-B). We also examined Clpp1 protease and ATF5 transcription factor. There are trends to reduction in their expression level however it didn't reach to significance (Fig 3.8 C-D). Also, the protein level

of ATF4 in liver lysates reduced in liver of AMG18 treated *Apoe* $^{-/-}$ mice. These findings also confirm results that are obtained from WT MEF treated with IRE1 kinase inhibitors in Fig 3.5 and Fig 3.7.

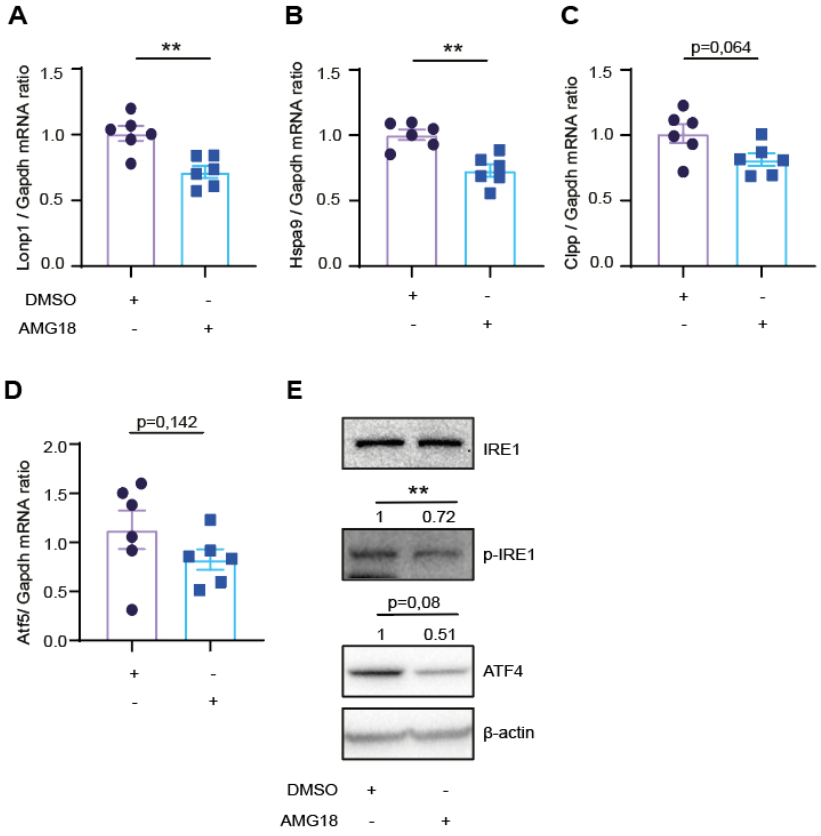

Figure 3. 8: IRE1 kinase inhibitor blocks hyperlipidemia-induced UPR^{mt} in mouse livers in vivo. (A-E) *Apoe* $^{-/-}$ mice were fed with WD for 12 weeks and injected with AMG18 (30 mg/kg) or vehicle (DMSO) twice per day in the final 4 weeks of the diet (A-D). Liver total RNA lysates were analyzed by qRT-PCR for Lonp1, Clpp, Hspa9, Atf5 and Gapdh (n=6 biological replicates). (E) Liver protein lysates were analyzed by Western blotting using specific antibodies for IRE1, p-IRE1, ATF4 and β-actin (n=5 biological replicates). Data information: All data are mean ± SEM; Mann-Whitney U test. *P ≤ 0.05, **P ≤ 0.01.

3.5 Inhibition of IRE1 RNase domain does not have an effect of TG induced UPR^{mt}.

Kinase activity of IRE1 has a profound effect in regulation of mitochondrial proteostasis and expression of UPRmt markers. Since IRE1 has two enzymatic activity, kinase and endoribonuclease, we also examined the effect of RNase domain activity on UPR^{mt}. Inhibition of IRE1 RNase domain by small inhibitor, 4μ8c, did not change the expression level of UPR^{mt}

markers in WT MEF cells (Fig 3.9 A-E) even though the inhibitor has worked efficiently by reducing sXBP1 transcription level (Fig3.9 F).

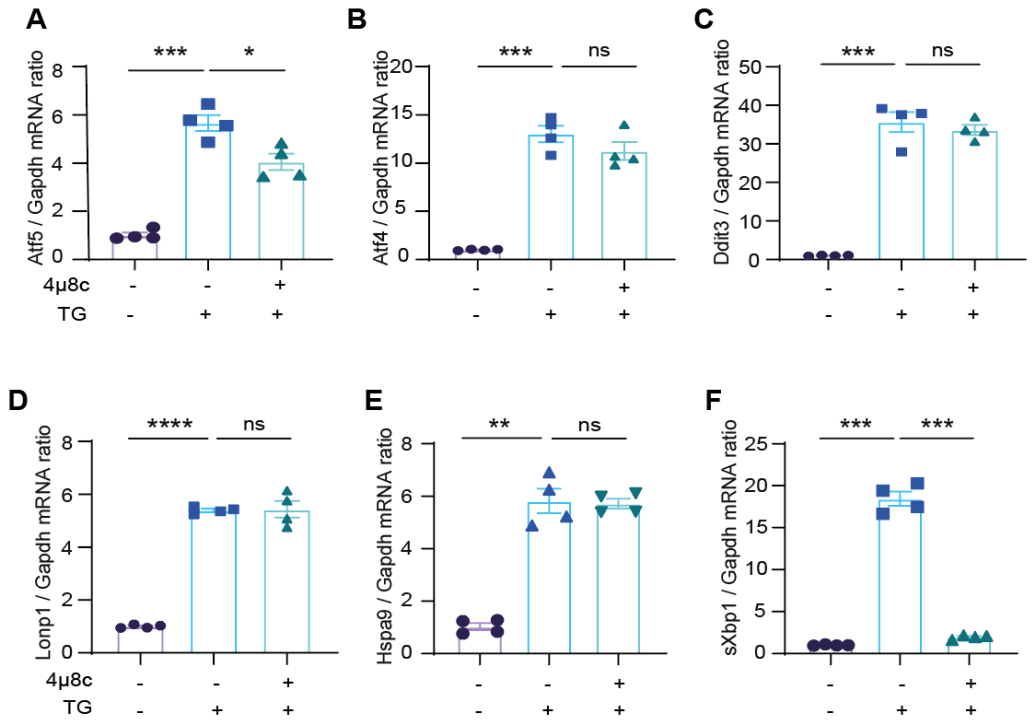

Figure 3. 9: Inhibition of IRE1 RNase domain does not have an effect of TG induced UPR^{mt}. (A-F) WT MEFs were treated with 4μ8c (100 nm) and TG (100 nM) for 12 hours and total RNA was analyzed by qRT-PCR for Atf5, Atf4, Ddit3, Lonp1, Hspa9, sXbp1 and Gapdh mRNA (n=4 biologial replicates). Data information: All data are mean ± SEM; (n = 4). Unpaired t-test with Welch's correction. * P ≤ 0.05, ** P ≤ 0.01, *** P ≤0.001, **** P ≤0.0001 ns=not significant.

We also examined effect of 4μ8c the mitochondrial protein levels. Inhibition of IRE1 RNAse domain icreases the level of TG-induced UPRmt related proteins such as LONP1, CLPP1 and mtHSP70 in WT MEF's mitochondrial fractions (Fig 3.10).

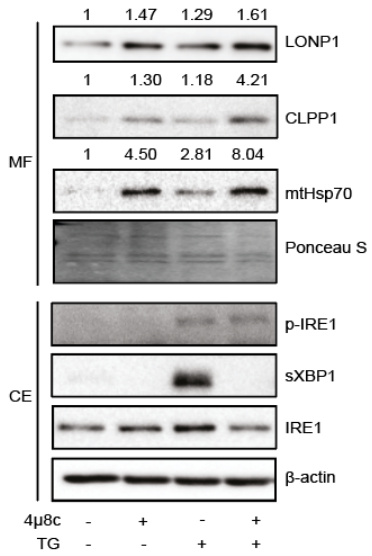

Figure 3. 10: IRE1 RNase inhibitor increase UPR^{mt} related mitochondrial protein levels. WT MEF cells were treated with 4μ8c (100 nm) and TG (100 nm) for 4 hours and MF protein lysates were analyzed by Western blotting using specific antibodies for LONP1, mtHSP70 and CLPP1 and CE protein lysates were analyzed with antibodies for p-IRE1, IRE1 and β-actin. The membrane was stained with Ponceau S. (n=3 biological replicates; a representative blot is shown).

3.6 Delineating SPL as IRE1 kinase substrate

The role of IRE1 RNase domain in response to ER stress has been studied extensively however the only target of IRE1 kinase function is itself since its activation requires autophosphorylation. Recently, the ER stress induced changes in the IRE1 interactome has been identified and reveals the proteins which are predicted to interact with IRE1 under stress condition (38). SPL, the enzyme that degrades S1P, is one of the candidates for IRE1 interacting proteins. S1P is a signaling lipid and its level is tightly controlled in the cell since small changes in S1P level can initiate robust cellular signaling response (162). Previous study show that mitochondrial stress can promote increased S1P level and result in potent UPRmt signaling in nematodes. In same study, deletion of SPL by RNAi results in elevated UPRmt under mitochondrial stress conditions (177). Here, we sought to whether interaction of IRE1 with SPL has an effect of SPL function under stress conditions.

3.6.1 Validation of interaction between IRE1 and SPL

First, we want to experimentally validate the predicted interaction between IRE1 and SPL occurs in mammalian cells. IRE1 and SPL plasmids were co-transfected into HEK293 cells, in which ER stress was induced by TG treatment. The results of coimmunoprecipitation experiment confirmed that IRE1 and SPL interact with each other under both basal and stress condition in HEK293T cells (Fig 3.11)

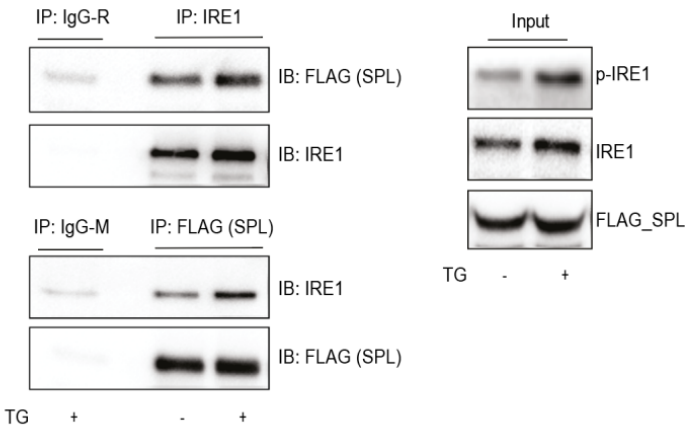

Figure 3. 11: IRE1 and SPL physically interact with each other. HEK293T cell were co-transfected with IRE1 and FLAG-SPL plasmids and treated with TG (600 nM; 4 hours). IRE1 and SPL were immunoprecipitated with total IRE1 and FLAG antibodies, respectively, and analyzed by Western blotting using antibodies specific for total IRE1 and FLAG. Normal IgG-Rabbit or normal IgG-Mouse antibodies were used to show specifity of IRE1 and FLAG antibodies, respectively.The cell lysate was also analyzed by Western blotting using antibodies specific for p-IRE1, total IRE1 and FLAG (n=4 biological replicates, a representative blot is shown).

3.6.2 IRE1 phosphorylates SPL

After validating physical interaction between IRE1 and SPL, we sought to investigate the consequences of this interaction. Since IRE1 is a serine threonine kinase, we examine the possibility of SPL phosphorylation by IRE1 through its kinase domain. To test this, Wild type (IRE_WT) and IRE1 kinase dead mutants (IRE1_KD; serine 599 mutated to an alanine) plasmids transfected with or without FLAG-tagged SPL and immunoprecipitated. These proteins were incubated together to perform *in vitro* kinase assay (where IRE1 was the kinase and SPL, the substrate). IRE1_WT phosphorylates SPL and itself *in vitro*, however IRE1_KD failed to phosphorylate SPL (Fig 3.12 A). We next tested this by doing cell-based kinase assay using a previously characterized ATP analog sensitive kinase allele of IRE1 (IRE1_ASKA). In this mutant, ATP binding cavity is slightly enlarged and it can be modulated by using bulky side-chain ATP analogs which cannot be used by wild type kinase. IRE1 _WT and IRE1_ASKA transfected HEK293T cells simultaneously treated with N6-furfuryl ATPγS, the bulky ATP analogue, with TG (to induce ER stress). These cell lysated are combined with cell lysates from SPL transfected cells. These data shows IRE_ASKA that can use bulky ATP analogue phosphorylates SPL by not IRE1_WT in cells (Fig 3.12 B).

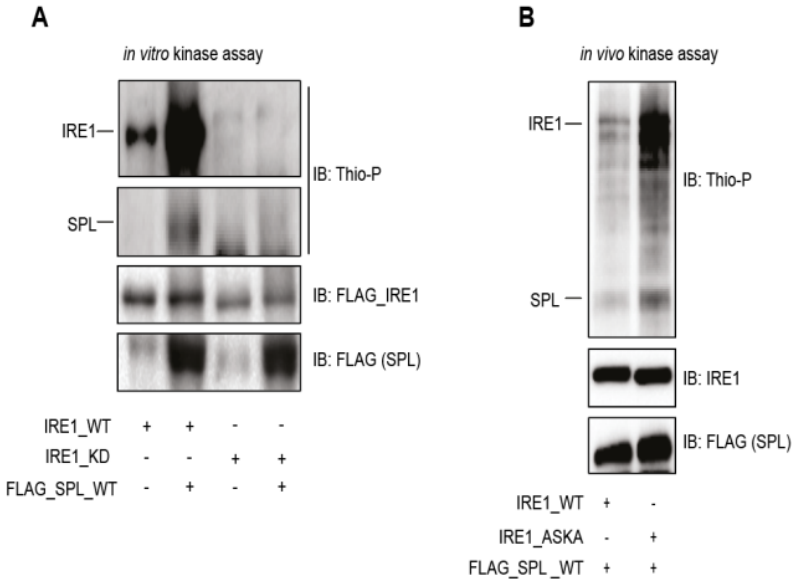

Figure 3. 12: SPL is phosphorylated by IRE1. (A) In vitro kinase assay: HEK293T cells were transfected with the indicated plasmids and treated with TG (1 mM; 2 hours). IRE1 and SPL were IP'd with FLAG antibodies and incubated together with ATPγS in a kinase reaction. The kinase reaction was analyzed by Western blotting using specific antibodies for thiophosphate ester and FLAG (n=3 biological replicates, a representative blot is shown). (B) In vivo kinase assay: HEK293T cells were transfected with the indicated plasmids and treated with TG (1 μM; 2 hours) followed by treatment with N-6 furfuryl ATPgS. Immunoprecipitated lysates were analyzed by Western blotting with specific antibodies for thiophospho-ester, total IRE1 and FLAG. (n=3 biological replicates; a representative blot is shown).

3.6.3 Discovering the specific amino acids on SPL possible phosphorylated by IRE1. After proving IRE1 phosphorylate SPL by using in vitro and in vitro kinase assay, we sought to discover which amino acids on SPL are phosphorylated by IRE1. For this purpose, we set an in vitro kinase assay with SPL (as substrate) in the presence or absence of IRE1_ WT (as kinase) and discover phosphorylated sites on SPL by using mass spectroscopy- based phosphor-proteomics. The analysis revealed serine (S286) and threonine 287 (T287) on SPL are phosphorylated by IRE1 kinase (Fig 3.13).

S/T Phosphosites on SPL in the presence of IRE1-- protein ID: H7BXL7/O95470 sequence coverage: 72,4 % ---- total score 6354

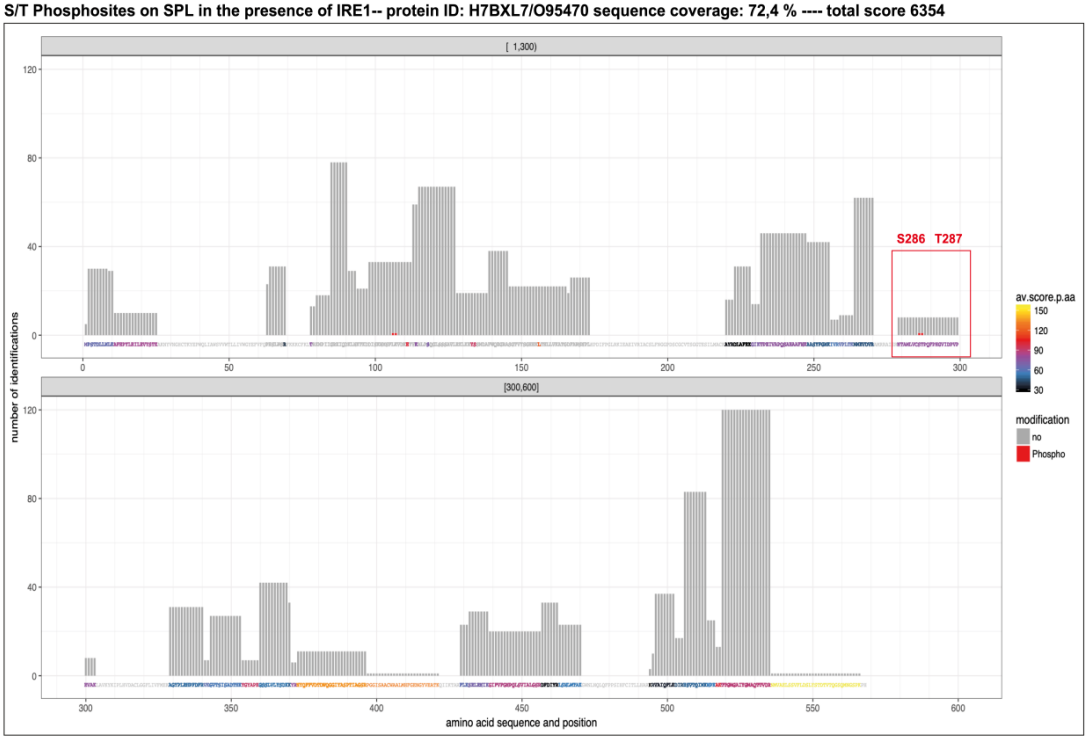

S/T Phosphosites on SPL in the absence of IRE1-- protein ID: H7BXL7/O95470 sequence coverage: 73,8 % ---- total score 6262

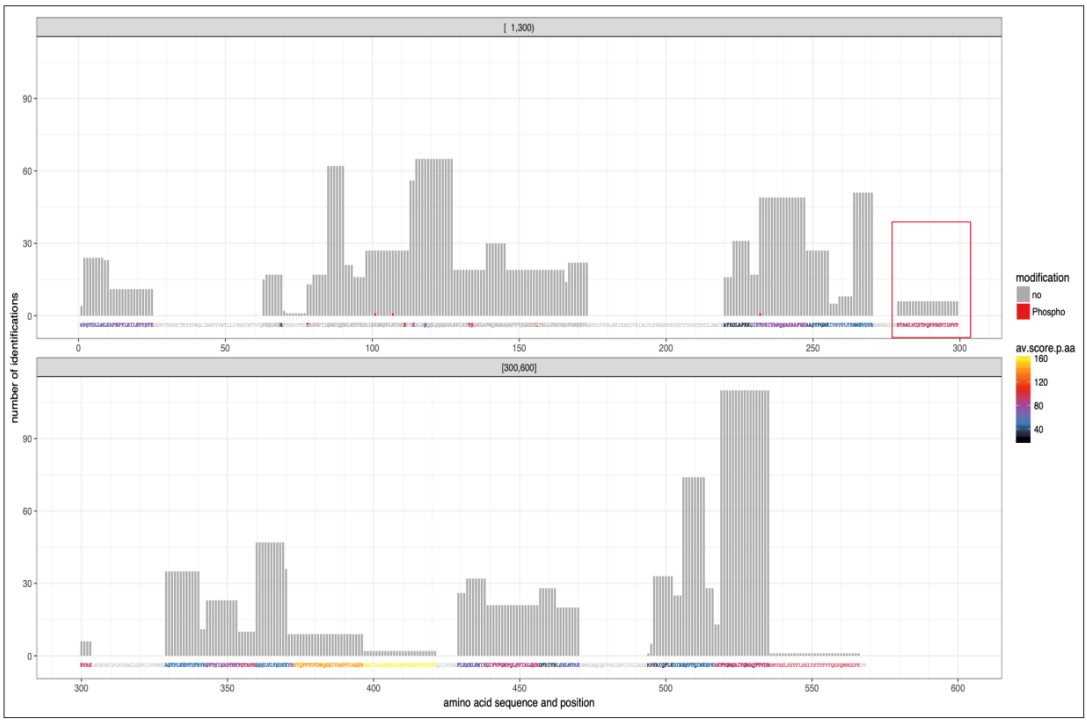

Figure 3. 13: IRE1-mediated phosphorylation sites on SPL amino acid sequence. HEK293T cells were transfected with IRE1_WT and FLAG_SPL_WT plasmids and treated with TG (1 mM; 2 hours). IRE1 and SPL were immunoprecipitated with total IRE1 and FLAG antibodies, respectively. FLAG immunoprecipitated lysates were incubated with ATPγS in a kinase reaction in the absence and presence of IRE1 immunoprecipitated lysates. Samples were separated by SDS_PAGE and stained with Coomassie blue. Bands corresponding to the molecular weight of IRE1 and SPL were cut from gel and digested with trypsin. Phosphorylation sites on SPL_WT were detected with liquid chromatography with tandem mass spectrometry (LC-MS/MS). The data was assessed using the Uniprot Homo sapiens proteome database (UP000005640)

After validating S286 and T287 as IRE1 phosphorylation targets on SPL, we checked the conservation status of these and their neighboring amino acids among species. It is revealed that these amino acinds are highly conserved among species (Fig 3.14 A). Next, we mutated T287 on SPL to alanine (SPL_MUT) to generate phospho-mutant SPL. We observed that SPL_WT can be phosphorylated by IRE1 but not SPL_MUT (Fig 3.14 B). Overall, these results demonstrate that IRE1 interacts with SPL and thus results in phosphorylation of T287 on SPL.

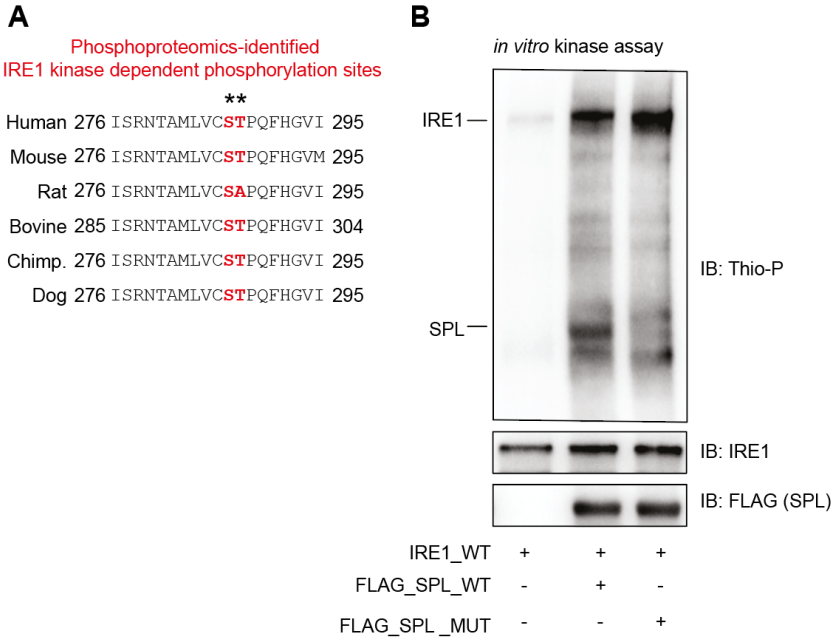

Figure 3. 14: IRE1 phosphorylates SPL on T287. (A) Multiple amino acid sequence alignment of SPL from different species: * indicates possible IRE1-mediated phosphorylation sites as determined by mass spectrometry. (B) In vitro kinase assay: HEK293T cells were transfected with the indicated plasmids and treated with TG (1 mM; 2 hours). IRE1 and SPL were immunoprecipitated with total IRE1 and FLAG antibodies, respectively, and incubated together with ATPγS in a kinase reaction. The kinase reaction was analyzed by Western blotting using specific antibodies for thiophospho ester, total IRE1 and FLAG (n=3; a representative blot is shown).

3.7 Investigating impact of SPL phosphorylation by IRE1 on SPL activity

SPL is an active lipid molecule, produced from Sph by 2 sphingosine kinases (SPHK1 and SPHK2) and is irreversibly degraded by SPL. Produced hexadecenal and ethanolamine-phosphate as a result of this reaction have several roles in cellular signaling pathways. Since this is one directional reaction, it is referred as exit point of sphingolipid metabolism (Fig 3.15)

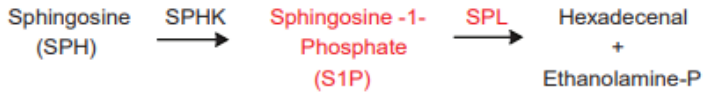

Figure 3. 15: Schematic representation of S1P degradation by SPL

3.7.1 Impact of IRE1 on SPL enzymatic activity

After revealing SPL is phosphorylated by IRE1, we sought to investigate what the consequences of this phosphorylation on SPL's enzymatic activity. To address this, we used cell based fluorogenic assay to measure SPL activity under several condition. We observed that ER stress induced by TG treatment led to inhibition of SPL activity. This is consistent with a previous study that elevated cellular S1P levels upon ER stress (172). Furthermore, inhibition of IRE1 kinase activity by KIRA6 reversed the effect of TG on SPL activity and inhibition of IRE1 RNase activity by 4μ8c did not in HEK293T cells (Fig 3.16 A). We also used another IRE1 kinase inhibitor, AMG18, to test this. AMG18 showed similar effect with KIRA6 by reversing TG-inhibited SPL activity in a dose dependent manner in HEK293T cells (Fig 3.16 B).

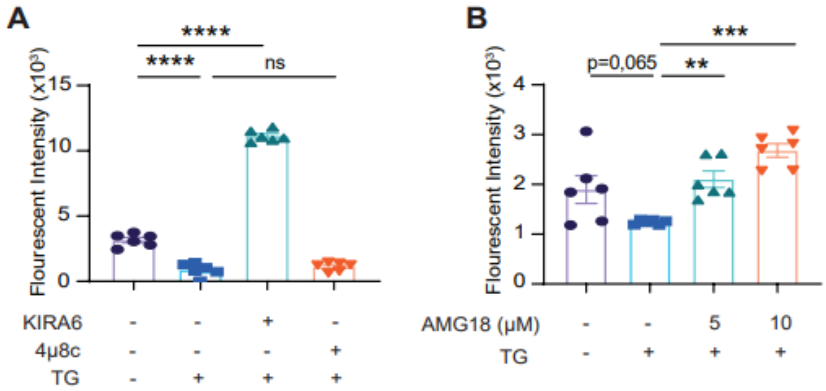

Figure 3. 16: IRE1 kinase domain is responsible for controlling SPL enzymatic activity. (A-B) SPL fluorogenic substrate assay was performed according to the manufacturer protocol on the cellular lysates from: (A) HEK293T cells that were treated with KIRA6 (20 μM) or 4μ8c (100 μM) and TG (600 nM; 2 hours) (n=6 biological replicates), (B) HEK293T cells were that were treated with AMG18 (5-10 μM) and TG (600 nM; 2 hours) (n=6 biological replicates). Data information: Data are mean ± SEM; Unpaired t-test with Welch's correction. * $P \leq 0.05$, ** $P \leq 0.01$, *** $P \leq 0.001$, **** $P \leq 0.0001$.

After showing inhibited SPL activity by TG is reversed by IRE1 kinase inhibition (KIRA6 and AMG18), we next sought to experimentally validate the effect of IRE1 overexpression on SPL activity under stress conditions. As it is expected overexpression of SPL_WT increased SPL

enzymatic activity and thus inhibited by TG in HEK293T cells. Moreover, co-transfection of SPL_WT with IRE1_WT has more profound inhibition effect under ER stress condition. Thus confirms that SPL activity is sensitive to TG-induced IRE1 activity (Fig 3.18).

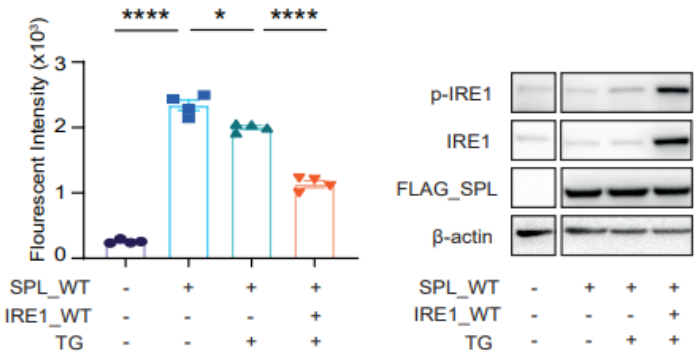

Figure 3. 17: SPL activity is sensitive to level of IRE1 activity. SPL fluorogenic substrate assay was performed according to the manufacturer protocol on the cellular lysates from HEK293T cells that were transfected with the indicated plasmids and treated with TG (600 nM; 2 hours) (n=4 biological replicates). Transfection and treatment efficiencies were analyzed by Western blotting using specific antibodies p-IRE1, total IRE1 and β-actin. Data are mean ± SEM; Unpaired t-test with Welch's correction. * $P \leq 0.05$, ** $P \leq 0.01$, *** $P \leq 0.001$, **** $P \leq 0.0001$.

3.7.1.1 Validation of mutant SPL activity under stress condition

As it is expected, SPL_WT overexpression induces SPL activity and this effect is reversed by ER stress, we next validated the activity of SPL_MUT (SPL T287A). We showed that TG has no effect of SPL_MUT, showing that SPL phosphorylation by IRE1 (on T287) is critical for SPL inhibition by ER stress (Fig 3.19)

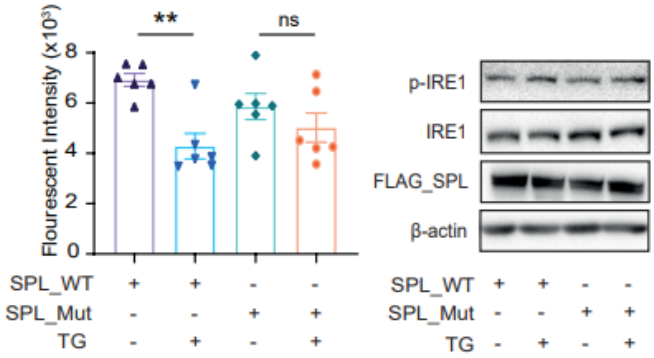

Figure 3. 18: SPL_MUT does not response to ER Stress. SPL fluorogenic substrate assay was performed according to the manufacturer protocol on the cellular lysates from HEK293T cells that were transfected with the indicated plasmids and treated with TG (600 nM; 2 hours) (n=4 biological replicates). Transfection and treatment efficiencies were analyzed by Western blotting using specific antibodies for p-IRE1, total IRE1 and β-actin. Data are mean ± SEM; Unpaired t-test with Welch's correction. * P ≤ 0.05, ** P ≤ 0.01, *** P ≤0.001, **** P ≤0.0001, ns= no significant

3.7.2 Impact of IRE1 on sphingolipids under ER stress condition

SPL deficiency or inhibition result in the change in level of several sphingolipid species and especially leads to accumulation of S1P in the cell (157, 204). After showing SPL phosphorylation by IRE1 upon ER stress inhibits SPL activity, we next assessed changes in sphingolipid levels during ER stress by using liquid chromatography-mass spectrometry (LC-MS). Consistent with previous study, acute ER stress resulted in a significant increase in intracellular S1P levels. Moreover, IRE1 kinase inhibitor, KIRA6, prevented S1P accumulation caused by TG treatment (Fig 3.19).

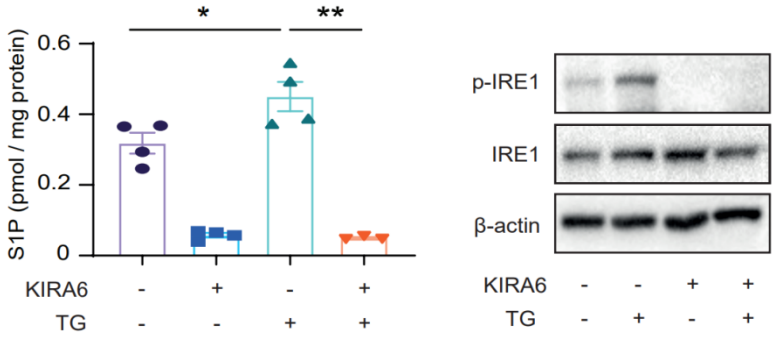

Figure 3. 19: Inhibition of IRE1 kinase activity prevents ER stress induces S1P accumulation. Lipid quantification was performed by LC-MS/MS from lysates of HEK293T that were pretreated with KIRA6 (20 µM; 1 hour) and then treated with TG (600 nM) or vehicle for 2 hours (n= 4 biological replicates for DMSO, KIRA6, and TG,n=3 biological replicates for KIRA6+TG). Peak areas of S1P were sequentially normalized by the internal standard and protein concentrations. Treatment efficiencies were analyzed by Western blotting using specific antibodies p-IRE1, total IRE1 and β-actin. Data information: Data are mean ± SEM; Unpaired t-test with Welch's correction. * P ≤ 0.05, ** P ≤ 0.01

Since regulation of sphingolipid metabolism is tightly controlled and also highly dynamic, we also analyzed level of other sphingolipids species under same conditions. It is appeared that TG treatment also increased SPH level that is precursor of S1P. Increased SPH levels also decreased by IRE1 kinase inhibitor KIRA6. Also, ER stress induced levels of ceramide (Total Cer) and total sphingomyelin (Total SM) prevented by inhibition of IRE1 kinase activity (Fig 3.20 A-C). Overall, these results reveal that IRE1 fulfills critical role in regulation of sphingolipid levels under stress condition as kinase domain dependent manner.

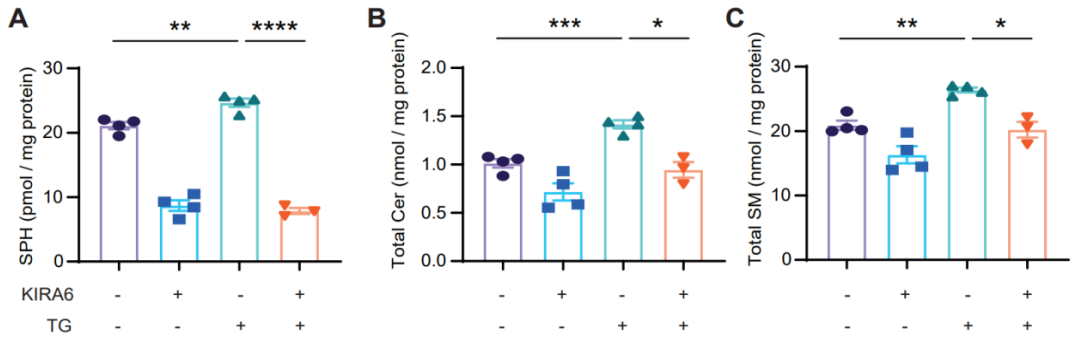

Figure 3. 20: Inhibition of IRE1 kinase activity prevents ER stress induced sphingolipid levels accumulation. Lipid quantification was performed by LC-MS/MS from lysates of HEK293T that were pretreated with KIRA6 (20 µM; 1 hour) and then treated with TG (600 nM) or vehicle for 2 hours (n= 4 biological replicates for DMSO, KIRA6, and TG, n=3 biological replicates for KIRA6+TG). Sph, Total Cer and Total SM levels were measured. Peak areas of sphingolipids were sequentially normalized by the internal standard and protein concentrations. Data information: Data are mean ± SEM; Unpaired t-test with Welch's correction. * P ≤ 0.05, ** P ≤ 0.01, *** P ≤0.001, **** P ≤0.0001.

To further confirm that IRE1 regulates intracellular S1P levels, we sought to examine the effect of deficiency of IRE1 on S1P. We knocked down IRE1 expression by its specific siRNA and analyzed S1P levels by LC-MS. Silencing IRE1 by siRNA had partial but strong inhibitory effect on TG- induced S1P accumulation (Fig 3.21)

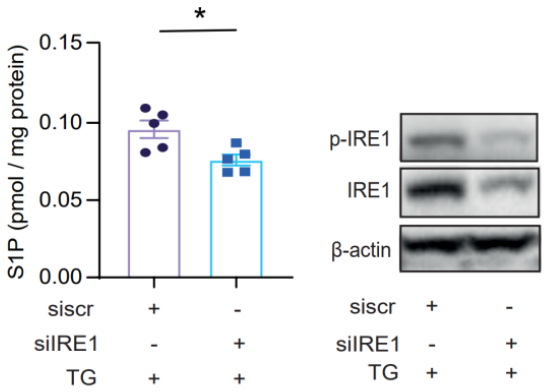

Figure 3. 21: Silencing of IRE1 reduced S1P levels upon ER stress. Lipid quantification was performed by LC-MS/MS from lysates of HEK293T that were transfected with scrambled (scr) or IRE1-specific (siIRE1) siRNA (50nmol) and treated with TG (600 nM; 1 hour) (n=5 biological replicates). Peak areas of S1P were sequentially normalized by the internal standard and protein concentrations. Transfection and treatment efficiencies were analyzed by Western blotting using specific antibodies p-IRE1, total IRE1 and β-actin. Data information: Data are mean ± SEM; Unpaired t-test. * P ≤ 0.05

To further prove our hypothesis, we also checked intracellular S1P levels in the presence of other IRE1 kinase inhibitor, AMG18, upon ER stress. AMG18 treatment also significantly

reduced TG-induced intracellular S1P accumulation (Fig 3.22). Collectively, these results demonstrate that suppression of IRE1 kinase can prevent ER stress-induced intracellular sphingolipid accumulation especially level of direct SPL target S1P.

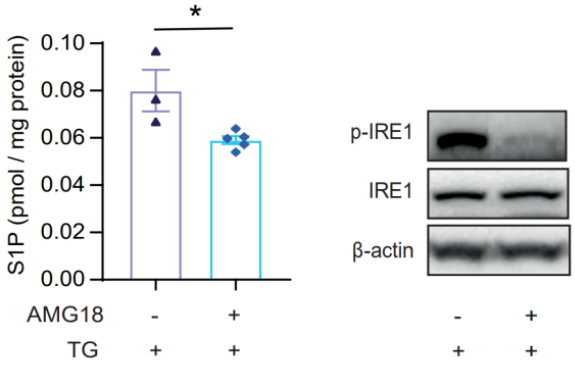

Figure 3. 22: IRE1 kinase activity inhibition alleviated intracellular S1P levels upon ER stress. Lipid quantification was performed by LC-MS/MS from lysates of HEK293T that were pretreated with AMG18 (5 µM; 1 hour), followed by TG (600 nM; 1 hour) treatment (n=4 biological replicates for TG and n=3 biological replicates for AMG18+TG). Peak areas of S1P were sequentially normalized by the internal standard and protein concentrations. Treatment efficiencies were analyzed by Western blotting using specific antibodies p-IRE1, total IRE1 and β-actin. Data information: Data are mean ± SEM; Unpaired t-test. * $P \leq 0.05$

3.8 Investigating the effect of SPL on UPR^{mt} upon ER stress

It has been shown that mitochondrial stress induces translocation of SPHK1 to the outer mitochondrial membrane and thus leads to UPR^{mt} activation initiated by increased S1P production in *C. elegans* (177). We showed that IRE1 kinase inhibition can prevent ER stress induced accumulation of intracellular sphingolipids especially S1P (Fig 3.19-20) simultaneous to UPR^{mt} induction. We investigated whether SPL has any impact on UPR^{mt} activation in mammalian cells. Overexpression of SPL leads to significantly higher SPL activity as expected which theoretically results in reduced S1P levels in the cell (3.23 A). We observed that SPL_WT blocked ER stress induced transcription level of UPRmt related genes (3.23 B-F).

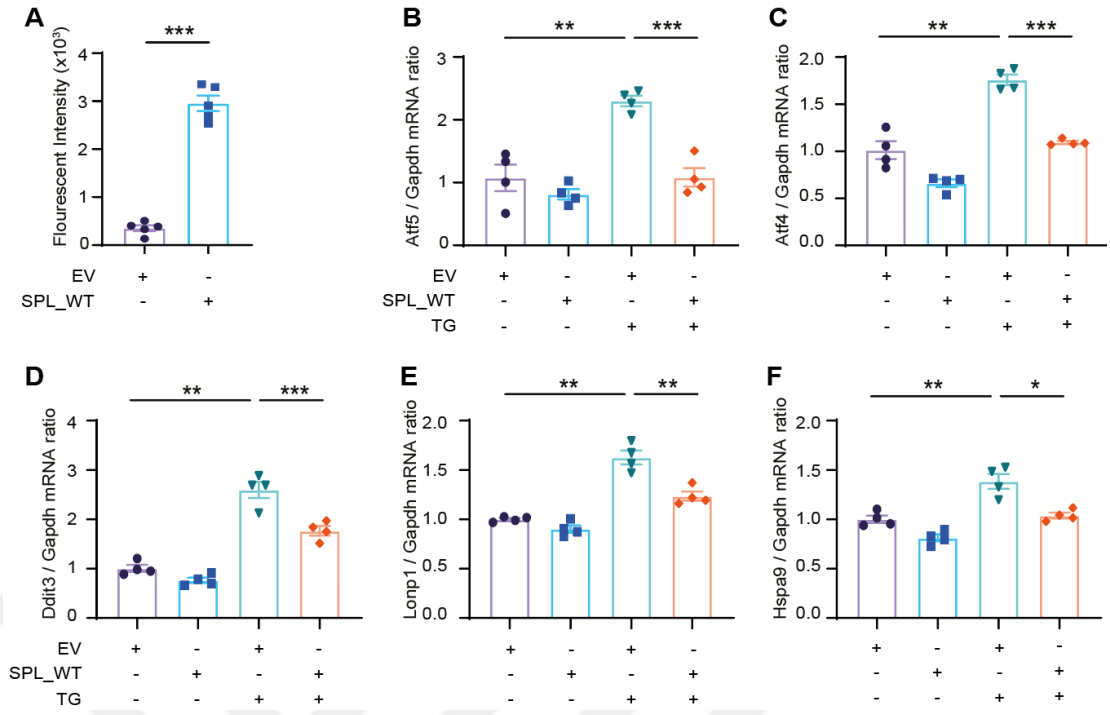

Figure 3. 23: SPL overexpression reduces ER stress induced UPR^{mt}. (A) HEK293T cells were transfected with either empty vector (EV) or SPL_WT plasmid, and the cell lysates were used to perform the SPL fluorogenic substrate assay according to manufacturer's protocol (n=4 biological replicates). (B-F) WT MEFs were transfected with either EV or SPL_WT and treated with TG (100 nM: 12 hours). Total RNA was analyzed by qRT-PCR for Atf5, Atf4, Ddit3, Lonp1, Hspa9 and Gapdh mRNA (n=4 biological replicates). Data information: All data are mean ± SEM; (n=4) Unpaired t-test with Welch's correction. * $P \leq 0.05$, ** $P \leq 0.01$, *** $P \leq 0.001$.

We next sought to confirm the impact of SPL_WT on UPR^{mt} related protein levels in mitochondria upon ER stress. We showed that TG-induced LONP1, CLPP1 and mtHSP70 proteins localization in mitochondria reduced in SPL_ WT overexpressed cells upon ER stress. Moreover, SPL overexpression inhibited eIF2α phosphorylation which is the shared component for UPR^{ER} and UPR^{mt} (Fig 3.24).

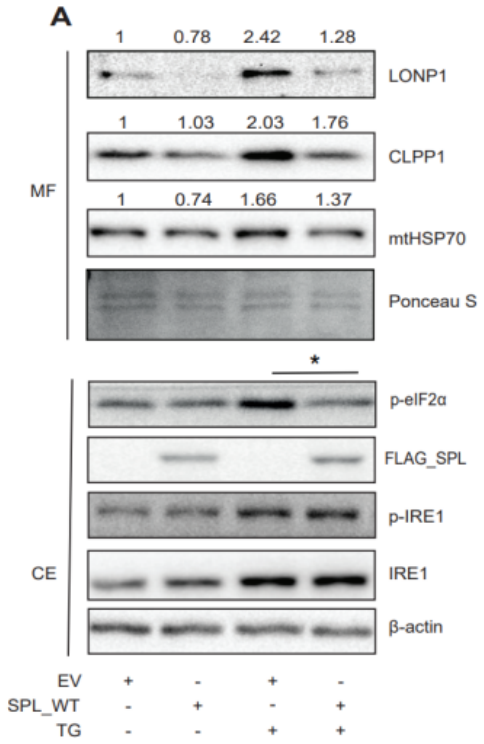

Figure 3. 24: Mitochondrial stress response reduces UPR^{mt} under ER stress condition. (A) WT MEF cells were transfected with the indicated plasmids and treated with TG (100 nM; 4 hours). MF protein lysates were analyzed by Western blotting using specific antibodies for LONP1, mtHSP70 and CLPP1 and CE protein lysates with antibodies for p-IRE1, IRE1, FLAG, p-eif2α and β-actin. The membrane was stained with Ponceau S. (n=3; a representative blot is shown).

After validating that SPL_WT overexpression reduces UPR^{mt}, we next sought to investigate the impact of SPL inhibition to further prove our hypothesis. We first checked the efficiency of specific SPL inhibitor, THI (2-acetyl-4-(tetrahydroxybutyl)imidazole). THI significantly blocks SPL enzymatic activity in WT MEFs (Figure 3.25).

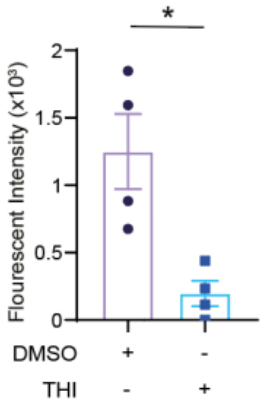

Figure 3. 25: SPL inhibitor THI significantly reduces SPL activity in WT MEF cells. SPL fluorogenic substrate assay was performed according to the manufacturer protocol on the cellular lysates from WT MEF cells treated with DMSO and THI (5mm) for 12 hours. All data are mean ± SEM; (n=4) Unpaired t-test with Welch's correction. * $P \leq 0.05$

We next asked whether THI has an impact on mitochondrial proteostasis. THI treatment significantly elevates TG-induced transcription of UPR^{mt} genes in WT MEF cells (Figure 3.26 A-E).

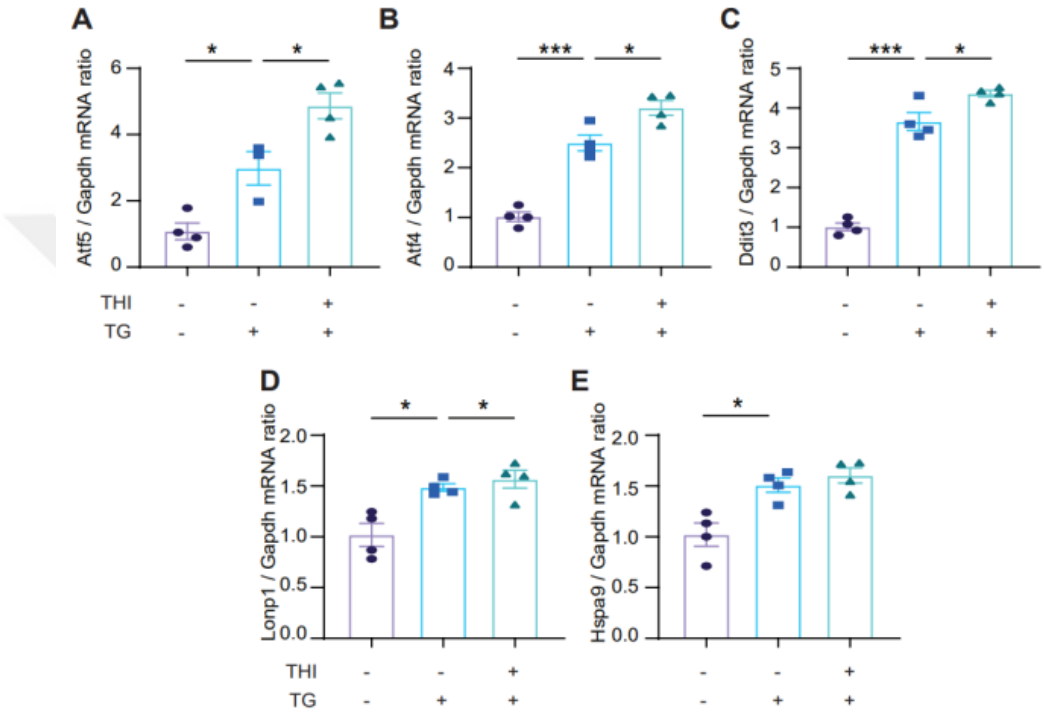

Figure 3. 26: TG-induced UPR^{mt} –related gene expression is enhanced by SPL inhibition. (A-E). WT MEFs were treated with THI (5 mm) and TG (100 nM) for 12 hours, and total RNA lysate was analyzed by qRT-PCR for Atf5, Atf4, Ddit3, Lonp1, Hspa9 and Gapdh mRNA (n=4 biological replicates. Data information: All data are mean ± SEM; (n=4) Unpaired t-test with Welch's correction. * $P \leq 0.05$, ** $P \leq 0.01$, *** $P \leq 0.001$.

Also mitochondrial protein level of mitochondrial proteases markers while SPL was inhibited by THI in WT MEF cells and knocked down by specific siRNA in HEK293T cells. Both SPL inhibitor THI and SPL knock down also potentiated ER stress-induced mitochondrial protein level of UPRmt related proteins (Fig 3.27 A-B).

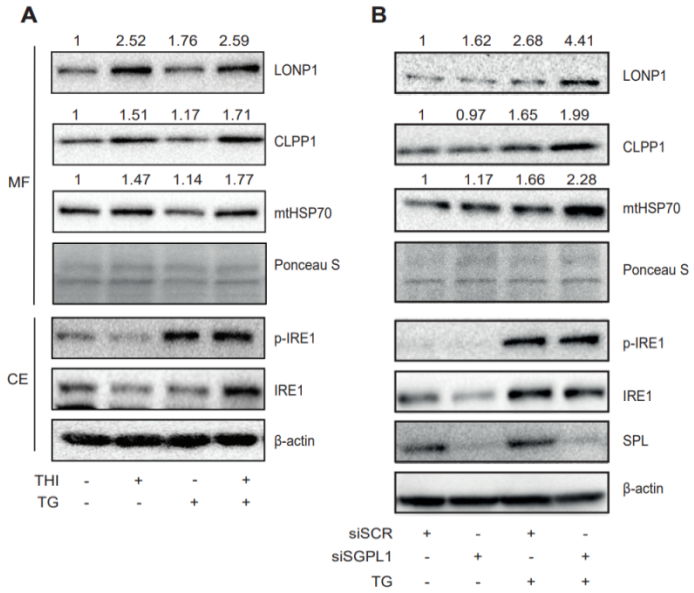

Figure 3. 27: Ablation of SPL activity elevates ER stress induced mitochondrial protein levels related to UPR^{mt}. WT MEFs were treated with THI (5 mm) and TG (100 nM) for 4 hours (A) and HEK293T cells were transfected with scrambled (scr) or SPL-specific (siSGPL1) siRNA (50nmol) and treated with TG (100 nM) for 8 hours (B). MF protein lysates were analyzed by Western blotting using specific antibodies for LONP1, mtHSP70 and CLPP1 and CE protein lysates were analyzed with antibodies for p-IRE1, IRE1, SPL and β-actin. The membrane was stained with Ponceau S. (n=3 biological replicates; a representative blot is shown).

As we demonstrated in Fig 3.14, IRE1 phosphorylates SPL on T287 and thus leads to inhibition of SPL enzymatic activity. To address the role of SPL phosphorylation by IRE1 in ER stress-induced UPRmt signaling, we next sought to validate the effect of SPL_MUT, which can not be phosphorylated by IRE1, on UPR^{mt} signaling upon ER stress. As a proof of our previous results, WT MEF cells overexpressing SPL_WT exhibited significant reduction in ER stress-induced UPR^{mt} signaling. However, this effect was diminished when IRE1-mediated phosphorylation site was mutated on SPL (Figure 3.28).

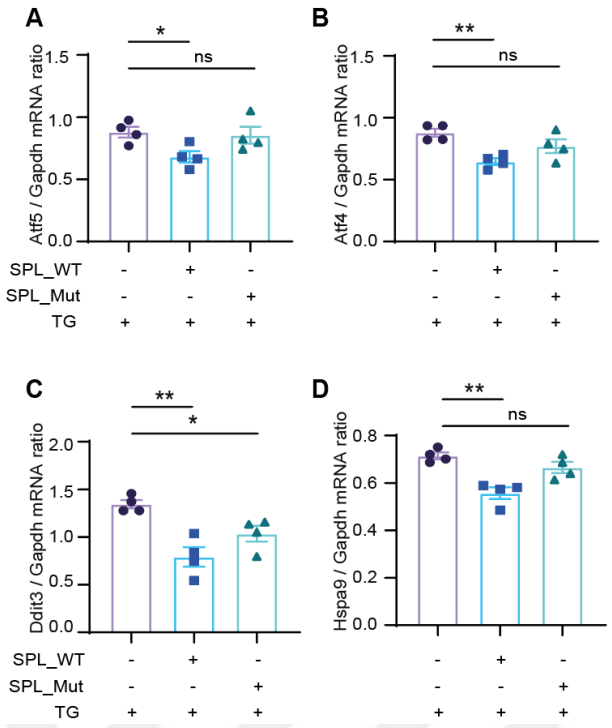

Figure 3. 28: Phosphorylation of SPL by IRE1 is crucial for UPR^{mt} regulation. WT MEFs were transfected with the indicated plasmids and treated with TG (100 nM; 20 hours). Total RNA lysate was analyzed by qRT-PCR for Atf5, Atf4, Ddit3, Hspa9 and Gapdh mRNA (n=4 biological replicates). Data information: All data are mean ± SEM; (n=4) Unpaired t-test with Welch's correction. * P ≤ 0.05, ** P ≤ 0.01

3.9 IRE1-SPL axis regulates UPR^{mt} through eif2α kinases, PKR and PERK

Common factor of UPR^{mt} and ISR is phosphorylation of eif2α. There are four eif2α kinase, PERK, PKR, GCN2 and HRI, in mammalian cells. To gain insight into mechanisms through which eif2α kinase is affected by IRE1-SPL axis to regulate UPR^{mt}, we first validated the effect of IRE1 ablation of activation of PKR and PERK kinases. IRE1 knocked down by specific siRNA caused a profound reduction in TG induced PRK and partially inhibition of TG-induced PERK phosphorylation. Consequently, ER stress induced eif2α phosphorylation significantly alleviated in the absence of IRE1 (Fig 3.29). This data confirms the effect of IRE1 ablation on blocked UPR^{mt} shown in Fig 3.1 and Fig 3.5.

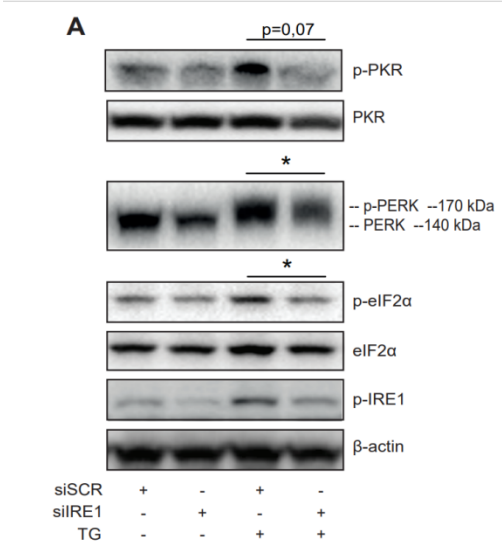

Figure 3. 29: IRE1 knock down prevents eif2α phosphorylation by suppressing PERK and PKR activation by ER stress. HEK293 cells were electroporated with either siSCR or siIRE1 (50 nmol) for 48 hours and then treated with TG (100 nM; 4h). Protein lysates were analyzed by Western blotting using specific antibodies for PERK, p-PKR, PKR, p-eif2α, eif2α, pIRE1 and beta actin. (n=3 biological replicates). Data information: All data are mean ± SEM; (n=3) Unpaired t-test. * $P \leq 0.05$, ** $P \leq 0.01$.

We have also examined the impact of IRE1 kinase domain inhibition on eif2α phosphorylation which we observed reduced UPR^{mt} induction upon ER stress. Inhibition of IRE1 kinase domain by KIRA6 leads to significant reduction in eif2α phosphorylation upon ER stress (Figure 3.30).

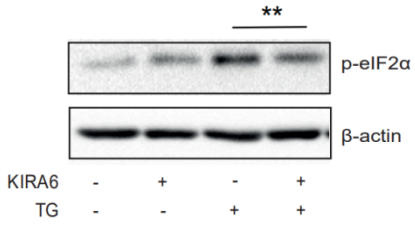

Figure 3. 30: IRE1 kinase inhibition leads to blocked eif2α phosphorylation. WT MEFs were treated with KIRA6 (5 mm) and TG (100 nM) for 4 hours, and protein lysates were analyzed by Western blotting using specific antibodies against p-eIF2α and β-actin (n=3 biological replicates; a representative blot is shown). Data information: All data are mean ± SEM; (n=3) Unpaired t-test. ** $P \leq 0.01$.

We next assessed the effect of SPL overexpression on phosphorylation of eif2α by PKR and PERK. SPL overexpression significantly reduced PKR and PERK phosphorylation upon ER stress. As a results of this, TG-induced eif2α phosphorylation profoundly inhibited in SPL overexpressing cells (Fig 3.31)

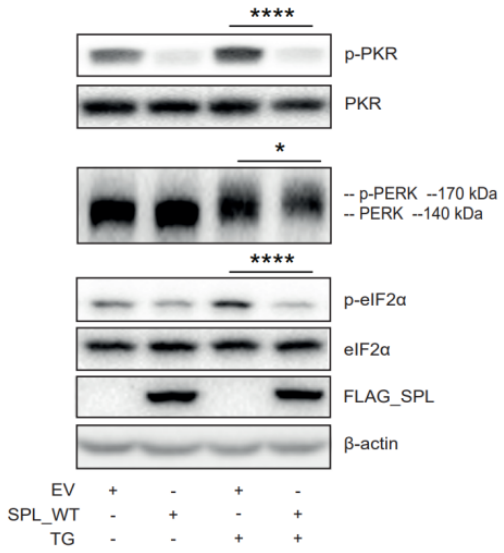

Figure 3. 31: SPL overexpression reduces ISR activation. HEK293 cells were transfected by either empty vector or SPL_WT plasmids for 24 hours and then treated with TG (100nM; 8 hours). Protein lysates were analyzed by Western blotting using specific antibodies for PERK, p-PKR, PKR, p-eif2α, eif2α, pIRE1, FLAG and β-actin. (n=3 biological replicates). All data are mean ± SEM; (n=3) Unpaired t-test with Welch's correction. * $P \leq 0.05$, ** $P \leq 0.01$, **** $P \leq 0.0001$

After observing hyper-inhibition of ISR pathway by overexpressing SPL_WT, next we addressed the effect of SPL inhibition on this pathway upon ER stress. Blocking SPL activity by its specific siRNA leads to significant increased level of p-PKR and p-eif2α but not p-PERK (Figure 3.32).

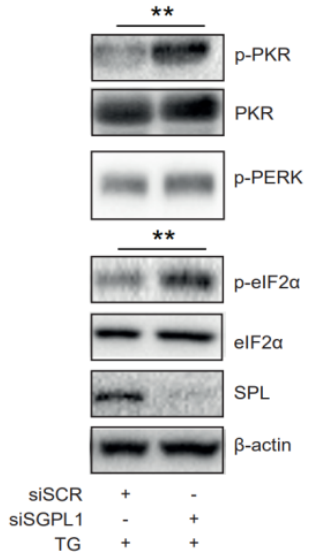

Figure 3. 32: SPL inhibition leads to ISR activation through PKR-eif2α pathway. HEK293 cells were electroporated with either siSCR or siIRE1 (50 nmol) for 48 hours and then treated with TG (100nM; 4h). Protein lysates were analyzed by Western blotting using specific antibodies for PERK, p-PKR, PKR, p-eif2α, eif2α, pIRE1 and β-actin (n=3 biological replicates). All data are mean ± SEM; (n=3) Unpaired t-test with Welch's correction. ** $P \leq 0.01$.

After validating which ISR kinases was affected by IRE1-SPL axis upon ER stress, we sought to investigate the impact of PKR and PEKR inhibitors on 3 main transcription factors involved in UPR^{mt}. Both PKR and PERK inhibitor blocks TG-induced transcription of ATF5, ATF4 and CHOP (Figure 3.9.5 A-C). Also, inhibition of PKR and PERK by their specific inhibitors significantly reduced phosphorylation of eif2α as it is expected in HEK293 cells (Fig 3.33 A-D)).

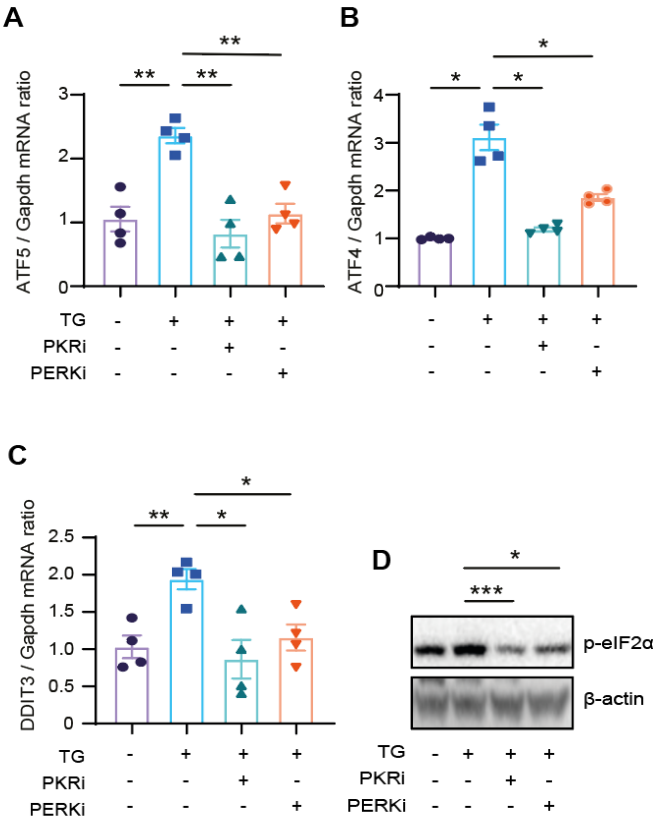

Figure 3. 33: Inhibition of PKR and PERK block TG-induced UPR^{mt} induction. (A-D) HEK293 cells were pretreated with either PKR inhibitor (2 mm) or PERK inhibitor (3 mm) for 1 hour and then treated with TG (100 nM; 16 hours). (A-C) total RNA lysate was analyzed by qRT-PCR for Atf5, Atf4 Ddit3 and Gapdh mRNA (n=4 biological replicates) while (D) protein lysate was analyzed by Western blotting using the indicated antibodies (n=3 biological replicates; a representative blot is shown). Data information: Data are mean ± SEM; (n = 4), Unpaired t-test with Welch's correction. * P ≤ 0.05, ** P ≤ 0.01.

Inhibition of PKR and PERK blocks UPR^{mt} related gene expression upon preventing phosphorylation of eif2α. We next sought to examine the effect of SPL inhibition when PKR and PERK were ablated. In Fig 3.27, we demonstrated that SPL inhibition by its specific inhibitor THI augments UPR^{mt} gene expression in WT MEFs. To test THI effect in the absence of PKR and PERK on UPR^{mt} regulation, we treated PKR$^{-/-}$ and PERK $^{-/-}$ MEF cells with THI and examined transcription level of ATF5 and ATF4 upon ER stress in comparison to WT MEFs treated with THI. SPL inhibition by THI could not enhance TG-induced UPR^{mt} in PKR- and PERK deficient MEF cells like it did in WT MEFs (Fig 3.34). Collectively these data exhibit IRE1-SPL axis impinges on phosphorylation of eif2α to induce a robust mitochondrial stress response during ER stress in mammalian cells.

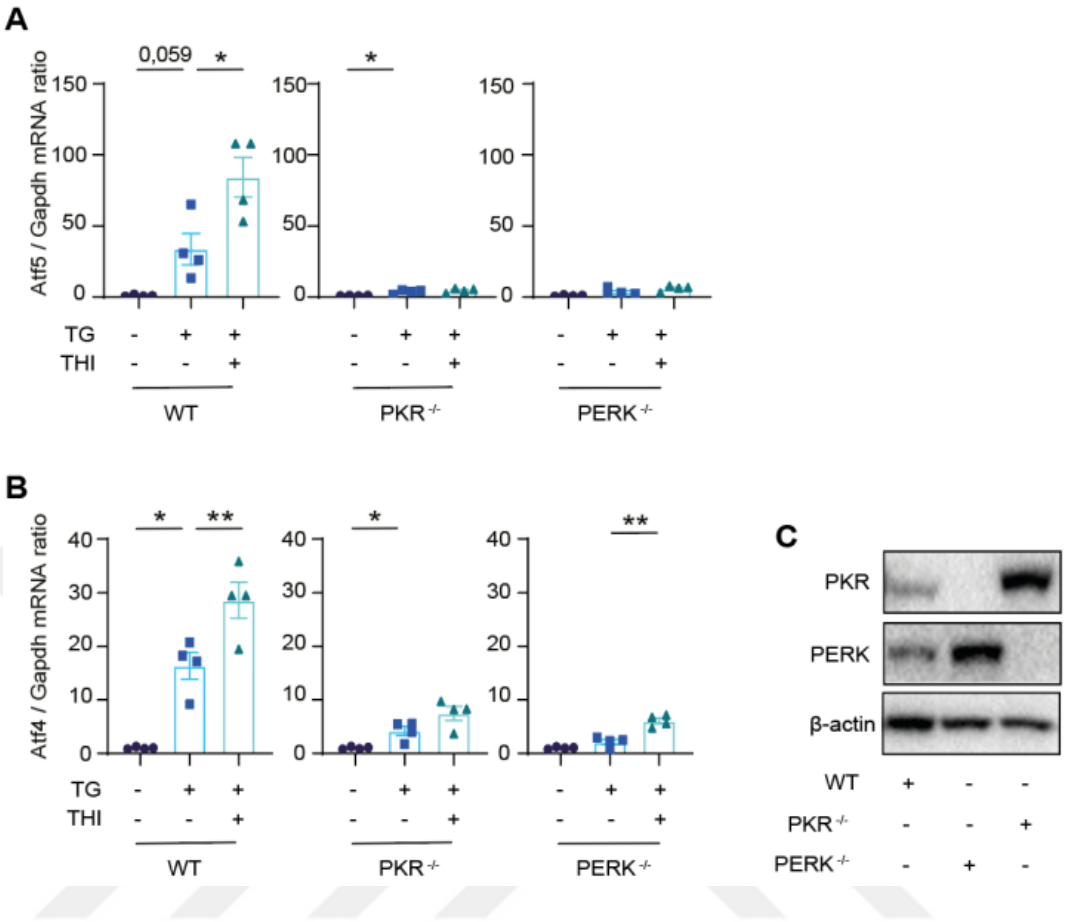

Figure 3. 34: SPL inhibition enhances UPR^{mt} as PKR and PERK dependent manner. (A-B) WT, PKR $^{-/-}$ and PERK$^{-/-}$ MEFs were treated with THI (5 mm) and TG (100 nM) for 12 hours, and total RNA lysate was analyzed by qRT-PCR for Atf5, Atf4 and Gapdh mRNA (n=4 biological replicates) while (C) protein lysates were analyzed by Western blotting using the indicated antibodies (n=3 biological replicates; a representative blot is shown). Data information: All data are mean ± SEM; (n=4) Unpaired t-test with Welch's correction. * P ≤ 0.05, ** P ≤ 0.01, *** P ≤0.001, **** P ≤0.0001. All data are mean ± SEM; (n=3) Unpaired t-test. * P ≤ 0.05, ** P ≤ 0.01.

Since PERK and PKR phosphorylates eif2α and leads to in activation of cellular proteostasis related gene transcription such as ATF4 and ATF5, we directly assessed the effect of IRE1 SPL axis on UPRmt when eif2α is phospho- mutant. To do this, we used eif2α S/S (WT) and eif2α A/A (phospho mutant) MEF cells and treated them with THI under ER stress condition. We found that THI is able to enhance TG-induced transcription of ATF5 and AT4 in eif2α S/S MEFs, however this effect of THI diminished when eif2α is phospho- mutant (Fig 3.35 A-B).

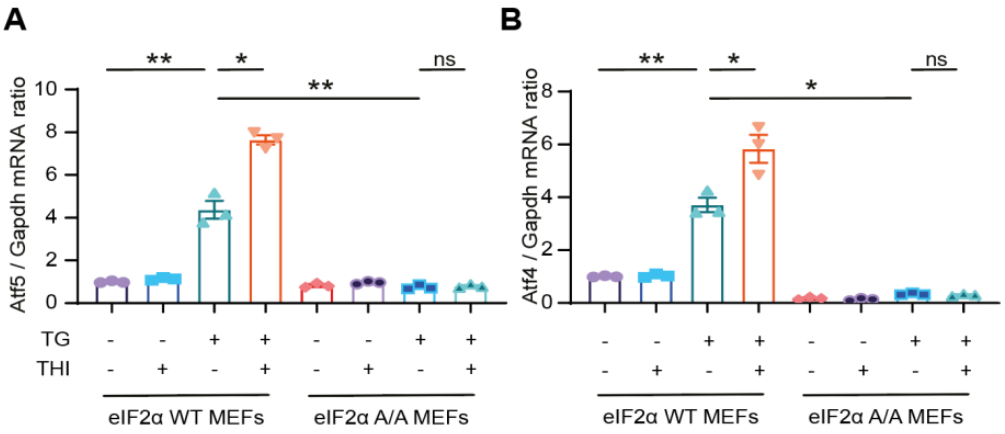

Figure 3. 35: IRE1-SPL axis modulates eif2α to regulate UPR^{mt}. (A-B) eif2α S/S (WT) and eif2α A/A (phospho mutant) MEF cells were treated with THI (5 mm) and TG (100 nM) for 12 hours, and total RNA lysate was analyzed by qRT-PCR for Atf5, Atf4 and Gapdh mRNA (n=4 biological replicates) Data information: All data are mean ± SEM; (n=3) Unpaired t-test with Welch's correction. t-test. * P ≤ 0.05, ** P ≤ 0.01.

To further confirm whether SPL phosphorylation by IRE1 regulates UPRmt through eif2α, we transfected eif2α S/S (WT) and eif2α A/A (phospho mutant) MEF cells with either SPL_WT or SPL_MUT and validated their effect under ER stress conditions. SPL_WT overexpression significantly reduced ER stress-induced UPRmt signaling in eif2α S/S (WT) MEFs and this effect was diminished when IRE1-mediated phosphorylation site was mutated on SPL. However, both SPL WT and SPL-MUT did not affect UPRmt signaling upon ER stress in eif2α A/A MEF cells (Fig 3.36).

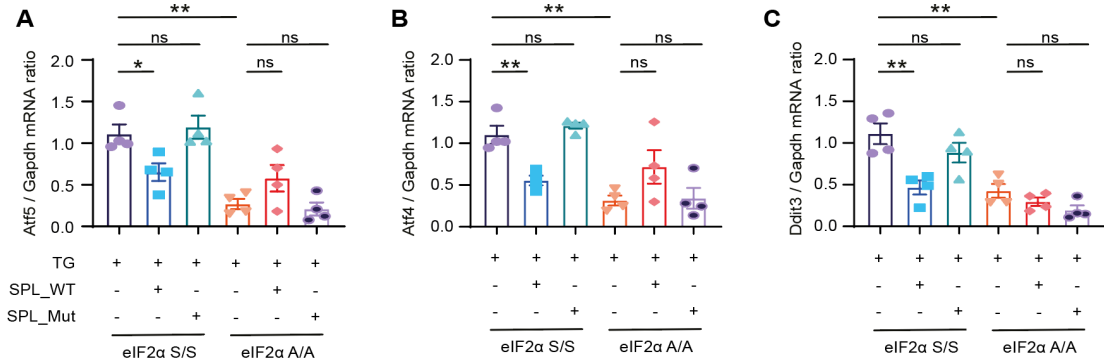

Figure 3. 36 : SPL phosphorylation by IRE1 leads to UPRmt inhibition through eif2α. (A-C) eif2α S/S and eif2α A/A MEFs were transfected with indicated plasmids and treated with treated TG (100 nM) for 16 hours, and total RNA lysate was analyzed by qRT-PCR for Atf5, Atf4, Ddit3 and Gapdh mRNA (n=4 biological replicates). Data information: All data are mean ± SEM; (n=4) Unpaired t-test with Welch's correction. * P ≤ 0.05, ** P ≤ 0.01, *** P ≤0.001, **** P ≤0.0001. All data are mean ± SEM; (n=3) Unpaired t-test. * P ≤ 0.05, ** P ≤ 0.01.

Collectively, these data demonstrate SPL phosphorylation by IRE1 impinges on eif2α phosphorylation to induce a robust UPRmt signaling during ER stress in mammalian cells

3.10 Validation of effect of IRE1-SPL axis on mitophagy

Mitochondrial proteostasis well-coordinated pathway and is maintained by balancing mitochondrial biogenesis, mitochondrial protein synthesis and clearance pathways related to mitochondria such as mitophagy. In this study we are demonstrating that, IRE1- SPL axis regulates mitochondrial proteostasis by controlling UPRmt. We also sought to investigate the effect of IRE1 SPL axis on mitophagy. We found that inhibition of IRE1 kinase domain and overexpression of SPL, both conditions result in UPRmt reduction, leads to activation of mitophagy by inducing the level of mitophagy-related adaptor proteins, such as PARKIN and p62 (Fig 3-37 A-B).

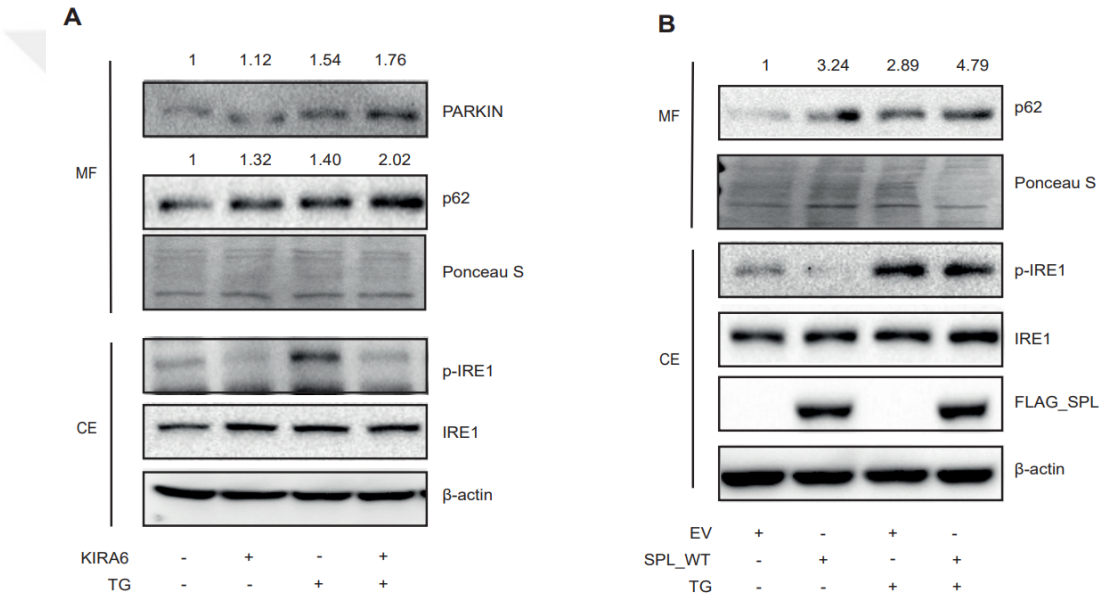

Figure 3. 37: Regulation of mitophagy by IRE1- SPL axis upon ER stress. (A)HEK293T cells were treated with with KIRA6 (5 mm) and TG (100 nM). MF protein lysates were analyzed by Western blotting using specific antibodies for Parkin and p62 while CE protein lysates were analyzed with antibodies for IRE1, p-IRE1 and β-actin. The membrane was stained with Ponceau S. (n=3, biological replicates; a representative blot is shown). (B) HEK293T cells were transfected with the indicated plasmids and treated with TG (100 nM). MF protein lysates were analyzed by Western blotting with antibody against p62 and total CE protein lysates were analyzed using antibodies against IRE1, p-IRE1, SPL and β-actin. Ponceau S was used as loading control. (n=3 biological replicates; a representative blot is shown).

3.11 Validation of effect of mitochondrial stress on ER stress

Until now, we demonstrated that ER stress induced IRE1 regulates mitochondrial proteostasis through its kinase substrate SPL. Inter-organelle stress has been extensively studied and it is obvious that stress is a bidirectional signal transferred to each other. From this end, we sought to examine the effect of mitochondrial stress on UPR^{ER}. To address this, we used doxyxcline, a mitochondrial stressor, and examined the UPR^{ER} and UPR^{mt}. We found that doxycycline induces the expression of both UPR^{ER} and UPR^{mt} genes as well as ER stress related protein

levels in WT MEFs and HEK293 cells (Fig 3.38). These results confirm that mitochondrial stress is sensed by ER and causes ER stress.

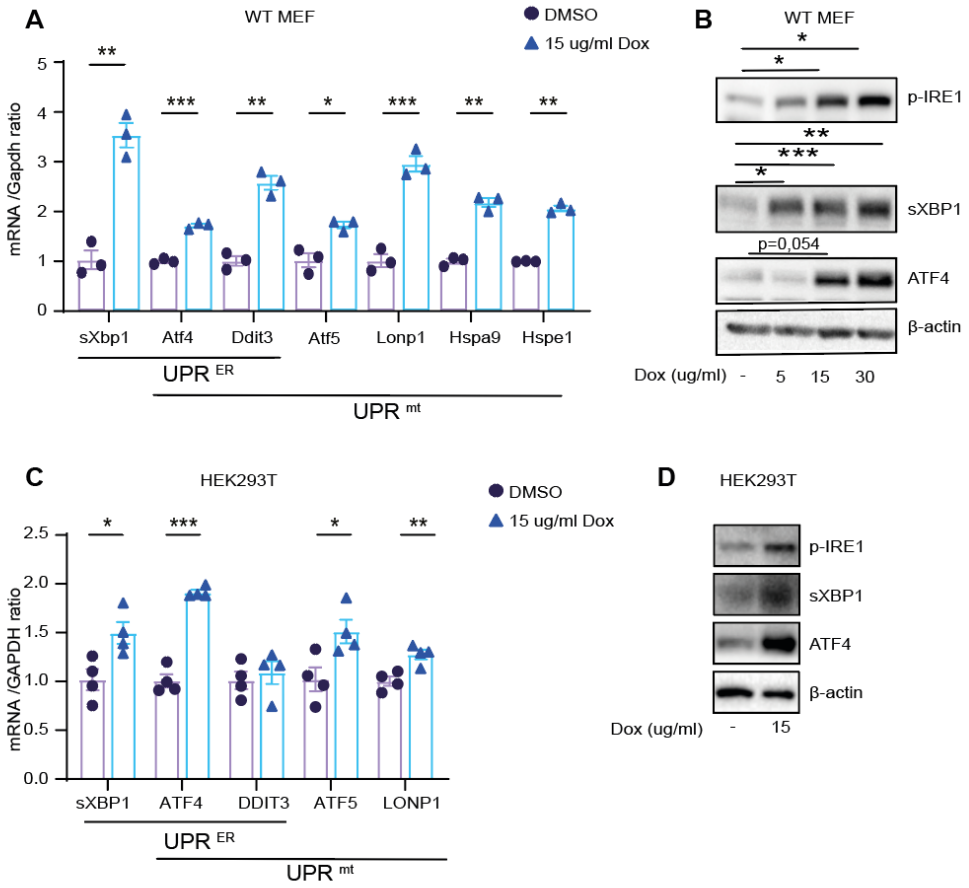

Figure 3. 38: Doxycyline induces ER stress. (A-B) WT MEFs were treated with doxycycline (Dox; 15 µg/ml) for 20 hours: (A) total RNA lysate was analyzed by qRT-PCR for sXbp1, Atf4, Ddit3, Atf5, Lonp1, Hspa9, Hspe1 and Gapdh mRNA (n=3 biological replicates) while (B) total protein lysate was analyzed by Western blotting using specific antibodies for p-IRE1, sXBP1, ATF4 and β-actin (n=3 biological replicates; a representative blot is shown). (C-D) HEK293T cells were treated with Dox (15 µg/ml; 20 hours): (C) total RNA lysate was analyzed by qRT-PCR for sXBP1, ATF4, DDIT3, ATF5, LONP1 and GAPDH (n=4 biological replicates) while (D) total cellular protein lysate was analyzed by Western blotting using specific antibodies for p-IRE1, sXBP1, ATF4 and β-actin (n=3 biological replicates; a representative blot is shown). Data information: All data in A and C are mean ± SEM. Unpaired t-test with Welch's correction. * P ≤ 0.05, ** P ≤ 0.01, *** P ≤0.001, ns=not significant. All data in B and D are mean ± SEM; (n = 3). Unpaired t-test. * P ≤ 0.05, ** P ≤ 0.01, *** P ≤0.001

3.12 Validation of used concentration of TG on mitochondrial Ca^{+2} levels.

To investigate the role of phosphorylation of SPL by IRE1 in mitochondrial proteostasis, we used 100nm TG. TG is a ER toxin which leads to inhibition of SERCA pumps. As a results of this, the Ca^{+2} concentrations in ER is reduced and cytoplasmic concentration is induced. To validate whether TG induces UPR^{mt} by chancing mitochondrial Ca^{+2} levels, we measured

mitochondrial $Ca^{+2}$by using a fluorescent labeling assay (RHOD2). We found that TG concentration used in this study induces UPR^{mt} without chancing mitochondrial Ca^{+2} levels (Fig 3.39).

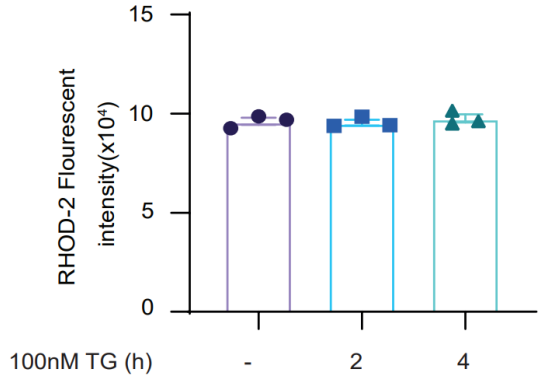

Figure 3. 39: Effect of TG concentration used in this study on mitochondrial Ca^{+2} levels
Mitochondrial Ca^{+2} levels in cells treated with 100 nM TG. WT MEFs were treated with TG (100 nM; 2-4 hours), incubated with RHOD-2AM fluorescent mitochondrial Ca^{+2} indicator and fluorescent readings were measured CytoFLEX analyzer (Beckman Coulter Life Sciences), according to manufacturer's protocol (n=3 biological replicates).

Chapter 4

The contribution of IRE1 in Kawasaki Disease Progression

4.1. Validating ER stress gene expression in Kawasaki disease

To investigate the role of ER stress on Kawasaki disease progression, we first sought to decipher the expression level of ER stress markers in Kawasaki disease set. ER stress gene signature has been determined according to published data and composed of 29 genes which are downstream of the three UPR arms (IRE1/XBP1, ATF6 and PERK/ATF4) **(Fig 4.1**).

UPR arms	Target genes
IRE1/XBP1	*DNAJB11, DNAJC3, EDEM1, EDEM2, EIF2A, ERN1, ERP29, ERP44, HSPA5, PDIA3, PDIA4, PDIA6, SOD2, SSR1, WIPI1, WFS1, XBP1*
ATF6	*CEBPB, DNAJB11, DNAJC3, EDEM1 HSPA5, OS9, PDIA3, PDIA4, PDIA6, RTN3, SEL1L, WIPI1, WFS1, XBP1*
PERK/ATF4	*ATF4, ATF6, CEBPB, DDIT3, EIF2A, EIF2AK2, EIF2AK3, ERP29, HSPA5, S100P, TRIB1, TRIB3*

Figure 4. 1: ER stress related genes which are downstream of UPR arms.

After determining the ER stress signature genes, we analyzed the changes in expression level of these signature genes from whole blood of KD patients compared with healthy controls (HC) in publicly available human transcriptomics datasets (200, 201). We observed that 18 ER stress signature genes were differentially expresses (DEG) in GSE68004 human

transcriptomics dataset and among these DEGs 11 genes from ER stress signature were up regulated in KD patients in comparison to their HC. We observed the similar results in GSE73461 human transcriptomics dataset. Expression level of 10 ER stress signature genes out of 15 DEG increased in KD patients (adjusted p-value (FDR) < 0.05, fold change (FC) > 1.5) **(Figure 4.2).**

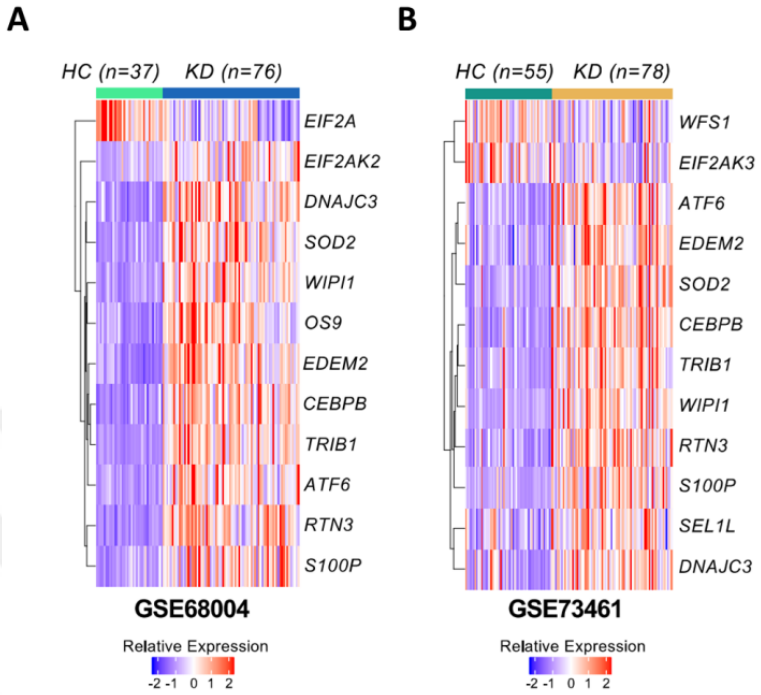

Figure 4. 2: ER stress signature genes expression increased during acute KD. (A, B) Heatmaps showing differentially expressed genes from acute KD patients compared with healthy controls (HC) (n=37 HCs and n=76 acute KD patients for GSE68004; n=55 HCs and n=78 acute KD patients for GSE73461). The statistical analysis has been done by using GEO2R and summary tables were generated with limma topTable function (adjusted p-value (FDR) < 0.05, fold change (FC) > 1.5).

Since patients with KD have high level of inflammatory markers, intravenous immunoglobulin (IVIG) is the gold standard treatment for KD vacuities. From this end, we analyzed ER stress signature gene expression in another data set to compare whole blood of IVIG-treated convalescent KD patients with acute KD patients (GSE63881) (202). We observed that resolution of acute KD progression with IVIG treatment is associated with reduced expression of ER stress signature genes in comparison to KD patients who are not subjected to IVIG treatment **(Figure 4.3)**. Overall, these results suggest disruption ER homeostasis may contribute KD vasculitis development.

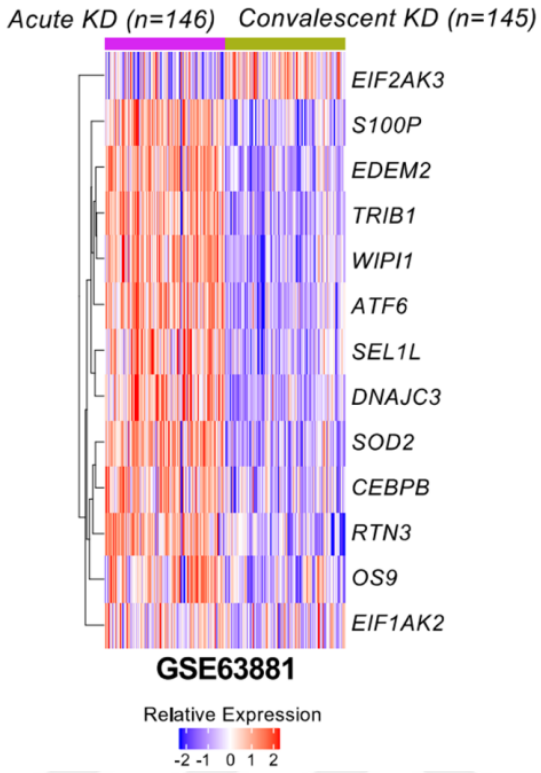

Figure 4. 3: IVIG treatment reduces expression of ER stress signature genes in KD vasculitis. Heatmap illustrating the expression of DEGS identified in Figure 4.2 in whole blood of acute KD compared with convalencent IVIG-treated KD patients (n=146 Acute KD and n=145 Convalescent IVIG-treated patients for GSE63881). The statistical analysis has been done by using GEO2R and summary tables were generated with limma topTable function (FDR < 0.05).

4.2. Determining ER stress gene signature in KD murine model

We next sought to investigate the results obtained from human datasets in mouse model mimicking KD progression. To achieve this, Lactobacillus casei cell wall extract (LCWE) was injected to mice for 1 week and assessed the heart vessel inflammation. As it is previously published (188, 189), LCWE-injection significantly increased heart vessel inflammation in comparison to PBS-injected littermates (Fig 4.4. A-B). We also assessed the impact of LCWE on abdominal aorta dilatation. LCWE-injected mice developed significantly induced infrarenal abdominal aorta aneurysms and dilatation (Fig 4.4. C-D).

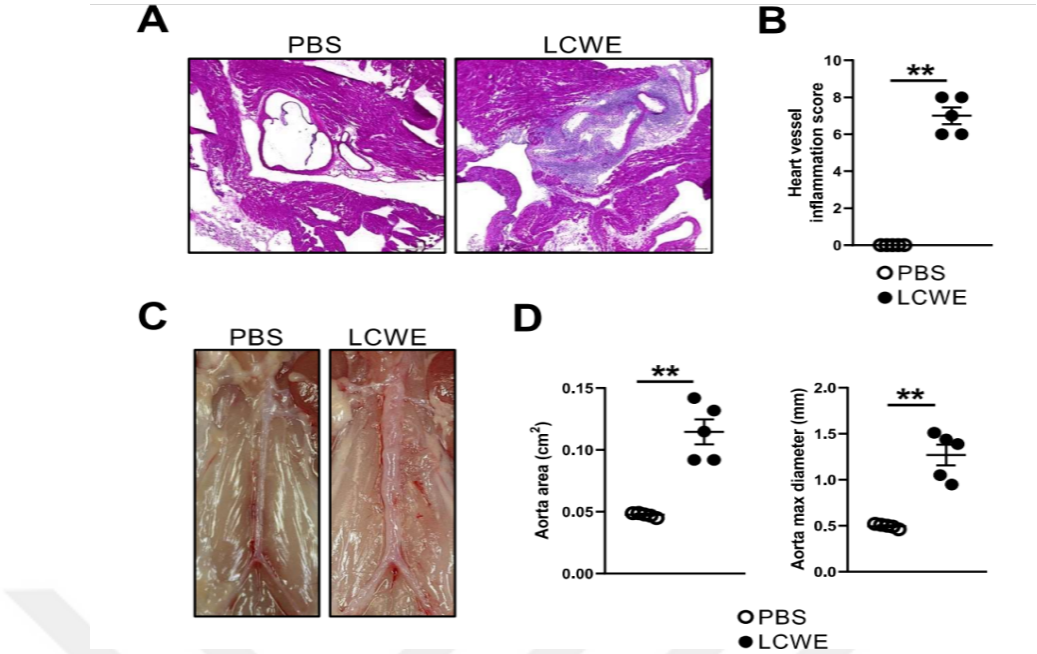

Figure 4. 4: Increased heart vessel inflammation and dilatation of aorta in LCWE-injected mice. (A, B) Representative H&E staining of heart sections (A) and heart vessel inflammation quantification (B) of either PBS- or LCWE-injected WT mice at one-week post-injection (n=5/group). Scale bars: 500µm. (C, D) Representative pictures of the abdominal aorta area (C), abdominal aorta area and maximal abdominal aorta diameter quatifications (D) of WT mice injected with either PBS and LCWE, one-week post-LCWE injection (n=5/group).

Next, we analyzed publicly available gene expression data set (mRNA-Seq) obtained from aortas of PBS- or LCWE-injected mice (GSE141072) (199). We exhibited that 10 ER stress signature genes were differentially expressed in LCWE-injected mice. From those, Cebpb (CCAAT Enhancer Binding Protein Beta) and Trib1 (Tribbles Pseudokinase 1) not only significantly induced in abdominal aorta of LCWE-injected mice but also consistently in the three transcriptomics dataset from acute KD patients (Figure 4.5). Expression of four of these DEGs (Eif2ak2 (Eukaryotic Translation Initiation Factor 2 Alpha Kinase 2), Os9 (OS9 Endoplasmic Reticulum Lectin), Cebpb and Trib1) increased in PBMC from acute KD patients and their expression reduced upon IVIG-treated convalescent KD patients

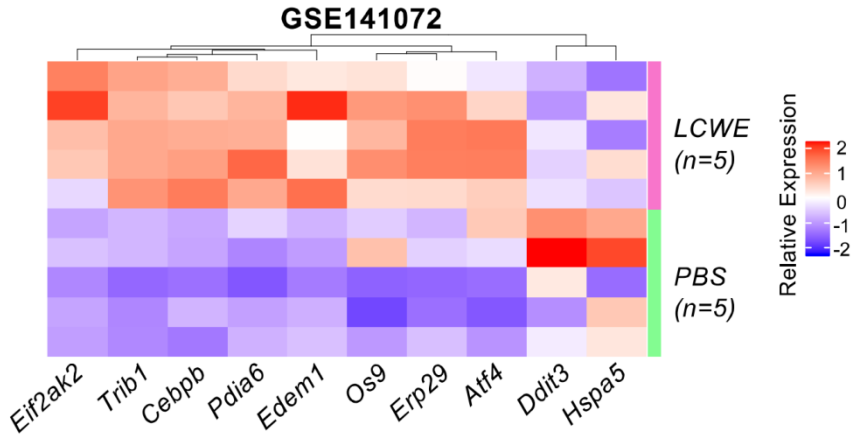

Figure 4. 5: Elevated expression of ER stress signature genes in abdominal aorta of Kawasaki murine model. Heatmap illustrating the expression of ER stress signature DEGs in abdominal aorta tissues of PBS and LCWE-injected mice (n=5/groups; GSE141072) (FDR < 0.05, FC > 1.5). Blue-red color gradient: low to high expression relative to the mean of each column.

Next, we sought to investigate which cellular subsets ER stress signature genes in KD murine model. To do this, we analyzed a published single cell RNA sequencing datasets (sc-RNA-seq) obtained from abdominal aortas collected from LCWE-injected (pool of n=7) compared with PBS-injected (pool of n=9) mice (GSE178765). In published dataset, it has been shown that LCWE injection results in intense immune cell infiltration in the abdominal aorta of LCWE injected mice. The cellular subsets were validated by flow cytometric analysis subsequently (190). We observed that ER stress signature genes were commonly expressed by fibroblast and other stromal cells such as vascular smooth muscle cells (VSMCs) in PBS-injected mice. However, LCWE injection caused the expression of ER stress signature genes in immune cells which are infiltrating to the abdominal aorta. We detected that Ern1, which encodes IRE1, and its endoribonuclease target Xbp1 expression induced in monocytes, macrophages, dendritic cells (DCs) and lymphocytes that infiltrated the abdominal aorta upon LCWE injections. As expected, expression profiles of specific Xbp1 target genes such as Erp44, Sod2, and Ssr1 showed similar cell type specific patterns. Since ER stress and its downstream pathways are well orchestrated and integrated by different ER stress sensor arms, we also analyzed the expression level of ER stress signature genes which are under control of Xbp1/Atf6 and Xbp1/Atf4. Sc-RNA-seq results exhibited that genes which are regulated by Xbp1/Atf6 such as Dnajc3, Dnajb11, Edem1, Hspa5, Pdia3 and Pdia4 and Xbp1/Atf4 such as Erp29, and Hspa5 were started to express in inflammatory cell types rather than stromal cells (Fig 4.6). Collectively, these findings indicate that LCWE-induced vasculitis may be driven by ER stress through promoting to vascular tissue inflammation.

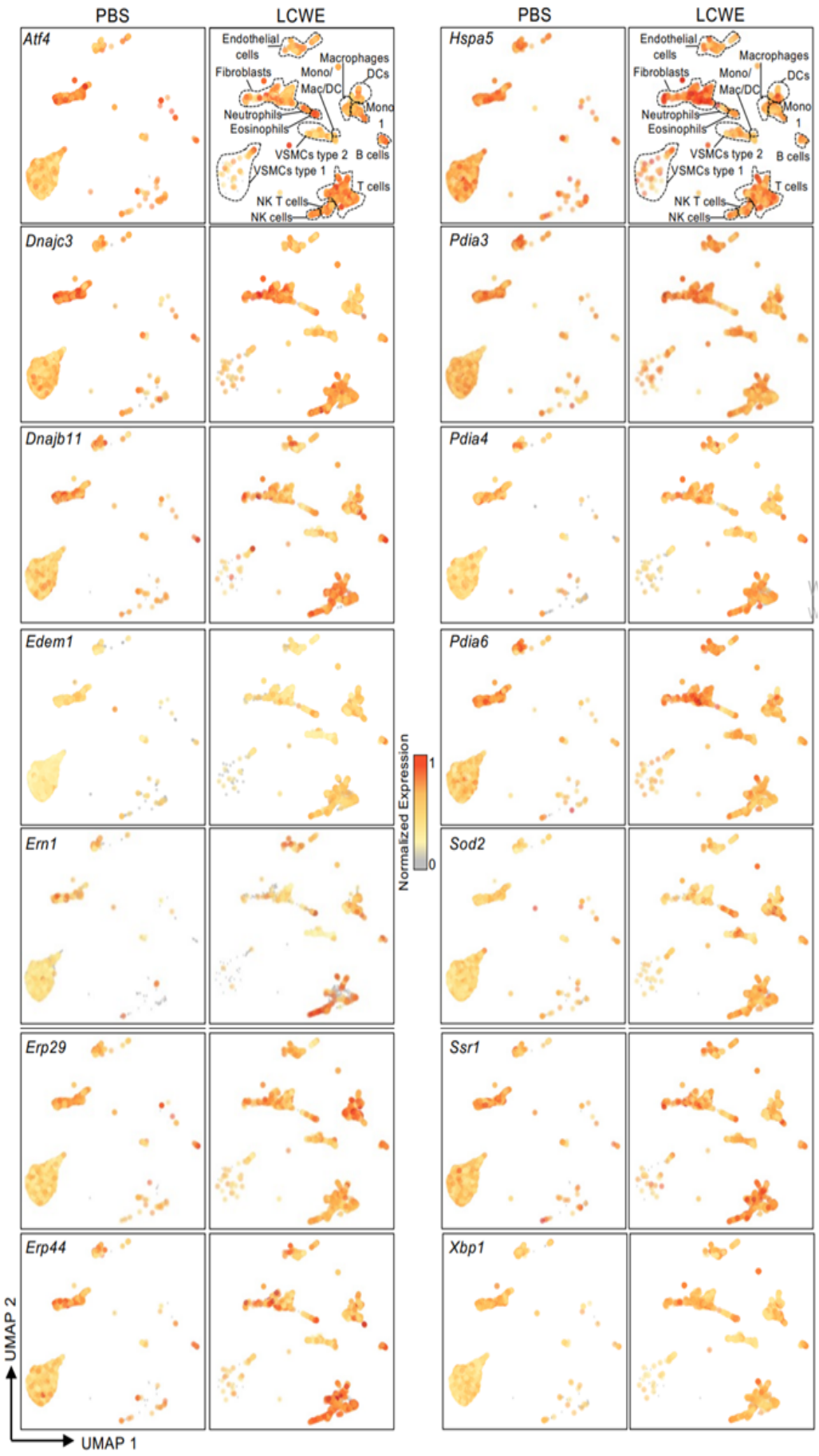
PBS
LCWE
PBS
LCWE
Atf4
Endothelial cells
Macrophages
Fibroblasts
Mono/ Mac/DC
DCs
Mono 1
Neutrophils
Eosinophils
VSMCs type 2
B cells
VSMCs type 1
T cells
NK T cells
NK cells
Hspa5
Dnajc3
Pdia3
Dnajb11
Pdia4
Edem1
Pdia6
Ern1
Sod2
Erp29
Ssr1
Erp44
Xbp1
Normalized Expression
1
0
UMAP 2
UMAP 1

Figure 4. 6: Immune cells infiltrating LCWE-induced abdominal aorta aneurysms express ER stress signature genes. Data generated from a previously published scRNAseq dataset generated from abdominal aorta tissues of PBS (n=9 tissues pooled) and LCWE-injected (n=6 tissues pooled) mice (GSE178765). UMAP visualization has been used and gradient expressions of selected ER stress signature genes were represented. Grey-yellow-red gradient: min-max normalization of CP10K expression. CP10K indicates counts per 10,000 reads; DCs, dendritic cells; Mono, monocytes; Mac, machrophages; NK, natural killer cells, VSMCs, vascular smooth muscle cells.

4.3 IRE1 activity increase upon LCWE-injection

After we validating increased ER stress related gene expression in publicly available transcriptomics and scRNA-seq data sets, we next sought to evaluate the altered protein levels of ER stress related genes in cardiovascular lesions. We injected WT mice with either PBS or LCWE for one week and we collected related tissues (Fig 4.7.A). ERp57, also known as protein disulfide-isomerase A3 (PDIA3) is shown to increase under ER stress conditions (205). We evaluate the protein level of ERp57 in LCWE-injected mice in comparison to PBS-injected mice. We observed that LCWE injection leads to increased protein levels of ERp57 in heart tissue indicating induced ER stress (Fig 4.7. B).To evaluate the IRE1 arm of UPR activation; we assessed the phosphorylation of IRE1 in the abdominal aorta of PBS- and LCWE-injected WT mice. IRE1 phosphorylation (p-IRE1) markedly increased in LCWE-injected mice in comparison to PBS-injected WT mice (Fig 4.7.C). To strengthen results showing IRE1 activation in abdominal aorta upon LCWE injection, we next immunoprecipitated total IRE1 from abdominal aorta of PBS- and LCWE injected WT mice and probed with p-IRE. Compared with PBS-injected WT mice, IRE1 phosphorylation is elevated in aortas of LCWE-injected WT mice (Figure 4.7.D). Overall, these results suggest that IRE1 is activated upon LCWE injection in KD murine model.

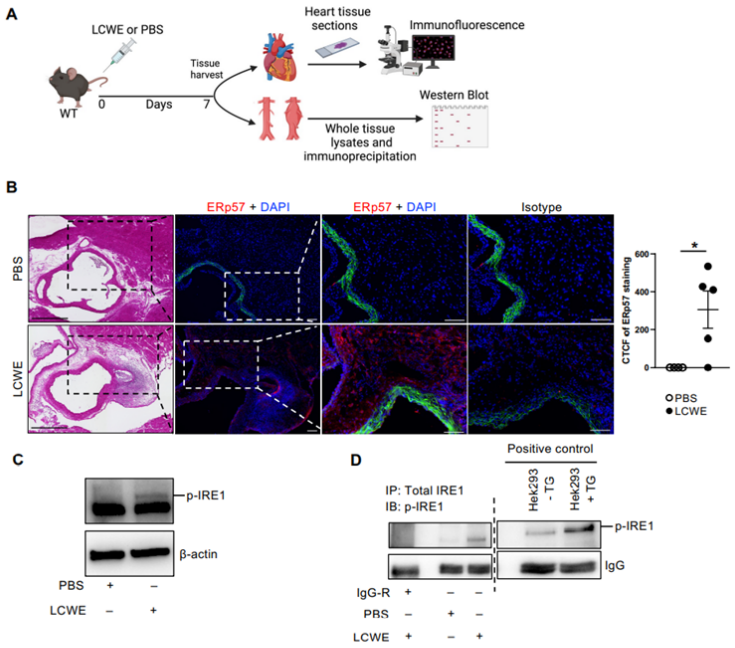

Figure 4. 7: IRE1 pathway-related proteins levels increase during LCWE-induced KD vasculitis. (A) Experimental schema of experimental setup. (B) H&E and immunofluorescent staining of ERp57 (Red) and DAPI (Blue) in heart sections of PBS or LCWE-injected, at one week of post injection (n=4-5/group). Scale bars, 100 μm. Quantification of ERp57 fluorescence intensity (right panel). (C) Tissue lysates of abdominal aorta tissues from PBS (n=3 tissues pooled/lane) and LCWE-injected mice (n=2 tissues pooled/lane) at one-week post-injection was probed with p-IRE1 and β-actin antibodies. (D) Abdominal aorta lysates from PBS and LCWE-injected mice (n=3/condition) were immunoprecipitated (IP) using anti-IRE1 antibody. IgG rabbit antibody was as an IP control. Western blot was performed using anti-phospho IRE1 (S747) antibody. Lysates from DMSO and TG- treated HEK293T cells were used as positive controls. *$p<0.05$ by Mann-Whitney test.

4.4 LCWE induces inflammation by activating IRE1 RNase domain

ER stress has been shown to involve in NLRP3 inflammation activation and IL-1β production in several inflammatory disease conditions. However, the role of ER stress and especially IRE1 arm on NLRP3 activation and IL-1β production is still needed to be investigated in KD progression. By using spatial transcriptomics of hearth tissue from PBS- and LCWE-injected WT mice, it has been shown that LCWE injected mice exhibited increased expression level of Nlrp3, Pycard, Casp1 and IL-1β in myeloid cells infiltrating the cardiovascular lesions in comparison to PBS-injected mice (190). Increased expression level of specific unit of inflammasome complex and its downstream activators may act as primary source of IL-1β secretion. Moreover, proinflammatory macrophages in cardiovascular lesions of LCWE injected mice exhibit caspase 1 activity and inhibited caspase-1 activity resulted in reduced LCWE-induced abdominal aorta aneurysms (189). Since our scRNAseq results also exhibited that LCWE injection increases expression of ER stress related genes in myeloid cells such as macrophages and monocytes, we next sought to investigate the impact of LCWE on ER stress activation in bone marrow-derived macrophages (BMDMs). BMDMs stimulated with LCWE leads to IRE1 activation and increased level of ERp57 protein. Well known ER stress inducer Tunicamycin was used as positive control (Fig 4.8 A). Previous study has been shown that inhibition of IRE1 RNase domain alleviates lipid induced inflammasome activation. We also examined the inhibition of which enzymatic activity of IRE1 responsible for NLRP3 inflammasome activation induced by LCWE stimulation. To test this, we used specific IRE1 kinase inhibitors, KIRA6 and AMG18, and specific IRE1 RNase inhibitor 4μ8c. LCWE stimulation led to a robust IRE1 activation which is inhibited by IRE1 kinase inhibitors but not by RNase inhibitor of IRE1, as expected. Inhibition of IRE1 RNase domain by 4μ8c decreased secreted level of both IL-1β and Caspase-1 (Fig 4.8 B).

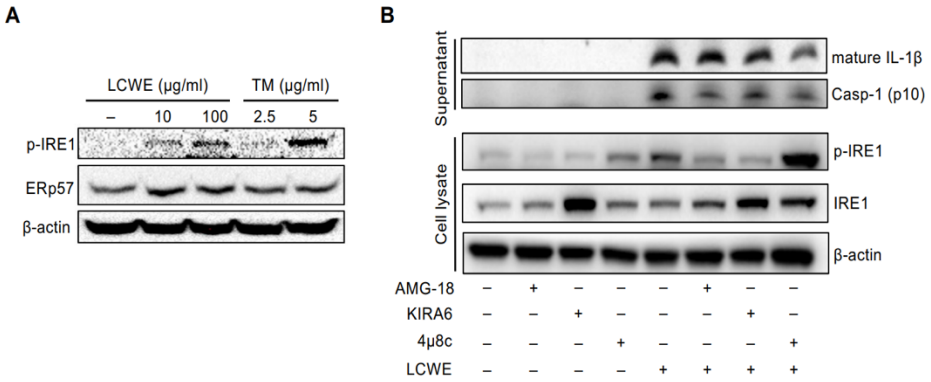

Figure 4. 8: LCWE induces IL-1β and Caspase 1 secretion through IRE1 RNase domain. **(A)** BMDMs obtained from WT mice were treated with indicated doses of LCWE for 16h. The ER stress inducer Tunicamycin (TM) was used as positive control. Protein lysates were analyzed by Western blotting using specific antibodies against p-IRE1, ERp57 and β-actin. **(B)** BMDMs obtained from WT mice were pre-treated with IRE1 kinase inhibitors AMG-18 (3µM), KIRA6 (15 µM) and Rnase inhibitor 4µ8c (100µM) for 1 hour and then treated with LCWE (75µg/ml) for 14 hours along with the inhibitors. The supernatants were collected and analyzed by western blotting for cleaved caspase-1 (p10) and mature IL-1β. Whole cell lysates were analyzed by western blotting using specific antibodies against p-IRE1, IRE1 and β-actin (n=3).

To further validate the IRE1 contribution in myeloid cells during LCWE-induced KD progression, we generated IRE1 deficiency by crossing Floxp-flanked *Ern1* (*Ern1*$^{fl/fl}$) mouse with Lyz2-Cre (*LysM*$^{Cre+}$) transgenic mouse to create myeloid cells-restricted *Ern1* knock-out (*LysM*$^{Cre+}$*Ern1*$^{Δ/Δ}$). LCWE stimulation markedly increased p-IRE1 and total IRE1 levels in BMDM obtained from *Ern1*$^{fl/fl}$ mice, indicating LCWE activates IRE1. However, these 2 proteins could not be detected in BMDM lysates of *LysM*$^{Cre+}$*Ern1*$^{Δ/Δ}$ mice, which confirmed specific IRE1 deletion in myeloid cell. We also assessed the effect of IRE1 in inflammasome activation by measuring mature IL-1β and caspase-1 secretion. We observed that LCWE-induced inflammasome activation in *Ern1*$^{fl/fl}$ mice reduced in IRE1 deficient BMDMs collected form *LysM*$^{Cre+}$*Ern1*$^{Δ/Δ}$ (Fig 4.9. A). LCWE stimulation also induced the expression level of spliced form of Xbp1 (sXbp1), which is IRE1 RNase domain target, in *Ern1*$^{fl/fl}$ BMDMs but not in in BMDMs generated from *LysM*$^{Cre+}$*Ern1*$^{Δ/Δ}$ mice. This is another layer of control to check the effect of LCWE on IRE1 activation in *Ern1*$^{fl/fl}$ BMDMs and IRE1 deficiency in *LysM*$^{Cre+}$*Ern1*$^{Δ/Δ}$ mice. LCWE stimulation induced the expression level of proinflammatory cytokines' gene expression such as IL-1β, Il-6 and Tnfα in *Ern1*$^{fl/fl}$ BMDMs. Furthermore, IRE1 deficiency significantly reduced LCWE- induced IL-1β and Il-6 gene expression (Fig 4.9. B).

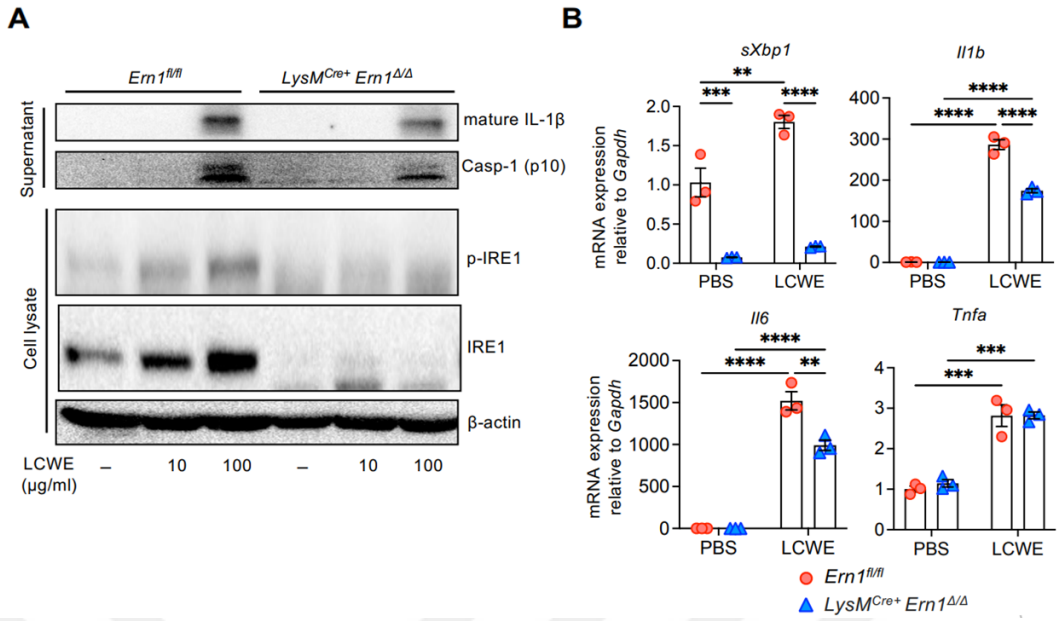

Figure 4. 9: IRE1 deficiency reduces LCWE-induced proinflammatory response. (A) BMDMs derived from *LysM*$^{Cre+}$*Ern1*$^{\Delta/\Delta}$ and littermate control *Ern1*$^{fl/fl}$ mice were treated with indicated doses of LCWE for 16h to activate the inflammasome. Supernatants were collected and analyzed by western blotting for mature IL-1β and cleaved caspase-1 (p10). Whole cell lysates were prepared from the same cells and analyzed by western blotting using specific antibodies against IRE1, p-IRE1, and β-actin (n=3). (B) qRT-PCR of sXbp1, IL-1β, Il-6 and Tnfα transcripts in BMDMs derived from *LysM*$^{Cre+}$*Ern1*$^{\Delta/\Delta}$ and littermate control *Ern1*$^{fl/fl}$ mice were treated with either PBS or LCWE. **p<0.01, ***p<0.001, ****p<0.0001 by 2-way ANOVA with Tukey's multiple comparison test.

4.5 IRE1 deficiency in myeloid cells reduces the development of LCWE-induced KD cardiovascular lesions

To further validate IRE1 contribution in myeloid cells upon LCWE-stimulated KD vasculitis in vivo, we injected LCWE to *LysM*$^{Cre+}$*Ern1*$^{\Delta/\Delta}$ and littermate control *Ern1*$^{fl/fl}$ mice. Myeloid cell specific IRE1 deficient mice exhibited reduced LCWE-induced heart vessel inflammation (Fig 4.10 A-B). We also assessed abdominal aorta aneurysms by measuring maximal aorta diameter and area. Myeloid specific IRE1 deficiency significantly reduced LCWE induced abdominal aorta aneurysms (Fig 4.10 C-D).

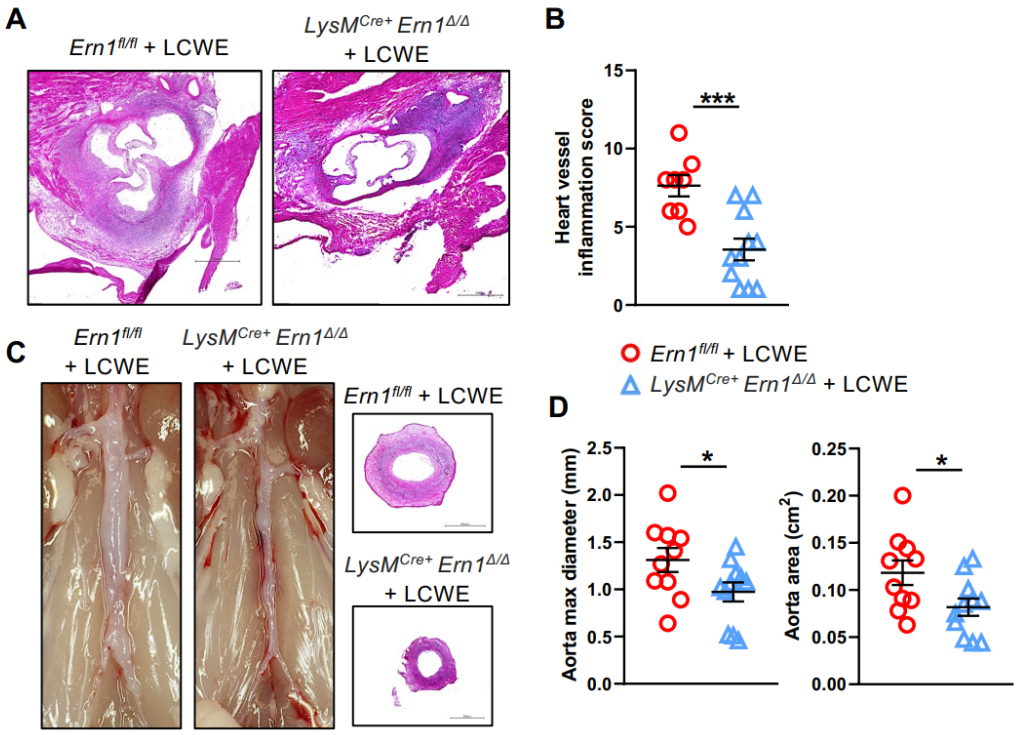

Figure 4. 10: Myeloid cell-specific IRE1 deficiency reduces the development of LCWE-induced KD cardiovascular lesions. (A, B) Representative H&E staining of heart sections (A) and heart vessel inflammation score (B) of LCWE-injected $Ern1^{fl/fl}$ (n=8) and LCWE-injected $LysM^{Cre+}Ern1^{\Delta/\Delta}$ (n=11) mice at two weeks post-LCWE injection. (C, D) Representative pictures of the abdominal aorta area, H&E staining of abdominal aorta cross-section (C) and maximal abdominal aorta diameter and aorta area measurements (D) of LCWE-injected $Ern1^{fl/fl}$ (n=10) and LCWE-injected $LysM^{Cre+}Ern1^{\Delta/\Delta}$ (n=11) mice at 2 weeks post-LCWE injection. Scale bars, 500µm. *p<0.05, **p<0.01, ***p<0.001 by Student's t test.

We additionally measured the caspase 1 activity by using fluorescent-labeled inhibitor of caspase assay (FLICA) in cardiovascular lesions. Caspase-1 activity significantly inhibited in myeloid cell specific IRE1 deficient mice compared to control littermates (Fig 4.11 A-B). In parallel to this, LCWE- induced serum IL-1β levels significantly reduced in $LysM^{Cre+}Ern1^{\Delta/\Delta}$ in comparison to control mice (Fig 4.11 C). Collectively these results exhibit the contribution of IRE1 in LCWE-induced inflammation in cardiovascular tissues.

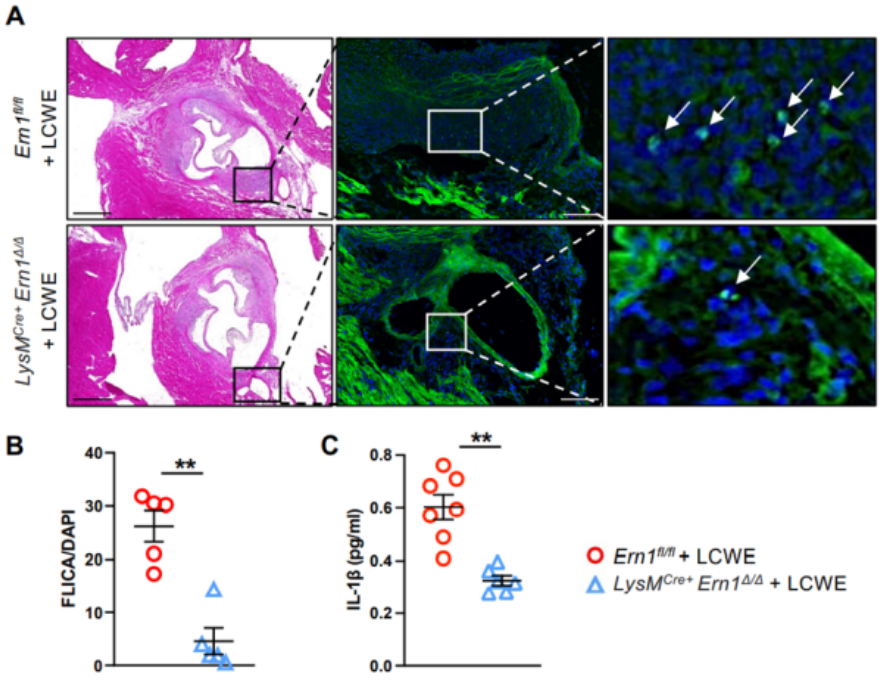

Figure 4. 11: Myeloid cell-specific IRE1 deficiency reduces LCWE-induced inflammatory markers. H&E staining, FLICA staining (A) and quantification of FLICA staining (B) in heart tissues of LCWE-injected *Ern1*$^{fl/fl}$ (n=5) and LCWE-injected *LysM*$^{Cre+}$*Ern1*$^{\Delta/\Delta}$ (n=5) at 2 weeks post-LCWE injection. FLICA+ cells were indicated with white arrows. Scale bars for H&E staining: 500µm; Scale bars for FLICA: 100 µm. (C) Serum IL-1β levels in LCWE-injected *Ern1*$^{fl/fl}$ (n=7) and LCWE-injected *LysM*$^{Cre+}$*Ern1*$^{\Delta/\Delta}$ (n=6) mice at two weeks post-LCWE injection. **p<0.01 by Mann-Whitney test. FLICA; fluorescent-labeled inhibitor of caspase assay.

4.6 Pharmacological inhibition of IRE1 RNase domain prevents KD progression

We next examined if pharmacological inhibition of IRE1 prevents or decreases the severity of LCWE-induced KD progression. Inhibition of IRE1 RNase domain has been shown to reduce IL-1β signaling pathway in atherosclerosis(33). Based on the published data showing effect of 4µ8c cardiovascular disease progression, we injected WT mice daily either with vehicle or 4µ8c beginning 2 days prior to LCWE injection to assess the contribution of IRE1 RNase domain in KD progression. We exhibited that inhibition of IRE1 RNase domain by using 4µ8c leads to reduced LCWE- induced heart inflammation (Fig 4.12 A-B). We also observed that, RNase domain inhibition of IRE1 leads to significant reduction in development of abdominal aorta dilation (Fig 4.12 C-D).

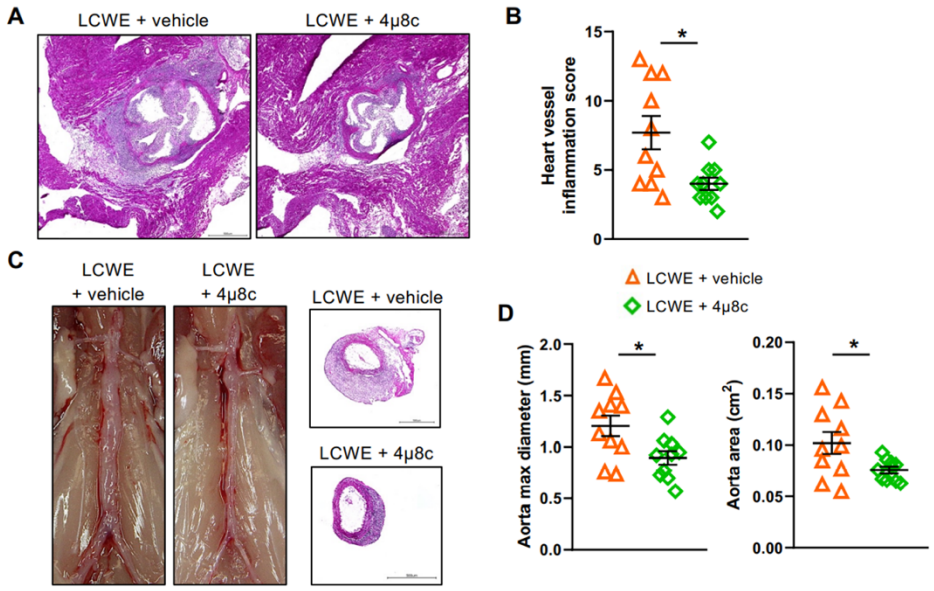

Figure 4. 12: IRE1 RNase domain inhibition with the small molecule inhibitor 4μ8c reduces cardiovascular lesion formation in the KD vasculitis murine model. (A, B) Representative H&E staining of heart sections (A) and heart vessel inflammation quantification (B) of LCWE-injected WT mice treated with either vehicle or 4μ8c (2 days prior injection), one week post-LCWE injection (n=10/group). (C, D) Representative pictures of the abdominal aorta area, H&E staining of abdominal aorta cross-section (C) and maximal abdominal aorta diameter and aorta area measurements (D) of LCWE-injected WT mice treated with vehicle or 4μ8c (2 days prior injection), one week post-LCWE injection (n=10/group). Scale bars, 500μm.

We also measured the Casp-1 activity by FLICA staining in LCWE-injected WT mice treated with either vehicle or 4μ8c. LCWE-induced caspase-1 activity

significantly blocked in mice received 4μ8c compared with vehicle-treated controls (Fig 4.13 A-B). Overall, these *in vivo* findings consistently confirm our *in vitro* observations and indicate that targeting IRE1 with genetic models or small molecules counteracts progression of LCWE-induced KD vasculitis.

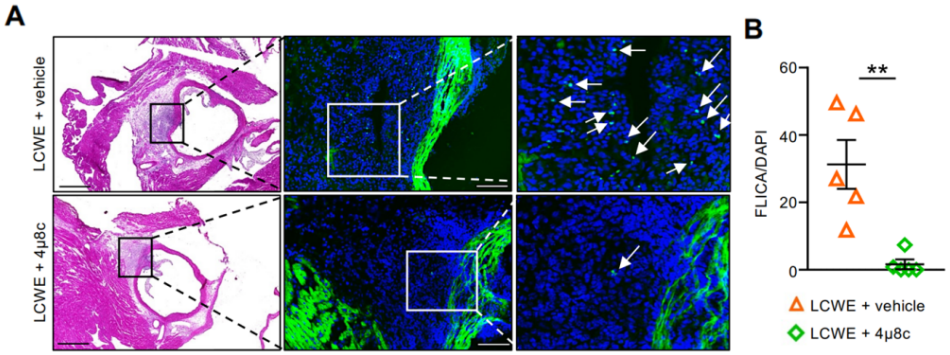

Figure 4. 13: Targeting IRE1 with 4μ8c counteracts LCWE-induced Caspase 1 activity. H&E staining, FLICA staining (A) and quantification (B) in heart tissues of LCWE-injected WT mice treated with either vehicle or 4μ8c, one week post injection (n=5/group). White arrows indicate FLICA+ cells. Scale bars H&E staining: 500μm; Scale bars FLICA: 100μm. **p<0.01 by Student's t test with Welch's correction. FLICA; fluorescent-labeled inhibitor of caspases assay.

Altogether, these findings are consistent with our in vitro observations and indicate that genetic or pharmacological targeting of IRE1 is protective against LCWE-induced KD vasculitis.

Chapter 5

ER membrane remodeling by bioactive lipid molecules

5.1 Blocking lipid induced inflammation activation and inflammation by using bioactive lipid

Excessive lipid stress leads to membrane- initiated UPR activation in macrophages. For example, IRE1 and PERK assembles into higher oligomers to transmit the stress within the organelles. Despite the activation of unfolded proteins, excessive lipid stress does not require ligand binding to induce ER stress. Saturated fatty acids (SFA), such as Palmitate have been shown to induce ER stress and leads to inflammasome activation (33, 49). On the other hand, as result of organ specific de novo lipogenesis (DNL), distinct bioactive lipids such as Palmitolate (PAO) can be generated. PAO regulates lipid metabolism and regulates lipid metabolism in liver and improves glucose utilization (206).
Here, we assessed the effect of PAO on SFA induced inflammation activation in macrophages. As earlier studies showed that treatment of PA induced the activation of NLRP3 inflammasome and IL-1β secretion in lipopolysaccharide (LPS) - primed BMDMs. PA treatment of LPS-primed BMDM activated caspase-1 secretion. Whereas cotreatment with PAO blocked both IL-1β and caspase-1 secretion (Figure 5.1.A-B). These results confirm, PAO suppresses SFA induced inflammasome activation.

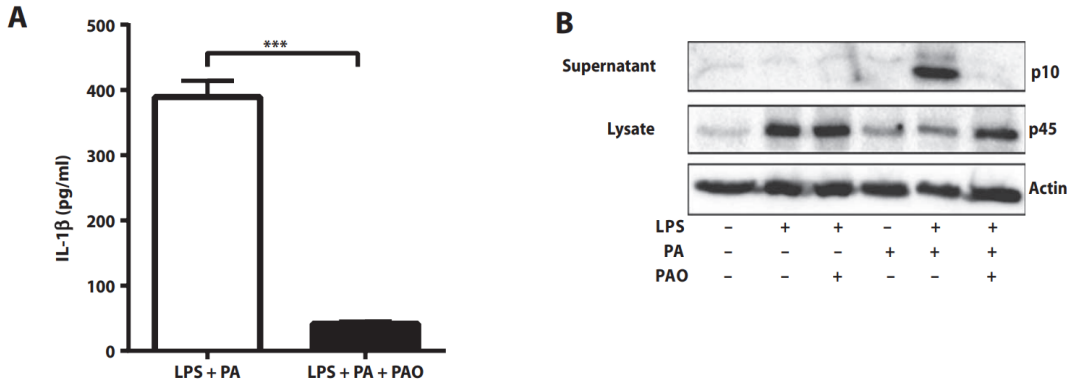

Figure 5. 1: PAO prevents lipid-induced proinflammatory cytokine expression and inflammasome activation in macrophages. (A) Concentrations of secreted IL-1b in supernatants of LPS-primed BMDM stimulated with PA or PAO, alone or together (n = 8). (B) Immunoblots for active caspase-1 (p10) from supernatant and pro–caspase1 (p45) and actin from cell lysate of BMDM. Blots shown are representative of three independent experiments.

5.2. Incorporation of PAO into ER membrane

Lipotoxicity, lipid- induced cellular dysfunction, is related to changes in lipid composition of cellular membranes (207, 208). Increased SFA or cholesterol in the cellular membranes lead to membrane stiffening and changes in ER structure. PAO induced lipidomics remodeling of cellular membranes and tissues may underlie the resilience of ER to lipotoxic stress. To investigate the mechanisms behind how PAO reduces SFA- induced inflammasome activation, we assessed the corporation of PAO into ER membranes in BMDM cells. We found that ER compartments from macrophages reflects the increase in total PAO and MUFA/SFA ratios after PAO treatment ($P < 0.05$, Figure.5.2. A; $P < 0.01$, Figure. 5.2 B). PAO is incorporated into all ER lipid species (Figure.5.2 .C).

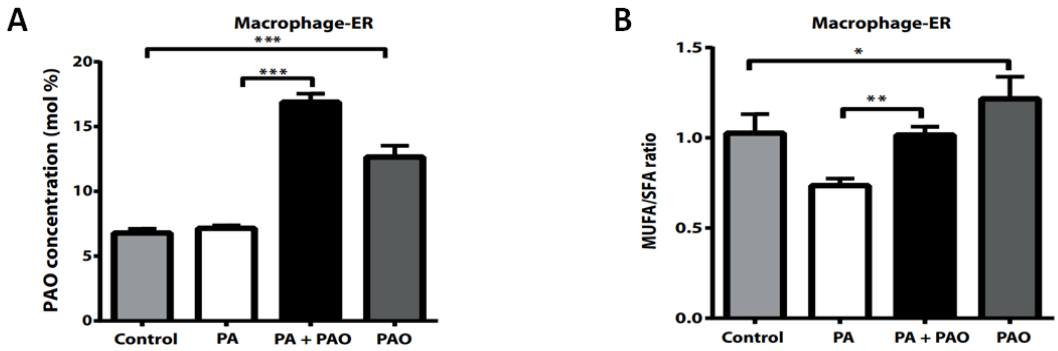

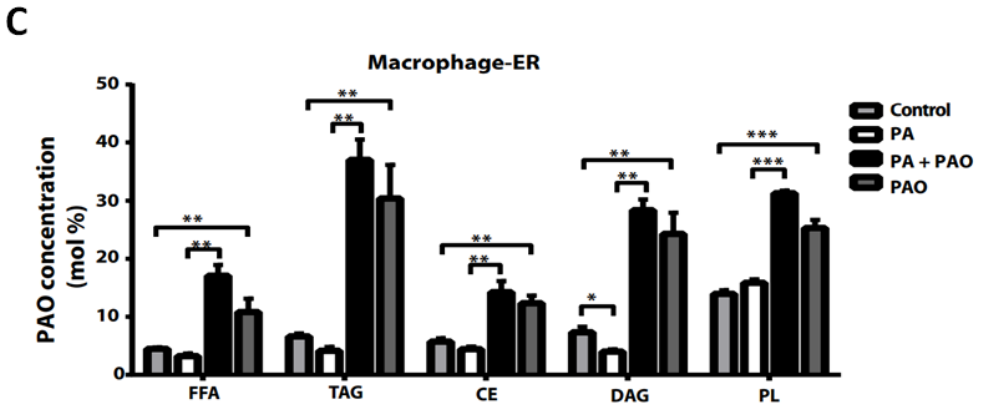

Figure 5. 2: PAO regulates lipid composition in the ERs from macrophages. ER fractions were isolated from RAW 293.6 macrophages and analyzed. (A) Mean concentration (mol %) of C16:1n7. (B) MUFA/SFA ratio. (C) Mean concentration (mol %) of C16:1n7 in various lipid classes. Data are means ± SEM. *P < 0.05, **P < 0.01, ***P < 0.001. n = 4. Nonparametric KruskalWallis test and unpaired two-tailed Student's t test were used for statistical analysis. Free fatty acids (FFA), TAG (triglycerides), cholesterol ester (CE), diacylglycerol(DAG), phospholipids (PL).

5.3 Resolving ER stress by reducing IRE1 oligomerization

Efficient incorporation of PAO into other lipid species together with an increase in MUFA/SFA ratio in the ER membrane suggests that PAO treatment could promote robust changes in membrane dynamics and reduces ER stiffness. Changes in lipid composition of ER membrane may alter oligomerization and activation of UPR sensors that are resident on ER membrane. To investigate that, we used HEK293 cells that are stably expressing GFP-IRE1 plasmid. We have found that PA induced formation of oligomerization of IRE1 largely prevented by cotreatment with PAO (Figure 5.3. A). We also revealed that PA induced IRE1 activation (as assessed by IRE1 phosphorylation and spliced XBP1 protein) was blocked by PAO (Figure 5.3. B)

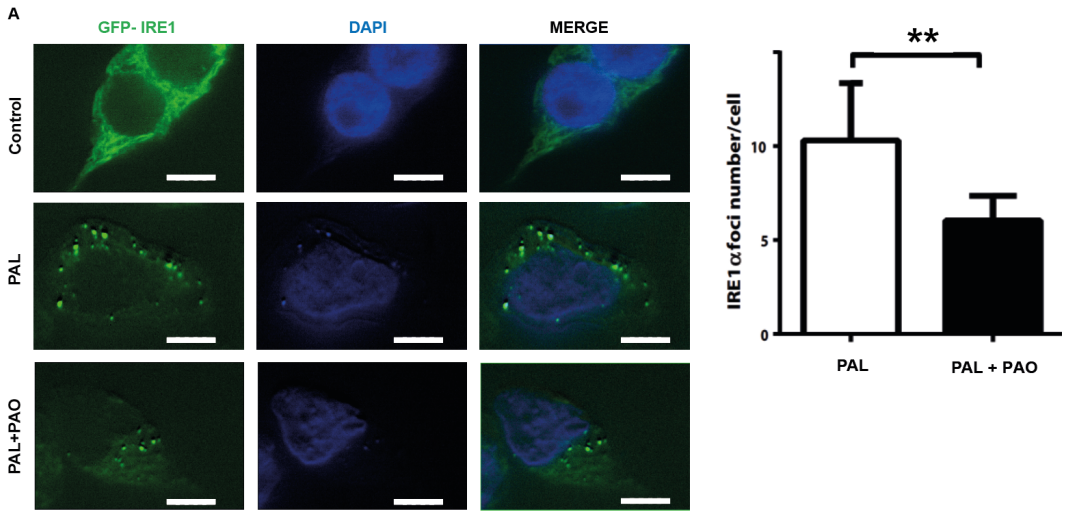

Figure 5. 3: PAO resolves ER stress by preventing IRE1 activation through oligomerization (A) HEK293 cells expressing GFP-IRE1 were treated with PA or PAO, alone or together, for 6 hours and analyzed for formation of discrete IRE1 oligomer foci (green dots) by imaging with a confocal microscope (blue, nuclei; green, GFP-IRE1). The graph depicts quantification of IRE1 oligomerization as reported distinct IRE1 foci per cell. Data are means ± SEM. **P < 0.01. n ≥ 100 cells from four experiments. To compare PA-treated versus cotreated with PA and PAO, Mann-Whitney U test was used for statistical analysis. Scale bar, 20 mm. DAPI, 4′,6-diamidino-2-phenylindole.

Chapter 6

Discussion

In the last decades, accumulated research into mechanisms how cells can sense and response to environmental changes has been done and several mechanisms are highlighted. Changes in environment cause stress in specific organelles such as ER and mitochondria and lead activation of downstream signaling pathways. Concomitantly, high level of communication in between organelles along with nucleus is required to restore cellular homeostasis. The ultimate purpose of these mechanisms is to restore cellular health by recovering organelles or elimination of organelles those that are beyond rescue. However, how the decision for recovering vs. elimination is taken in mammalian cells is now well understood. Chronic organelle stress is associated with progression of several diseases such as obesity, diabetes and atherosclerosis (33, 49, 209). In this study, I aimed to identify the putative roles of ER stress sensor protein IRE1 under different stress conditions by modulating distinct enzymatic functions of IRE1. In the first part of my thesis, I demonstrated the mechanisms underlying how IRE1 kinase function affect cellular sphingolipid levels and regulates mitochondrial proteostasis. In the second part, I focused to investigate the ER stress signature gene profiles and the role of RNase domain of IRE1 in Kawasaki disease progression. These two different functions of IRE1 provide new integrated signaling cascades into signaling and inflammation pathways which are crucial for progression of metabolic disease.

Under excessive stress conditions, ER senses the environmental changes and response. ER is the organelle that is responsible for folding and maturation of soluble proteins. Disruptions in protein homeostasis called as 'proteostasis' induces UPR^{ER} and initiates required signaling pathways coordinated with nucleus. Besides ER's role in proteostasis, ER also maintains metabolic flux by controlling calcium storage, balancing cholesterol synthesis and providing a hub for sphingolipids metabolism related enzymes. All these functions of ER are coordinated with each other to sustain cellular homeostasis (22). On the other hand, mitochondria are another crucial organelle to sustain functionality of the cells and mitochondrial dysfunction is closely associated with metabolic diseases. Since it is the power house of the cell by producing ATP, sustaining mitochondrial health determine cell fate (65). Mitochondria have their own genomes, mtDNA, which encodes only 13 genes and the rest of mitochondrial proteome is encoded by nucleus (70). From this end, balancing nucleus- and mitochondrial- encoded

proteins need complex and tightly controlled networks to maintain proteostasis of mitochondria. Since ER and mitochondria physically associate through MAMs and have overlapping functions, unresolved stress in one organelle can be sense by the other one and initiates signaling cascades (4). Due to overlapping functions in between ER and mitochondria, unresolved ER stress leads to mitochondrial dysfunction and triggers inflammation by inducing mitochondrial oxidative stress. ER stress also increases calcium transfer from ER to mitochondria and inhibits PERK induced mitophagy (49). Conversely, defects in mitochondria also are sensed by ER and initiates UPR^{ER}. For example, ER's role in protein folding and chaperoning require high level of ATP produced by mitochondria and defects affect the cellular energy status influence the folding/chaperoning of ER. More recently, it has been shown that unfolded proteins formed in ER can be transported into mitochondria and causes impaired mitochondrial function. This mechanism is called as ER-associated mitochondrial sequestration (ERAMS) system and adds a new layer for integrity of interorganelle crosstalk (210). In conjunction with the published studies, our studies identified that ER-and mitochondrial proteostasis system is well coordinated and sensed by each other.

IRE1, ER stress sensor protein, is a serine/threonine kinase which activates itself through autophosphorylation. A recent study showed that IRE1 interactome has been changed under ER stress condition (38). In this study, IRE1 is interacting SPL, enzyme catabolizing S1P irreversibly. S1P is a sphingolipid based bioactive molecule and its level is tightly controlled by sphingolipid kinases and phosphatases in addition to SPL (118, 120). Here in this study, I showed that IRE1 and SPL interact with each other under ER stress condition. By using *in vitro*/ cell-based kinase assay approaches in addition to phospho- proteomics results, we proofed that this interaction caused the phosphorylation of SPL by IRE1. This is a strongest proof to show that SPL is kinase substrate of IRE1. In IRE1 interactome study SPL is the only enzyme which is related to sphingolipid metabolism. The reason behind that may be SPL is also an ER resident protein and has a domain flanking to cytosol(162). Since ER stress change the lipid composition of ER membrane and stiffness, IRE1 and SPL may come together, and this may increase the chance of SPL phosphorylation by IRE1. In parallel to this, amino acids on SPL which are possible phosphorylated by IRE1 appeared in the flanking cytosolic region of SPL.

In this study, we demonstrated that ER stress inhibits SPL enzymatic activity as IRE1 kinase domain dependent manner. Inhibition of IRE1 kinase domain by using specific inhibitors, respectively KIRA6 and AMG18, but not RNase domain reversed the TG-inhibited SPL enzymatic activity. SPL is the enzyme which degrades S1P irreversible. In literature, ablation of SPL activity by using SPL specific inhibitor, THI, or knocking out SPL leads to increased level of sphingolipid species in the cells. We found that level of S1P increased in the condition that SPL activity is inhibited (under ER stress) which is reversed when IRE1 kinase domain is inhibited by inhibitors and IRE1 is silenced. In addition to S1P, level of other sphingolipids such as sphingomyelin and ceramide are also reduced when IRE1 kinase domain was inhibited. Sphingolipid metabolism is tightly controlled mechanisms. Levels of sphingolipids are transiently and strictly regulated by the activity of multiple enzymes. Any changes in level of one of these lipids sense by the cells and fluid is forced to regain the balance by over activating or slowing down the related enzymes(18, 118). As it was conducted, our study does not address the activity of others sphingolipid related enzymes such as SPTLC, the rate limiting enzyme of the pathway, or sphingosine kinases. This should be further assessed in future studies.

In this study, I identified that kinase function of IRE1 inhibits ER stress-induced cellular sphingolipid levels by regulating the activity of SPL. S1P can be secreted to extracellular space. S1P in the extracellular space bind to high density lipoprotein (HDL) and travels in the plasma (211). This may attribute to S1P another role that it can transfer the stress to the other cells. Indeed, extrinsic S1P treatment can induce ER stress (212). In parallel to our findings, it has been shown that IRE1 deficiency results in release of sphingolipid loaded extracellular sphingolipids to extracellular space. In addition, IRE1 controls cell-cell communication in C.

elegans, however whether this is conserved in mammals is not known. Also, the contribution of S1P to this mechanism is also not addressed. In C. elegans, activation of IRE1 in neuronal cells leads to the release of small clear vesicles carrying a secreted ER stress signal (SERSS). These SERSS is sensed by intestinal cells to activate a cell non-autonomous signaling mechanisms and enhance proteostasis and longevity (213, 214). As we shown in this study, S1P levels controlled by IRE1 hypothetically could be another layer of inter-cellular communication and transfer to the stress signal to the other cells. In this context, circulating S1P has a crucial role in progression of coronary artery disease and also atherosclerosis. ER and mitochondrial stress promote pro-inflammatory gene expression in atherosclerotic plaques. Our findings in this study highlight another layer in complex regulation of mammalian proteostasis and warrant future investigation into IRE1-mediated inter-organ communication by secreted S1P.

Besides types of sphingolipids, their cellular localization also defines their roles. In this study we measured the intracellular level of sphingolipids regardless of their subcellular compartments. For example, S1P in mitochondria binds to Prohibitin 2 and this binding is crutial for mitochondrial complex assembly and respiration (149). ER stress induced sphingolipid metabolites such as S1P and ceramide can locate in the mitochondria. Since slight changes in the level of these sphingolipids cause big differences, their accumulation in mitochondria may affect mitochondrial bioenergetics and function. S1P accumulation in the outer membrane of mitochondria induces UPRmt in C. elegans (177), it is worth to examine the role of IRE1-controlled S1P levels in mitochondrial function. Besides mitochondria, S1P-produced in nucleus binds to histone modifying enzymes and regulates the gene transcription (167). S1P levels induced IRE1 has a potential to transport into nucleus and bind to the specific transcription factors. It is possible that S1P can bind to UPRER and UPRmt related transcription factors to regulate cellular proteostasis.

IRE1 has been shown to locate on MAMs and IRE1 deficiency leads to changes in mitochondrial bioenergetics in mammalian cells (30). More recently, SPL has been shown to locate outer membrane of mitochondria in Trypanosoma brucei (165) and speculated to be located on MAM(162) Interaction between IRE1 and SPL which are both located on MAMs may provide another layer of control for mitochondrial S1P levels. Reduction in SPL activity under ER stress conditions may increase local S1P levels in mitochondria. S1P-produced in mitochondria by SPHK2 has been shown to bind to mitochondrial protein, prohibitin 2 (PHB2). Interaction between mitochondrial S1P and PHB2 is important for cytochrome-c oxidase assembly and mitochondrial respiration (149). Regulation of S1P levels by IRE1 through modulation of SPL activity may change the mitochondrial energetic and lead to activation of UPRmt.

S1P has been shown to promote mitochondrial biogenesis through increased mitochondrial DNA replication and elevated mitochondrial mass via stimulation of peroxisome proliferator-activated receptor-gamma coactivator 1α (PGC1α), one of the main transcription factors regulate mitochondrial biogenesis (215). Increased UPR^{mt} as a result of TG-induced S1P through SPL inhibition may increase uncontrolled mitochondrial DNA replication. Thus, may lead to accumulation of unwanted mitochondrial proteins in the mitochondria which causes UPRmt. There should be balanced mitochondrial biogenesis and degradation to regain mitochondrial homeostasis (71). Our results showing IRE1 kinase inhibition and SPL overexpression (result in S1P reduction) reduces UPR^{mt} and induces mitochondrial clearance pathways increases the possibility that IRE1-SPL axis maintain mitochondrial health by balancing several pathways related to mitochondrial proteostasis.

Dysregulation in mechanisms which regulate proteostasis is implicated with progression of several disease such as Alzheimer disease and cardiovascular disease. The severity of these diseases increases with age and differs in males and females (216, 217). Since activation of mild UPR mechanisms in specific organelles has also been shown to enhance health and life span, the development of safe and efficacious treatment could promote healthy aging, delaying

the onset of age-related diseases. Recent experimental studies in aged mice suggest that there exist significant sex-dependent differences in S1P-mediated vascular changes (218). While currently most studies investigate S1P effects in male animals exclusively, there is a need to involve both male and female animals in future in vivo studies as sex may significantly affect action of IRE1-SPL axis.

S1P gradient between various tissues promotes S1P- dependent regulation of immune cells to fulfill their action. It has been shown that S1P regulates immune cell trafficking and migration, angiogenesis and vascular permeability. S1P also has roles in modulating the functions of immune cells such as macrophages and neutrophiles (219). Since progression of various disease such as atherosclerosis and Kawasaki disease initiate upon immune cell infiltration into arteries (220, 221), modulation of S1P by IRE1 kinase domain may has critical roles in cardiovascular disease.

S1P is carried by HDL- bound Apolipoprotein M (APOM) in blood circulation. Most prominent HLD functions shown to depend on binding of S1P to HDL. The molecular determinants of HDL dysfunction are still insufficiently understood. HDL dysfunction is a common feature in patients with atherosclerotic disease, diabetes mellitus, metabolic syndrome and chronic kidney disease and presents with compromised anti-oxidative, anti-inflammatory, anti-apoptotic, vasodilative and cholesterol efflux properties(222). Accordingly, any HDL constituent such as S1P that is identified to participate in HDL function becomes a candidate for investigation in clinical disease settings and the contribution of IRE1-SPL axis in the level of HDL bound S1P is crucial for delineating mechanisms underlying cardiovascular disease progression.

Our data provides strong evidence for IRE1-S1P axis induced by ER stress has a central role in UPR^{mt} induction in mammalian cells. However, there could be additional mechanisms. One possible mechanism could be affecting mitochondrial proteostasis by ER stress. Recently, the presence of ER surface-mediated (ER-SURF) mitochondrial protein targeting pathway has been shown (223). In this model, newly synthetized mitochondrial proteins are initially located and bound to the ER surface. Specialized ER chaperons interact with certain mitochondrial protein precursor and modulate re-routing of these mitochondrial precursors to OMM. ER-SURF pathway is identified only in yeast. Since critical protein in this pathway encoded by EMA19 in yeast) is conserved and this suggest mammalian counterparts of this pathway exist. It can be speculated that impairment of mammalian counterpart of the ER-SURF pathway could inhibit translocation of mitochondrial protein precursor to mitochondria and initiate UPRmt. This exciting possibility can be addressed by future studies focusing on understanding whether ER stress can prevent proper mitochondrial localization of certain proteins in mammalian cells.

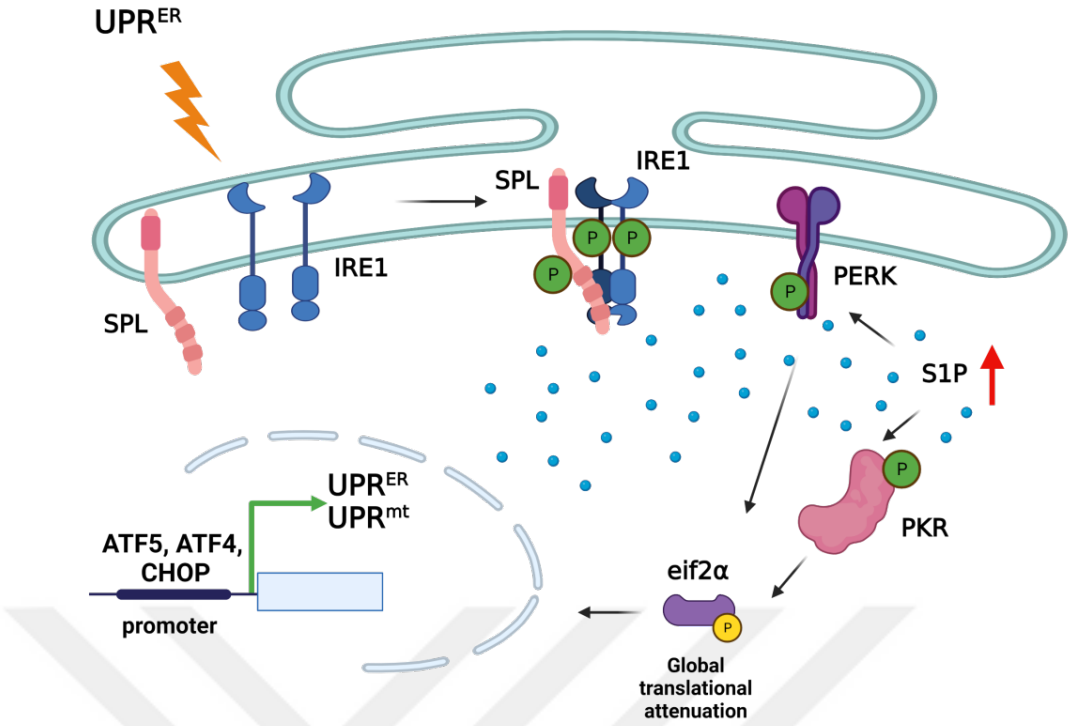

Figure 6. 1: ER stress- induced SPL phosphorylation by IRE1 potentiates the UPR^{mt}. IRE1-SPL axis impinges on eif2α phosphorylation through modulating PERK and PKR activities and establishes an additional layer of control over UPR^{mt} induction during ER stress in mammalian cells. Activated by ER stress, IRE1 phosphorylates SPL that is found on the ER membranes. IRE1-mediated phosphorylation leads to inactivation to SPL and increased S1P levels in cells. IRE1-SPL axis mainly regulates PKR activity and eif2α phosphorylation, a critical upstream event in the activation of mammalian UPRmt signaling.

In last decades, cardiovascular health problems have dramatically increased worldwide. Intense research into mechanisms of cardiovascular disease revealed that chronic inflammation caused by organelle stress is the common reasons of disease progression. Upon intense stress, functions of organelles such as ER and mitochondria impaired and initiate inflammatory pathways. However, the mechanisms underlying disease progression are still needed to be investigated. In the second part of this thesis study, we sought to investigate the contribution of ER stress on Kawasaki disease vasculitis.

ER stress has been implicated with inflammation-driven metabolic disease such as atherosclerosis and obesity. It has been shown that activation of ER stress sensor proteins, IRE1 and PERK, by metabolic stress cause NLRP3 activation and pro-inflammatory cytokine production. On the other hand, NLRP3 proinflammatory cytokine secretion is the main reasons in cardiovascular lesion development in human and murine models of KD vasculitis. However, the link between ER stress and KD vasculitis has not been investigated until now. Here, we sought to investigate whether ER stress has a role in KD vasculitis. We show that KD development is associated with increased level of ER stress signature gene expressions, including IRE1/XBP1 by using publicly available human transcriptomics data sets and scRNA Seq from murine KD vasculitis model. Furthermore, we revealed that ER stress markers, such as IRE1 activation and ERp57 protein levels are increased in the tissues of LCWE-injected mice. Our data is consistent with literature showing a strong relationship between ER stress and cardiovascular disease such as heart disease, hypertension, and atherosclerosis.

Here in this study, we showed that IRE1 activation was increased in abdominal aorta of LCWE-injected mice. Activation of IRE1 by autophosphorylation under extensive stress conditions leads to activation of inflammatory processes in cardiovascular disease through NLRP3 activation and IL1 beta secretion. In parallel to literature, our data revealed that IRE1 activation causes cardiovascular lesion formation in LCWE-induced KD vasculitis in mice models. Indeed, LCWE treatment leads to increase in level of ER stress related proteins in BMDM cells obtained from WT mice. This is logical because myeloid cells are such as BMDMs are the main source of IL1b in LCWE induced cardiovascular disease. Moreover, circulating peripheral blood monocytes are the main producers of IL1beta transcripts in acute KD patients. In this study we also assed the contribution of IRE1 pathway in myeloid cells in KD vasculitis progression. We generated myeloid specific IRE1 deficient mice, $LysM^{Cre+}$ $Ern1^{\Delta/\Delta}$ mice. IRE1 deficiency results in reduced IL1beta transcription in BMDMs after stimulation with LCWE. Consistent with previous findings in other types of cardiovascular disease, these findings suggest that IRE1 inhibition may lead to NLRP3 reduction in KD vasculitis. Protein levels of secreted caspase 1 and IL1beta were also down regulated in BMDMs from $LysM^{Cre+}$ $Ern1^{\Delta/\Delta}$ mice in comparison to WT counterparts. Consistent with these observations, $LysM^{Cre+}$ $Ern1^{\Delta/\Delta}$ mice displayed reduced heart inflammation and abdominal aorta aneurysm development. These findings proof that ER stress activation driven by IRE1 plays a crucial role in the LCWE murine model of KD vasculitis.

IRE1 has 2 different enzymatic activities which function corporately. IRE1 kinase domain autophosphorylates itself and this leads to activation of IRE1. Besides this, IRE1 RNAase domain has non-conventional function. RNase domain of IRE1 spices XBP1 mRNAs and this leads to production of short mRNA which can be translated. sXBP1 protein act as a transcription factor and translocates into the nucleus. sXBP1 is responsible for transcription of ER stress related genes as well as pro-inflammatory cytokine. In this study, we used small molecule inhibitor of IRE1 to define which domain of IRE1 has roles in KD vasculitis progression. Inhibition of IRE1 RNase domain but not IRE1 kinase domain reduced LCWE induced IL1beta and caspase 1 secretion in BMDM cells. In consistent with these results, targeting RNase domain of IRE1 by 4μ8c reduced heart inflammation and abdominal aorta aneurysm formation in LCWE injected mice. In literature it has been shown that 4μ8c treatment led to attenuation of NLRP3 inflammasome complex activity and reduced IL1 beta production in an atherosclerotic model. In consistent with previous studies, our combined in vitro and in vivo data strongly suggest that IRE1 inhibition attenuates cardiovascular lesion formation in the murine KD vasculitis by diminishing NLRP3 activation.

Besides their roles in exchanging information and signaling molecules, contacts sites between ER and mitochondria function as platforms for NLRP3 inflammasome assembly. Stress in each organelle is efficiently transferred to the other and results in ROS production. Increased ROS levels in both organelle lead to robust activation of the NLRP3 inflammasome by formation of damage-associated molecular patterns.

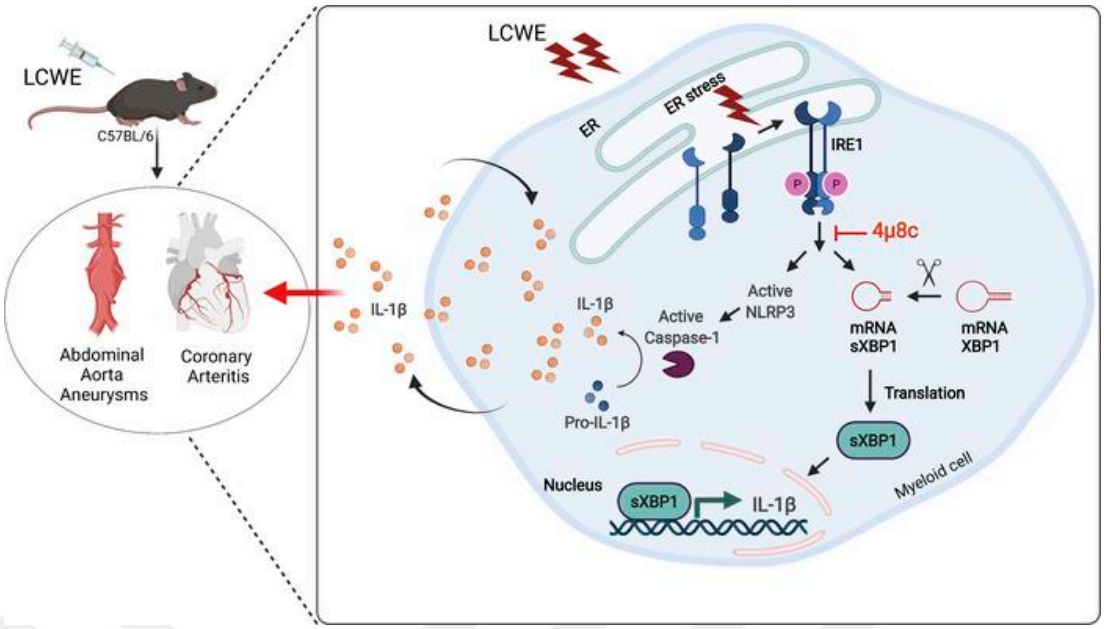

Figure 6. 2: Targeting IRE1 endoribonuclease activity alleviates cardiovascular lesions in a murine model of Kawasaki disease vasculitis.

In the third and final part of my thesis, we showed that PAO effectively replaces other FAs, resulting in increased MUFA/SFA ratio in macrophages, but without expanding any of the lipid classes. The marked incorporation of PAO into multiple PL species implies dynamic membrane remodeling of organelles through desaturation by PAO. Further lipidomic analysis of isolated ER fractions from macrophages confirmed that PAO effectively incorporates into most lipid compartments, especially PLs and cholesterol, in this organelle and increases the MUFA/SFA ratio. Extensive ER membrane remodeling can thus be achieved through PAO-induced desaturation and may have wider implications, such as altered membrane biophysical properties and UPR signaling emanating from these membranes. Proximal UPR regulators form high-order oligomers on ER membranes upon ER stress induction by chemicals (224).

Here, we show that PA evokes IRE1 oligomerization on ER membranes, which can be blocked by PAO cotreatment. The outcome of these experiments strongly supports the idea that dynamic remodeling of membranes by desaturation with PAO underlies ER resistance to stress induced by PA. One limitation of our study is that we do not know the extent of remodeling in other intracellular organelles' membranes because we only analyzed the ER via lipidomics. However, our study provides proof of principle that organelle membrane remodeling by nutritional supplementation with a bioactive lipid could be an effective strategy for the treatment of metabolic diseases.

This study and others support the conclusion that PAO supplementation can mitigate more than one component of metabolic syndrome, including insulin resistance and atherosclerosis (225-227). PAO is a potent inhibitor of lipid-induced ER stress and inflammasome activation in mouse. These beneficial changes are associated with dynamic lipidomic remodeling of ER membranes. Our findings show that it is possible to modify organelle stress responses and suppress inflammasome activity through nutritional supplementation with PAO. These results warrant future investigation to assess PAO's therapeutic potential in human disease.

Chapter 7

Future Perspectives

Cellular protein homeostasis so called as ‘proteostasis’ is crucial for cellular health and disruption in proteostasis is causally associated with disease progression. Every organelle has unique mechanisms such as balancing protein synthesis and degradation, readapting metabolic flux and activating transcriptional machineries to cope with stress(7, 100, 228). All these mechanisms require intraorganellar communication. In the past, malfunctioning of an individual organelle type was considered as the only specific pathology for disease progression. More recent studies start to highlight the intraorganelle communication as therapeutic targets of various human diseases.

Here, in this study, we explored different roles of ER stressor IRE1 under various stress condition to understand molecular targets of IRE1 for controlling cellular homeostasis and developing related inhibitors and agonists as potential treatment of human diseases.

As our first investigation, we identified IRE1 kinase domain function in mitochondrial stress response. PERK arm of UPRER and its effect of global translational attenuation via eif2α is well studied to understand collaboration between UPRER and UPRmt. Unexpected roles of IRE1 kinase domain shown in this study for regulating mitochondrial proteostasis rises need for developing new therapeutical strategies to specifically target IRE1 kinase domain. Systemic administration of IRE1 kinase domain inhibitor, KIRA6, has been shown to increase insulin levels and ameliorate hyperglycemia (37). However, as it has done in that specific study, interperitoneally injection of KIRA6 twice a day with high dose indicates that KIRA6 has short half-life and many cause toxicity. This also limits application of this drugs in clinics. To increase the specificity of IRE1 kinase inhibitors such as KIRA6, nano-particle based methodologies can be developed.

Identification of SPL as IRE1 kinase domain substrate provides a new layer for modulating intraorganelle crosstalk and initiating related transcriptional machineries. IRE1-SPL axis activates retrograde signaling from mitochondria to nucleus to initiate UPRmt -related gene transcription. SPL phosphorylation by IRE1 kinase domain consequently results in increased S1P levels in the cell. However, we did not examine the specific cell compartments where S1P may accumulate under ER stress conditions. IRE1 mediated SPL inhibition may lead to induction in local S1P levels in mitochondria and nucleus. S1P accumulating in specific sub compartments may directly affect their function and cellular response. For instance, S1P-binding to Prohibitin in the mitochondria impairs mitochondrial respiration capacity (149). Moreover, S1P produced by SPHK1 in nucleus also binds to histone modifying enzymes and impact chromatin remodeling and gene transcription (229). In conjunction with this knowledge, S1P controlled by IRE1 kinase domain activity may interact to unidentified proteins and mediate mitochondrial function and proteostasis. New protein partners of S1P under stress condition must be elucidated to better understand the mechanisms related to how IRE1-SPL axis controls UPR^{mt}.

Systemic induction in S1P levels has been shown as lipid mediator and activates autocrine and paracrine signaling by binding to G-protein coupled S1P receptors (S1PRs) on cell surfaces. Since S1P levels controlled by multiple enzymes which modulate action of S1P in opposite directions(120, 138, 230), it is important to validate effect of S1P in individual concepts. Identification of intracellular targets of S1P has been challenging since it has opposing effect in same disease concepts. Probably the most challenging difficulty of targeting S1P signaling for disease treatment is to gain the required specificity for certain pathways at the right time.

SPL phosphorylation by IRE1 results in reduction of UPRmt. Mitochondrial proteostasis has been shown to associate with progression of several disease such as neurodegenerative disease and cardiovascular disease. UPR^{mt} is protective in chronic and acute cardiac injury (231, 232). However, and seemingly contradictory, deletion of UPR^{mt} related proteins impairs heart function(233). It is possible that moderate UPR^{mt} activity has cardioprotective effect and may be beneficial for removing damaged/ unwanted proteins in the mitochondria. When there is excessive and prolonged stress, UPRmt activation may leads to uncontrolled cleavage of mitochondrial proteins and promoting mitochondrial dysfunction. From this end, fine tuning of SPL activity and balancing intracellular S1P by IRE1 kinase domain provide a strategy to control severity of UPR^{mt} and determine cellular fate in between health and death.

In the second part of this study, we identified that ER stress plays a central role in KD vasculitis. There are there ER stressors, IRE1, PERK and ATF6. All these stressors modulate ER stress- related gene transcriptions individually and cooperatively according to type and severity of stress conditions. Expressions of several ER stress signature gene are upregulated in LCWE-induced KD murine model and human transcriptomics data cells. These data confirmed that three arms of UPR^{ER} is activated in KD vasculitis. However, we only validated the contribution of IRE1 in KD progression and effects of PERK and ATF6 arms still need to be elucidated.

Activation of inflammatory pathways have been identified as driven players in KD vasculitis. ER stress is also associated with other cardiovascular disease such as atherosclerosis by inducing inflammatory pathways. Here we showed that inhibition of IRE1 RNase domain by 4μ8c inhibits IL-1β and cleaved caspase 1 secretion. Targeting IRE1 with 4μ8c also partially

inhibited the expression level of IL-1 and IL-6. This partial effect may observe because PERK and ATF6 arm of UPR may be still active and are needed to be addressed with further studies.

LCWE-induced KD vasculitis is associated with impaired autophagy/mitophagy and increased ROS production in inflamed vascular tissues, which promotes NLRP3 inflammasome activation and the development of cardiovascular lesions in LCWE-injected mice (234). We revealed that targeting IRE1 by 4μ8c or inflammation activation and reduces plaque size. Specific targets of IRE1 RNase domain have been studied extensively. Blocking of RNase target reduces mitochondrial ROS levels and reveals beneficial effect on cardiovascular diseases such as atherosclerosis (33). We did not investigate how IRE1 inhibition mechanistically blocks NLRP3 activation in the concept of KD. As previously shown, reduction of ROS levels and induction of mitochondrial clearance pathways by inhibition of IRE1 RNase domain may be one mechanistic possibility also in KD vasculitis.

Studies report that circulating levels of IL-1β are increased during the acute phase of KD and reduced following IVIG treatment (234). Transcriptomics analysis of whole blood from patients with KD that is responsive or resistant to IVIG treatment also indicates increased abundance of multiple genes belonging to the IL-1 pathway in IVIG-resistant patients (235). These observations led us to investigate new pharmacological agents to cure KD vasculitis. In this thesis study, we demonstrate that pharmacological modulation and myeloid specific deletion of the IRE1 pathway hampers NLRP3 inflammasome activation and IL-1β secretion, resulting in decreased development of cardiovascular lesions. These findings highlight IRE1 as a therapeutic target in KD. Whether IVIG-resistant KD patients would benefit from targeting of organelle stress responses or whether treatment with IRE1 inhibitors could prevent long-term cardiovascular sequelae warrant deeper investigation. The ongoing efforts to discover next-generation IRE1 kinase and RNase inhibitors make these exciting times to further explore the potential of IRE1 modulation in KD vasculitis.

Recent studies have shown several bioactive lipid species are produced by DNL including several endogenous ligands for nuclear receptors and PAO possess specific biological activities and exert potent metabolic effects (236). In the last part of this thesis study, we investigate that bioactive lipid molecule PAO incorporate the ER membrane and leads to remodeling of lipid composition. Integration of PAO into cellular membranes reduces ER stress by blocking IRE1 clusters and activation via autophosphorylation. By preventing ER stress, PAO blocks lipid-induced inflammasome activation in mouse macrophages. In conjunction with studies in literature, our findings exciting findings confirm bioactive lipid molecules such PAO serve beneficial effects for metabolic remodeling and requires future investigation to assess PAO's therapeutic potential in human disease.

Here in this thesis study, we investigated the different roles of IRE1-mediated ER stress in organelle crosstalk and inflammatory disease progression. Since, IRE1 has such diverse function, exploring the potentials of IRE1 is needed to investigate different disease pathologies.

References

1. Westrate, L. M., J. E. Lee, W. A. Prinz, and G. K. Voeltz. 2015. Form Follows Function: The Importance of Endoplasmic Reticulum Shape. *Annual Review of Biochemistry* 84: 791-811.
2. Schwarz, D. S., and M. D. Blower. 2016. The endoplasmic reticulum: structure, function and response to cellular signaling. *Cell Mol Life Sci.* 73: 79-94.
3. Phillips, M. J., and G. K. Voeltz. 2016. Structure and function of ER membrane contact sites with other organelles. *Nature Reviews Molecular Cell Biology* 17: 69-82.
4. van Vliet, A. R., and P. Agostinis. 2018. Mitochondria-Associated Membranes and ER Stress. *Curr Top Microbiol Immunol.* 414:73-102.
5. Braakman, I., and D. N. Hebert. 2013. Protein folding in the endoplasmic reticulum. *Cold Spring Harb Perspect Biol.* 5(5):a013201.
6. Pool, M. R. 2005. Signal recognition particles in chloroplasts, bacteria, yeast and mammals (review). *Mol Membr Biol* . 22(1-2):3-15.
7. Araki, K., and K. Nagata. 2011. Protein folding and quality control in the ER. *Cold Spring Harb Perspect Biol.* 3(11):a007526.
8. Jaffe, L. F. 1983. Sources of calcium in egg activation: a review and hypothesis. *Dev Biol* . 99(2):265-276.
9. Clapham, D. E. 1995. Calcium signaling. *Cell* 80: 259-268.
10. Treiman, M. 2002. Regulation of the endoplasmic reticulum calcium storage during the unfolded protein response--significance in tissue ischemia? *Trends Cardiovasc Med* . 12(2):57-62.
11. Fagone, P., and S. Jackowski. 2009. Membrane phospholipid synthesis and endoplasmic reticulum function. *Journal of Lipid Research* 50: S311-S316.
12. Lange, Y. 1991. Disposition of intracellular cholesterol in human fibroblasts. *J Lipid Res* . 32(2):329-339.
13. Radhakrishnan, A., J. G. Goldstein Jl Fau - McDonald, M. S. McDonald Jg Fau - Brown, and M. S. Brown. 2008. Switch-like control of SREBP-2 transport triggered by small changes in ER cholesterol: a delicate balance. *Cell Metab* . 8(6):512-521.
14. Adams, C. M., J. L. Goldstein, and M. S. Brown. 2003. Cholesterol-induced conformational change in SCAP enhanced by Insig proteins and mimicked by cationic amphiphiles. *Proceedings of the National Academy of Sciences* 100: 10647.
15. Goldstein, J. L., M. S. DeBose-Boyd Ra Fau - Brown, and M. S. Brown. 2006. Protein sensors for membrane sterols. *Cell* . 124(1):35-46.
16. van Meer, G., D. R. Voelker, and G. W. Feigenson. 2008. Membrane lipids: where they are and how they behave. *Nature Reviews Molecular Cell Biology* 9: 112-124.
17. Merrill A.H., W., E., Hargrove, J. L. 1985. Hepatic enzymes of sphingolipid and glycerolipid biosynthesis in rats from Spacelab 3. *Physiologist* . 28(6 Suppl):S229.
18. Tidhar, R., and A. H. Futerman. 2013. The complexity of sphingolipid biosynthesis in the endoplasmic reticulum. *Biochimica et Biophysica Acta (BBA) - Molecular Cell Research* 1833: 2511-2518.
19. Taouji, S., S. Wolf, and E. Chevet. 2013. Chapter Seventeen - Oligomerization in Endoplasmic Reticulum Stress Signaling. *In* Progress in Molecular Biology and Translational Science. J. Giraldo and F. Ciruela, editors. Academic Press. 465-484.
20. Sehgal, P., P. A.-O. Szalai, C. A.-O. Olesen, H. A.-O. Praetorius, P. A.-O. Nissen, S. B. Christensen, N. A.-O. Engedal, and J. V. Møller. Inhibition of the sarco/endoplasmic reticulum (ER) Ca(2+)-ATPase by thapsigargin analogs induces cell death via ER Ca(2+) depletion and the unfolded protein response.
21. Hetz, C., F. Martinon, D. Rodriguez, and L. H. Glimcher. 2011. The Unfolded Protein Response: Integrating Stress Signals Through the Stress Sensor IRE1α. *Physiological Reviews* 91: 1219-1243.
22. Hetz, C. 2012. The unfolded protein response: controlling cell fate decisions under ER stress and beyond. *Nature Reviews Molecular Cell Biology* 13: 89-102.
23. Ron, D., and S. R. Hubbard. 2008. How IRE1 Reacts to ER Stress. *Cell* 132: 24-26.

24. Tabas, I., and D. Ron. 2011. Integrating the mechanisms of apoptosis induced by endoplasmic reticulum stress. *Nature Cell Biology* 13: 184-190.
25. Park, K., S. E. Lee, K.-O. Shin, and Y. Uchida. 2019. Insights into the role of endoplasmic reticulum stress in skin function and associated diseases. *The FEBS Journal* 286: 413-425.
26. Yoshida, H., A. Matsui T Fau - Yamamoto, T. Yamamoto A Fau - Okada, K. Okada T Fau - Mori, and K. Mori. 2001. XBP1 mRNA is induced by ATF6 and spliced by IRE1 in response to ER stress to produce a highly active transcription factor. *Cell* . 107(7):881-891.
27. Wang, S., and R. J. Kaufman. 2012. The impact of the unfolded protein response on human disease. *Journal of Cell Biology* 197: 857-867.
28. Adams, C. J., M. C. Kopp, N. Larburu, P. R. Nowak, and M. M. U. Ali. 2019. Structure and Molecular Mechanism of ER Stress Signaling by the Unfolded Protein Response Signal Activator IRE1. *Frontiers in Molecular Biosciences* 6.
29. Urra, H., P. Pihan, and C. Hetz. 2020. The UPRosome - decoding novel biological outputs of IRE1alpha function. *J Cell Sci* 133.
30. Carreras-Sureda, A., F. Jaña, H. Urra, S. Durand, D. E. Mortenson, A. Sagredo, G. Bustos, Y. Hazari, E. Ramos-Fernández, M. L. Sassano, P. Pihán, A. R. van Vliet, M. González-Quiroz, A. K. Torres, C. Tapia-Rojas, M. Kerkhofs, R. Vicente, R. J. Kaufman, N. C. Inestrosa, C. Gonzalez-Billault, R. L. Wiseman, P. Agostinis, G. Bultynck, F. A. Court, G. Kroemer, J. C. Cárdenas, and C. Hetz. 2019. Non-canonical function of IRE1α determines mitochondria-associated endoplasmic reticulum composition to control calcium transfer and bioenergetics. *Nature Cell Biology* 21: 755-767.
31. Yoshida, H., M. Oku, M. Suzuki, and K. Mori. 2006. pXBP1(U) encoded in XBP1 pre-mRNA negatively regulates unfolded protein response activator pXBP1(S) in mammalian ER stress response. *Journal of Cell Biology* 172: 565-575.
32. Hamid, S. M., M. Citir, E. M. Terzi, I. Cimen, Z. Yildirim, A. E. Dogan, B. Kocaturk, U. I. Onat, M. Arditi, C. Weber, A. Traynor-Kaplan, C. Schultz, and E. Erbay. 2020. Inositol-requiring enzyme-1 regulates phosphoinositide signaling lipids and macrophage growth. *EMBO reports* 21: e51462.
33. Tufanli, O., P. Telkoparan Akillilar, D. Acosta-Alvear, B. Kocaturk, U. I. Onat, S. M. Hamid, I. Çimen, P. Walter, C. Weber, and E. Erbay. 2017. Targeting IRE1 with small molecules counteracts progression of atherosclerosis. *Proceedings of the National Academy of Sciences* 114: E1395.
34. Upton, J.-P., L. Wang, D. Han, E. S. Wang, N. E. Huskey, L. Lim, M. Truitt, M. T. McManus, D. Ruggero, A. Goga, F. R. Papa, and S. A. Oakes. 2012. IRE1α cleaves select microRNAs during ER stress to derepress translation of proapoptotic Caspase-2. *Science (New York, N.Y.)* 338: 818-822.
35. Zhou, J., C. Y. Liu, S. H. Back, R. L. Clark, D. Peisach, Z. Xu, and R. J. Kaufman. 2006. The crystal structure of human IRE1 luminal domain reveals a conserved dimerization interface required for activation of the unfolded protein response. *Proceedings of the National Academy of Sciences* 103: 14343.
36. Urano, F., X. Wang, A. Bertolotti, Y. Zhang, P. Chung, P. Harding Heather, and D. Ron. 2000. Coupling of Stress in the ER to Activation of JNK Protein Kinases by Transmembrane Protein Kinase IRE1. *Science* 287: 664-666.
37. Ghosh, R., L. Wang, Eric S. Wang, B. Gayani K. Perera, A. Igbaria, S. Morita, K. Prado, M. Thamsen, D. Caswell, H. Macias, Kurt F. Weiberth, Micah J. Gliedt, Marcel V. Alavi, Sanjay B. Hari, Arinjay K. Mitra, B. Bhhatarai, Stephan C. Schürer, Erik L. Snapp, Douglas B. Gould, Michael S. German, Bradley J. Backes, Dustin J. Maly, Scott A. Oakes, and Feroz R. Papa. 2014. Allosteric Inhibition of the IRE1α RNase Preserves Cell Viability and Function during Endoplasmic Reticulum Stress. *Cell* 158: 534-548.
38. Acosta-Alvear, D., G. E. Karagöz, F. Fröhlich, H. Li, T. C. Walther, and P. Walter. 2018. The unfolded protein response and endoplasmic reticulum protein targeting machineries converge on the stress sensor IRE1. *eLife* 7: e43036.

39. Liu, Z., Y. Lv, N. Zhao, G. Guan, and J. Wang. 2015. Protein kinase R-like ER kinase and its role in endoplasmic reticulum stress-decided cell fate. *Cell Death & Disease* 6: e1822-e1822.
40. Harding, H. P., I. Novoa, Y. Zhang, H. Zeng, R. Wek, M. Schapira, and D. Ron. 2000. Regulated Translation Initiation Controls Stress-Induced Gene Expression in Mammalian Cells. *Molecular Cell* 6: 1099-1108.
41. Cullinan Sara, B., D. Zhang, M. Hannink, E. Arvisais, J. Kaufman Randal, and J. A. Diehl. 2003. Nrf2 Is a Direct PERK Substrate and Effector of PERK-Dependent Cell Survival. *Molecular and Cellular Biology* 23: 7198-7209.
42. Akai, R., A. Hosoda, M. Yoshino, and T. Iwawaki. 2015. Constitutive role of GADD34 and CReP in cancellation of phospho-eIF2α-dependent translational attenuation and insulin biosynthesis in pancreatic β cells. *Genes to Cells* 20: 871-886.
43. Thuerauf, D. J., P. J. Marcinko M Fau - Belmont, C. C. Belmont Pj Fau - Glembotski, and C. C. Glembotski. 2007. Effects of the isoform-specific characteristics of ATF6 alpha and ATF6 beta on endoplasmic reticulum stress response gene expression and cell viability. *J Biol Chem* . 282(31):22865-22878.
44. Haze, K., H. Yoshida, H. Yanagi, T. Yura, and K. Mori. 1999. Mammalian Transcription Factor ATF6 Is Synthesized as a Transmembrane Protein and Activated by Proteolysis in Response to Endoplasmic Reticulum Stress. *Molecular Biology of the Cell* 10: 3787-3799.
45. Shen, J., L. Chen X Fau - Hendershot, R. Hendershot L Fau - Prywes, and R. Prywes. 2002. ER stress regulation of ATF6 localization by dissociation of BiP/GRP78 binding and unmasking of Golgi localization signals. *Dev Cell* . 3(1):99-111.
46. Schröder, M., and R. J. Kaufman. 2005. THE MAMMALIAN UNFOLDED PROTEIN RESPONSE. *Annual Review of Biochemistry* 74: 739-789.
47. Vekich, J. A., D. J. Belmont Pj Fau - Thuerauf, C. C. Thuerauf Dj Fau - Glembotski, and C. C. Glembotski. 2012. Protein disulfide isomerase-associated 6 is an ATF6-inducible ER stress response protein that protects cardiac myocytes from ischemia/reperfusion-mediated cell death. *J Mol Cell Cardiol* . 53(2):259-267.
48. Wek, R. C., T. G. Jiang Hy Fau - Anthony, and T. G. Anthony. 2006. Coping with stress: eIF2 kinases and translational control. *Biochem Soc Trans* . 34(Pt 1):7-11.
49. Onat Umut, I., D. Yildirim Asli, Ö. Tufanli, I. Çimen, B. Kocatürk, Z. Veli, M. Hamid Syed, K. Shimada, S. Chen, J. Sin, K. Shah Prediman, A. Gottlieb Roberta, M. Arditi, and E. Erbay. 2019. Intercepting the Lipid-Induced Integrated Stress Response Reduces Atherosclerosis. *Journal of the American College of Cardiology* 73: 1149-1169.
50. Cole, J. L. 2007. Activation of PKR: an open and shut case? *Trends Biochem Sci* . 32(2):57-62.
51. Vazquez de Aldana, C. R., R. C. Wek, P. S. Segundo, A. G. Truesdell, and A. G. Hinnebusch. 1994. Multicopy tRNA genes functionally suppress mutations in yeast eIF-2 alpha kinase GCN2: evidence for separate pathways coupling GCN4 expression to unchanged tRNA. *Molecular and Cellular Biology* 14: 7920-7932.
52. Han, A.-P., C. Yu, L. Lu, Y. Fujiwara, C. Browne, G. Chin, M. Fleming, P. Leboulch, S. H. Orkin, and J.-J. Chen. 2001. Heme-regulated eIF2α kinase (HRI) is required for translational regulation and survival of erythroid precursors in iron deficiency. *The EMBO Journal* 20: 6909-6918.
53. Chefalo, P. J., J. Oh, M. Rafie-Kolpin, B. Kan, and J.-J. Chen. 1998. Heme-regulated eIF-2α kinase purifies as a hemoprotein. *European Journal of Biochemistry* 258: 820-830.
54. Bruns, G. P., and I. M. London. 1965. The effect of hemin on the synthesis of globin. *Biochemical and Biophysical Research Communications* 18: 236-242.
55. Pakos-Zebrucka, K., I. Koryga, K. Mnich, M. Ljujic, A. Samali, and A. M. Gorman. 2016. The integrated stress response. *EMBO reports* 17: 1374-1395.
56. Guo, X., G. Aviles, Y. Liu, R. Tian, B. A. Unger, Y.-H. T. Lin, A. P. Wiita, K. Xu, M. A. Correia, and M. Kampmann. 2020. Mitochondrial stress is relayed to the cytosol by an OMA1–DELE1–HRI pathway. *Nature* 579: 427-432.

57. Fessler, E., E.-M. Eckl, S. Schmitt, I. A. Mancilla, M. F. Meyer-Bender, M. Hanf, J. Philippou-Massier, S. Krebs, H. Zischka, and L. T. Jae. 2020. A pathway coordinated by DELE1 relays mitochondrial stress to the cytosol. *Nature* 579: 433-437.
58. Hinnebusch Alan, G. 2011. Molecular Mechanism of Scanning and Start Codon Selection in Eukaryotes. *Microbiology and Molecular Biology Reviews* 75: 434-467.
59. Lee, Y. Y., E. Cevallos Rc Fau - Jan, and E. Jan. 2009. An upstream open reading frame regulates translation of GADD34 during cellular stresses that induce eIF2alpha phosphorylation. *J Biol Chem* . 284(11):6661-6673.
60. Palam, L. R., R. C. Baird Td Fau - Wek, and R. C. Wek. 2011. Phosphorylation of eIF2 facilitates ribosomal bypass of an inhibitory upstream ORF to enhance CHOP translation. *J Biol Chem* . 286(13):10939-10949.
61. Novoa, I., H. Zeng, H. P. Harding, and D. Ron. 2001. Feedback Inhibition of the Unfolded Protein Response by GADD34-Mediated Dephosphorylation of eIF2α. *Journal of Cell Biology* 153: 1011-1022.
62. Harding, H. P., H. Zhang Y Fau - Zeng, I. Zeng H Fau - Novoa, P. D. Novoa I Fau - Lu, M. Lu Pd Fau - Calfon, N. Calfon M Fau - Sadri, C. Sadri N Fau - Yun, B. Yun C Fau - Popko, R. Popko B Fau - Paules, D. F. Paules R Fau - Stojdl, J. C. Stojdl Df Fau - Bell, T. Bell Jc Fau - Hettmann, J. M. Hettmann T Fau - Leiden, D. Leiden Jm Fau - Ron, and D. Ron. 2003. An integrated stress response regulates amino acid metabolism and resistance to oxidative stress. *Mol Cell* . 11(3):619-633.
63. Ameri, K., and A. L. Harris. 2008. Activating transcription factor 4. *The International Journal of Biochemistry & Cell Biology* 40: 14-21.
64. Mick, E. A.-O. X., D. A.-O. Titov, O. A.-O. Skinner, R. Sharma, A. A.-O. Jourdain, and V. A.-O. X. Mootha. 2020. Distinct mitochondrial defects trigger the integrated stress response depending on the metabolic state of the cell. LID - 10.7554/eLife.49178 [doi] LID - e49178. *Elife* . 9:e49178.
65. Friedman, J. R., and J. Nunnari. 2014. Mitochondrial form and function. *Nature* 505: 335-343.
66. Zinser, E., C. D. Sperka-Gottlieb, E. V. Fasch, S. D. Kohlwein, F. Paltauf, and G. Daum. 1991. Phospholipid synthesis and lipid composition of subcellular membranes in the unicellular eukaryote Saccharomyces cerevisiae. *Journal of Bacteriology* 173: 2026-2034.
67. de Kroon, A. I. P. M., D. Dolis, A. Mayer, R. Lill, and B. de Kruijff. 1997. Phospholipid composition of highly purified mitochondrial outer membranes of rat liver and Neurospora crassa. Is cardiolipin present in the mitochondrial outer membrane? *Biochimica et Biophysica Acta (BBA) - Biomembranes* 1325: 108-116.
68. Zorova, L. D., V. A. Popkov, E. Y. Plotnikov, D. N. Silachev, I. B. Pevzner, S. S. Jankauskas, V. A. Babenko, S. D. Zorov, A. V. Balakireva, M. Juhaszova, S. J. Sollott, and D. B. Zorov. 2018. Mitochondrial membrane potential. *Analytical Biochemistry* 552: 50-59.
69. Robin, E. D., and R. Wong. 1988. Mitochondrial DNA molecules and virtual number of mitochondria per cell in mammalian cells. *Journal of Cellular Physiology* 136: 507-513.
70. Taanman, J.-W. 1999. The mitochondrial genome: structure, transcription, translation and replication. *Biochimica et Biophysica Acta (BBA) - Bioenergetics* 1410: 103-123.
71. Moehle, E. A., K. Shen, and A. Dillin. 2019. Mitochondrial proteostasis in the context of cellular and organismal health and aging. *J Biol Chem* . 294(14):5396-5407.
72. Dolezal, P., V. Likic, J. Tachezy, and T. Lithgow. 2006. Evolution of the Molecular Machines for Protein Import into Mitochondria. *Science* 313: 314-318.
73. Schmidt, O., N. Pfanner, and C. Meisinger. 2010. Mitochondrial protein import: from proteomics to functional mechanisms. *Nature Reviews Molecular Cell Biology* 11: 655-667.
74. Young, J. C., N. J. Hoogenraad, and F. U. Hartl. 2003. Molecular Chaperones Hsp90 and Hsp70 Deliver Preproteins to the Mitochondrial Import Receptor Tom70. *Cell* 112: 41-50.
75. Neupert, W., and J. M. Herrmann. 2007. Translocation of Proteins into Mitochondria. *Annual Review of Biochemistry* 76: 723-749.

76. Saitoh, T., M. Igura, T. Obita, T. Ose, R. Kojima, K. Maenaka, T. Endo, and D. Kohda. 2007. Tom20 recognizes mitochondrial presequences through dynamic equilibrium among multiple bound states. *The EMBO Journal* 26: 4777-4787.
77. Chacinska, A., A. E. Lind M Fau - Frazier, J. Frazier Ae Fau - Dudek, C. Dudek J Fau - Meisinger, A. Meisinger C Fau - Geissler, A. Geissler A Fau - Sickmann, H. E. Sickmann A Fau - Meyer, K. N. Meyer He Fau - Truscott, B. Truscott Kn Fau - Guiard, N. Guiard B Fau - Pfanner, P. Pfanner N Fau - Rehling, and P. Rehling. 2005. Mitochondrial presequence translocase: switching between TOM tethering and motor recruitment involves Tim21 and Tim17. *Cell* . 120(6):817-829.
78. Chacinska, A., M. van der Laan, S. Mehnert Carola, B. Guiard, U. Mick David, P. Hutu Dana, N. Truscott Kaye, N. Wiedemann, C. Meisinger, N. Pfanner, and P. Rehling. 2010. Distinct Forms of Mitochondrial TOM-TIM Supercomplexes Define Signal-Dependent States of Preprotein Sorting. *Molecular and Cellular Biology* 30: 307-318.
79. Vögtle, F. N., R. P. Wortelkamp S Fau - Zahedi, D. Zahedi Rp Fau - Becker, C. Becker D Fau - Leidhold, K. Leidhold C Fau - Gevaert, J. Gevaert K Fau - Kellermann, W. Kellermann J Fau - Voos, A. Voos W Fau - Sickmann, N. Sickmann A Fau - Pfanner, C. Pfanner N Fau - Meisinger, and C. Meisinger. 2009. Global analysis of the mitochondrial N-proteome identifies a processing peptidase critical for protein stability. *Cell* . 139(2):428-439.
80. Koppen, M., and T. Langer. 2007. Protein Degradation within Mitochondria: Versatile Activities of AAA Proteases and Other Peptidases. *Critical Reviews in Biochemistry and Molecular Biology* 42: 221-242.
81. Sinha, D., S. Srivastava, L. Krishna, and P. D'Silva. 2014. Unraveling the Intricate Organization of Mammalian Mitochondrial Presequence Translocases: Existence of Multiple Translocases for Maintenance of Mitochondrial Function. *Molecular and Cellular Biology* 34: 1757-1775.
82. Pagliarini, D. J., B. Calvo Se Fau - Chang, S. A. Chang B Fau - Sheth, S. B. Sheth Sa Fau - Vafai, S.-E. Vafai Sb Fau - Ong, G. A. Ong Se Fau - Walford, C. Walford Ga Fau - Sugiana, A. Sugiana C Fau - Boneh, W. K. Boneh A Fau - Chen, D. E. Chen Wk Fau - Hill, M. Hill De Fau - Vidal, J. G. Vidal M Fau - Evans, D. R. Evans Jg Fau - Thorburn, S. A. Thorburn Dr Fau - Carr, V. K. Carr Sa Fau - Mootha, and V. K. Mootha. 2008. A mitochondrial protein compendium elucidates complex I disease biology. *Cell* . 134(1):112-123.
83. Morgenstern, M., S. B. Stiller, P. Lübbert, C. D. Peikert, S. Dannenmaier, F. Drepper, U. Weill, P. Höß, R. Feuerstein, M. Gebert, M. Bohnert, M. van der Laan, M. Schuldiner, C. Schütze, S. Oeljeklaus, N. Pfanner, N. Wiedemann, and B. Warscheid. 2017. Definition of a High-Confidence Mitochondrial Proteome at Quantitative Scale. *Cell Rep* . 19(13):2836-2852.
84. Hansen, K. G., and J. M. Herrmann. 2019. Transport of Proteins into Mitochondria. *The Protein Journal* 38: 330-342.
85. Kang, P.-J., J. Ostermann, J. Shilling, W. Neupert, E. A. Craig, and N. Pfanner. 1990. Requirement for hsp70 in the mitochondrial matrix for translocation and folding of precursor proteins. *Nature* 348: 137-143.
86. Srivastava, S., M. A. Savanur, D. Sinha, A. Birje, V. R, P. P. Saha, and P. D'Silva. 2017. Regulation of mitochondrial protein import by the nucleotide exchange factors GrpEL1 and GrpEL2 in human cells. *J Biol Chem* . 292(44):18075-18090.
87. Horst, M., W. Oppliger, S. Rospert, H.-J. Schönfeld, G. Schatz, and A. Azem. 1997. Sequential action of two hsp70 complexes during protein import into mitochondria. *The EMBO Journal* 16: 1842-1849.
88. Deshwal, S., K. U. Fiedler, and T. Langer. 2020. Mitochondrial Proteases: Multifaceted Regulators of Mitochondrial Plasticity. *Annual Review of Biochemistry* 89: 501-528.
89. Quirós, P. M., A. Mottis, and J. Auwerx. 2016. Mitonuclear communication in homeostasis and stress. *Nature Reviews Molecular Cell Biology* 17: 213-226.
90. Goard, C. A., and A. D. Schimmer. 2014. Mitochondrial matrix proteases as novel therapeutic targets in malignancy. *Oncogene* 33: 2690-2699.
91. Sauer, R. T., and T. A. Baker. 2011. AAA+ Proteases: ATP-Fueled Machines of Protein Destruction. *Annual Review of Biochemistry* 80: 587-612.

92. Wong, K. S., and W. A. Houry. 2019. Recent Advances in Targeting Human Mitochondrial AAA+ Proteases to Develop Novel Cancer Therapeutics. *In* Mitochondria in Health and in Sickness. A. Urbani and M. Babu, editors. Springer Singapore, Singapore. 119-142.
93. Ondrovicová, G., K. Liu T Fau - Singh, B. Singh K Fau - Tian, H. Tian B Fau - Li, O. Li H Fau - Gakh, D. Gakh O Fau - Perecko, J. Perecko D Fau - Janata, Z. Janata J Fau - Granot, J. Granot Z Fau - Orly, E. Orly J Fau - Kutejová, C. K. Kutejová E Fau - Suzuki, and C. K. Suzuki. 2005. Cleavage site selection within a folded substrate by the ATP-dependent lon protease. *J Biol Chem* . 280(26):25103-25110.
94. Voos, W., and K. Pollecker. 2020. The Mitochondrial Lon Protease: Novel Functions off the Beaten Track? *Biomolecules* 10.
95. Truscott, K. N., A. Bezawork-Geleta, and D. A. Dougan. 2011. Unfolded protein responses in bacteria and mitochondria: A central role for the ClpXP machine. *IUBMB Life* 63: 955-963.
96. Ripstein, Z. A., S. Vahidi, W. A. Houry, J. L. Rubinstein, and L. E. Kay. 2020. A processive rotary mechanism couples substrate unfolding and proteolysis in the ClpXP degradation machinery. *eLife* 9: e52158.
97. Fischer, F., J. D. Langer, and H. D. Osiewacz. 2015. Identification of potential mitochondrial CLPXP protease interactors and substrates suggests its central role in energy metabolism. *Scientific Reports* 5: 18375.
98. Zhao, Q., J. Wang, I. V. Levichkin, S. Stasinopoulos, M. T. Ryan, and N. J. Hoogenraad. 2002. A mitochondrial specific stress response in mammalian cells. *The EMBO journal* 21: 4411-4419.
99. Berry, B. J., T. O. Nieves, and A. P. Wojtovich. 2021. Decreased Mitochondrial Membrane Potential Activates the Mitochondrial Unfolded Protein Response. *microPublication biology* 2021: 10.17912/micropub.biology.000445.
100. Haynes, C. M., and D. Ron. 2010. The mitochondrial UPR – protecting organelle protein homeostasis. *Journal of Cell Science* 123: 3849-3855.
101. Haynes, C. M., K. Petrova, C. Benedetti, Y. Yang, and D. Ron. 2007. ClpP Mediates Activation of a Mitochondrial Unfolded Protein Response in C. elegans. *Developmental Cell* 13: 467-480.
102. Bennett, C. F., H. Vander Wende, M. Simko, S. Klum, S. Barfield, H. Choi, V. V. Pineda, and M. Kaeberlein. 2014. Activation of the mitochondrial unfolded protein response does not predict longevity in Caenorhabditis elegans. *Nature Communications* 5: 3483.
103. Runkel, E. D., R. Liu S Fau - Baumeister, E. Baumeister R Fau - Schulze, and E. Schulze. 2013. Surveillance-activated defenses block the ROS-induced mitochondrial unfolded protein response. *PLoS Genet.* 9(3):e1003346.
104. Nargund Amrita, M., W. Pellegrino Mark, J. Fiorese Christopher, M. Baker Brooke, and M. Haynes Cole. 2012. Mitochondrial Import Efficiency of ATFS-1 Regulates Mitochondrial UPR Activation. *Science* 337: 587-590.
105. Wrobel, L., U. Topf, P. Bragoszewski, S. Wiese, M. E. Sztolsztener, S. Oeljeklaus, A. Varabyova, M. Lirski, P. Chroscicki, S. Mroczek, E. Januszewicz, A. Dziembowski, M. Koblowska, B. Warscheid, and A. Chacinska. 2015. Mistargeted mitochondrial proteins activate a proteostatic response in the cytosol. *Nature* 524: 485-488.
106. Wang, X., and X. J. Chen. 2015. A cytosolic network suppressing mitochondria-mediated proteostatic stress and cell death. *Nature* 524: 481-484.
107. Fiorese, Christopher J., Anna M. Schulz, Y.-F. Lin, N. Rosin, Mark W. Pellegrino, and Cole M. Haynes. 2016. The Transcription Factor ATF5 Mediates a Mammalian Mitochondrial UPR. *Current Biology* 26: 2037-2043.
108. Zhou, D., L. Palam Lr Fau - Jiang, J. Jiang L Fau - Narasimhan, K. A. Narasimhan J Fau - Staschke, R. C. Staschke Ka Fau - Wek, and R. C. Wek. 2008 Phosphorylation of eIF2 directs ATF5 translational control in response to diverse stress conditions. *J Biol Chem.* 283(11):7064-73.

109. Jousse, C., A. Bruhat, V. Carraro, F. Urano, M. Ferrara, D. Ron, and P. Fafournoux. 2001. Inhibition of CHOP translation by a peptide encoded by an open reading frame localized in the chop 5′UTR. *Nucleic Acids Research* 29: 4341-4351.
110. Aldridge, J. E., T. Horibe, and N. J. Hoogenraad. 2007. Discovery of genes activated by the mitochondrial unfolded protein response (mtUPR) and cognate promoter elements. *In* PloS one. e874.
111. Horibe, T., and N. J. Hoogenraad. 2007. The chop gene contains an element for the positive regulation of the mitochondrial unfolded protein response. *PloS one* 2: e835-e835.
112. Watatani, Y., N. Ichikawa K Fau - Nakanishi, M. Nakanishi N Fau - Fujimoto, H. Fujimoto M Fau - Takeda, N. Takeda H Fau - Kimura, H. Kimura N Fau - Hirose, S. Hirose H Fau - Takahashi, Y. Takahashi S Fau - Takahashi, and Y. Takahashi. 2008. Stress-induced translation of ATF5 mRNA is regulated by the 5'-untranslated region. *J Biol Chem* . 283(5):2543-2553.
113. Rainbolt, T. K., J. C. Atanassova N Fau - Genereux, R. L. Genereux Jc Fau - Wiseman, and R. L. Wiseman. 2013. Stress-regulated translational attenuation adapts mitochondrial protein import through Tim17A degradation. *Cell Metab* . 18(6):908-919.
114. Poveda-Huertes, D. A.-O., A. A. Taskin, I. A.-O. Dhaouadi, L. Myketin, A. Marada, L. A.-O. Habernig, S. A.-O. Büttner, and F. A.-O. Vögtle. 2021. Increased mitochondrial protein import and cardiolipin remodelling upon early mtUPR. *PLoS Genet* . 17(7):e1009664.
115. Zurita Rendón, O., and A. Shoubridge Eric. LONP1 Is Required for Maturation of a Subset of Mitochondrial Proteins, and Its Loss Elicits an Integrated Stress Response. *Molecular and Cellular Biology* 38: e00412-00417.
116. Bezawork-Geleta, A., E. J. Brodie, D. A. Dougan, and K. N. Truscott. 2015. LON is the master protease that protects against protein aggregation in human mitochondria through direct degradation of misfolded proteins. *Scientific Reports* 5: 17397.
117. Shin, C.-S., S. Meng, S. D. Garbis, A. Moradian, R. W. Taylor, M. J. Sweredoski, B. Lomenick, and D. C. Chan. 2021. LONP1 and mtHSP70 cooperate to promote mitochondrial protein folding. *Nature Communications* 12: 265.
118. Hannun, Y. A., and L. M. Obeid. 2008. Principles of bioactive lipid signalling: lessons from sphingolipids. *Nature Reviews Molecular Cell Biology* 9: 139-150.
119. Thudichum, M. D. 1884. A Treatise on the Chemical Constitution of the Brain: Based Throughout upon Original Researches. *Glasgow Medical Journal* 22: 363-364.
120. Hannun, Y. A., and L. M. Obeid. 2018. Sphingolipids and their metabolism in physiology and disease. *Nature Reviews Molecular Cell Biology* 19: 175-191.
121. Gault, C. R., L. M. Obeid, and Y. A. Hannun. 2010. An Overview of Sphingolipid Metabolism: From Synthesis to Breakdown. *In* Sphingolipids as Signaling and Regulatory Molecules. C. Chalfant and M. D. Poeta, editors. Springer New York, New York, NY. 1-23.
122. Han, G., S. D. Gupta, K. Gable, S. Niranjanakumari, P. Moitra, F. Eichler, R. H. Brown, J. M. Harmon, and T. M. Dunn. 2009. Identification of small subunits of mammalian serine palmitoyltransferase that confer distinct acyl-CoA substrate specificities. *Proceedings of the National Academy of Sciences* 106: 8186.
123. Bode, H., F. Bourquin, S. Suriyanarayanan, Y. Wei, I. Alecu, A. Othman, A. Von Eckardstein, and T. Hornemann. 2016. HSAN1 mutations in serine palmitoyltransferase reveal a close structure–function–phenotype relationship. *Human Molecular Genetics* 25: 853-865.
124. Breslow, D. K., S. R. Collins, B. Bodenmiller, R. Aebersold, K. Simons, A. Shevchenko, C. S. Ejsing, and J. S. Weissman. 2010. Orm family proteins mediate sphingolipid homeostasis. *Nature* 463: 1048-1053.
125. Pewzner-Jung, Y., A. H. Ben-Dor S Fau - Futerman, and A. H. Futerman. 2006. When do Lasses (longevity assurance genes) become CerS (ceramide synthases)?: Insights into the regulation of ceramide synthesis. *J Biol Chem* . 281(35):25001-25005.
126. Kraveka, J. M., Z. M. Li L Fau - Szulc, J. Szulc Zm Fau - Bielawski, B. Bielawski J Fau - Ogretmen, Y. A. Ogretmen B Fau - Hannun, L. M. Hannun Ya Fau - Obeid, A. Obeid Lm Fau - Bielawska, and A. Bielawska. 2007. Involvement of dihydroceramide desaturase in cell cycle progression in human neuroblastoma cells. *J Biol Chem* . 282(23):16718-16728.

127. Hanada, K., K. Kumagai, S. Yasuda, Y. Miura, M. Kawano, M. Fukasawa, and M. Nishijima. 2003. Molecular machinery for non-vesicular trafficking of ceramide. *Nature* 426: 803-809.
128. Huitema, K., J. van den Dikkenberg, J. F. H. M. Brouwers, and J. C. M. Holthuis. 2004. Identification of a family of animal sphingomyelin synthases. *The EMBO journal* 23: 33-44.
129. Ikeda, M., A. Kihara, and Y. Igarashi. 2004. Sphingosine-1-phosphate lyase SPL is an endoplasmic reticulum-resident, integral membrane protein with the pyridoxal 5′-phosphate binding domain exposed to the cytosol. *Biochemical and Biophysical Research Communications* 325: 338-343.
130. Maceyka, M., K. B. Harikumar, S. Milstien, and S. Spiegel. 2012. Sphingosine-1-phosphate signaling and its role in disease. *Trends in Cell Biology* 22: 50-60.
131. Dempsey, L. A. 2019. Distinct S1PR roles. *Nature Immunology* 20: 517-517.
132. Kharel, Y., S. Lee, A. H. Snyder, S. L. Sheasley-O'Neill, M. A. Morris, Y. Setiady, R. Zhu, M. A. Zigler, T. L. Burcin, K. Ley, K. S. K. Tung, V. H. Engelhard, T. L. Macdonald, S. Pearson-White, and K. R. Lynch. 2005. Sphingosine Kinase 2 Is Required for Modulation of Lymphocyte Traffic by FTY720*. *Journal of Biological Chemistry* 280: 36865-36872.
133. Maria L Allende , T. S., Hiromichi Kawai , Ana Olivera , Yide Mi , Gerhild van Echten-Deckert , Richard Hajdu , Mark Rosenbach , Carol Ann Keohane , Suzanne Mandala , Sarah Spiegel , Richard L Proia. 2004. Mice deficient in sphingosine kinase 1 are rendered lymphopenic by FTY720. *J Biol Chem* . ;279(50):52487-52492.
134. Pham, T. H., M. Okada T Fau - Matloubian, C. G. Matloubian M Fau - Lo, J. G. Lo Cg Fau - Cyster, and J. G. Cyster. 2008. S1P1 receptor signaling overrides retention mediated by G alpha i-coupled receptors to promote T cell egress. *Immunity* . 28(1):122-133.
135. Brinkmann, V., A. Billich, T. Baumruker, P. Heining, R. Schmouder, G. Francis, S. Aradhye, and P. Burtin. 2010. Fingolimod (FTY720): discovery and development of an oral drug to treat multiple sclerosis. *Nature Reviews Drug Discovery* 9: 883-897.
136. Liu, H., D. Chakravarty, M. Maceyka, S. Milstien, and S. Spiegel. 2002. Sphingosine kinases: A novel family of lipid kinases. *In* Progress in Nucleic Acid Research and Molecular Biology. Academic Press. 493-511.
137. Ogretmen, B. 2018. Sphingolipid metabolism in cancer signalling and therapy. *Nature Reviews Cancer* 18: 33-50.
138. Alvarez, S. E., S. Milstien, and S. Spiegel. 2007. Autocrine and paracrine roles of sphingosine-1-phosphate. *Trends in Endocrinology & Metabolism* 18: 300-307.
139. Kate E Jarman , P. A. B. M., Julia R Zebol , Stuart M Pitson. 2010. Translocation of sphingosine kinase 1 to the plasma membrane is mediated by calcium- and integrin-binding protein 1. *J Biol Chem* . 285(1):483-492.
140. Nishino, S., H. Yamashita, M. Tamori, M. Mashimo, K. Yamagata, H. Nakamura, and T. Murayama. 2019. Translocation and activation of sphingosine kinase 1 by ceramide-1-phosphate. *Journal of Cellular Biochemistry* 120: 5396-5408.
141. Alvarez, S. E., K. B. Harikumar, N. C. Hait, J. Allegood, G. M. Strub, E. Y. Kim, M. Maceyka, H. Jiang, C. Luo, T. Kordula, S. Milstien, and S. Spiegel. 2010. Sphingosine-1-phosphate is a missing cofactor for the E3 ubiquitin ligase TRAF2. *Nature* 465: 1084-1088.
142. Parham, K. A., J. R. Zebol, K. L. Tooley, W. Y. Sun, L. M. Moldenhauer, M. P. Cockshell, B. L. Gliddon, P. A. Moretti, G. Tigyi, S. M. Pitson, and C. S. Bonder. 2015. Sphingosine 1-phosphate is a ligand for peroxisome proliferator-activated receptor-γ that regulates neoangiogenesis. *The FASEB Journal* 29: 3638-3653.
143. Liu, H., V. E. Sugiura M Fau - Nava, L. C. Nava Ve Fau - Edsall, K. Edsall Lc Fau - Kono, S. Kono K Fau - Poulton, S. Poulton S Fau - Milstien, T. Milstien S Fau - Kohama, S. Kohama T Fau - Spiegel, and S. Spiegel. Molecular cloning and functional characterization of a novel mammalian sphingosine kinase type 2 isoform.
144. Ding, G., H. Sonoda, H. Yu, T. Kajimoto, S. K. Goparaju, S. Jahangeer, T. Okada, and S. I. Nakamura. 2007. Protein kinase D-mediated phosphorylation and nuclear export of sphingosine kinase 2. *J Biol Chem* . 282(37):27493-27502.

145. Ebenezer, D. L., E. V. Berdyshev, I. A. Bronova, Y. Liu, C. Tiruppathi, Y. Komarova, E. V. Benevolenskaya, V. Suryadevara, A. W. Ha, A. Harijith, R. M. Tuder, V. Natarajan, and P. Fu. 2019. Pseudomonas aeruginosa stimulates nuclear sphingosine-1-phosphate generation and epigenetic regulation of lung inflammatory injury. *Thorax* 74: 579-591.
146. Hait Nitai, C., J. Allegood, M. Maceyka, M. Strub Graham, B. Harikumar Kuzhuvelil, K. Singh Sandeep, C. Luo, R. Marmorstein, T. Kordula, S. Milstien, and S. Spiegel. 2009. Regulation of Histone Acetylation in the Nucleus by Sphingosine-1-Phosphate. *Science* 325: 1254-1257.
147. Hait, N. C., L. E. Wise, J. C. Allegood, M. O'Brien, D. Avni, T. M. Reeves, P. E. Knapp, J. Lu, C. Luo, M. F. Miles, S. Milstien, A. H. Lichtman, and S. Spiegel. 2014. Active, phosphorylated fingolimod inhibits histone deacetylases and facilitates fear extinction memory. *Nature Neuroscience* 17: 971-980.
148. Fu, P., R. Ramchandran, T. Sudhadevi, P. P. K. Kumar, Y. Krishnan, Y. Liu, Y. Zhao, N. L. Parinandi, A. Harijith, J. Sadoshima, and V. Natarajan. 2021. NOX4 Mediates Pseudomonas aeruginosa-Induced Nuclear Reactive Oxygen Species Generation and Chromatin Remodeling in Lung Epithelium. *Antioxidants* 10.
149. Strub, G. M., M. Paillard, J. Liang, L. Gomez, J. C. Allegood, N. C. Hait, M. Maceyka, M. M. Price, Q. Chen, D. C. Simpson, T. Kordula, S. Milstien, E. J. Lesnefsky, and S. Spiegel. 2011. Sphingosine-1-phosphate produced by sphingosine kinase 2 in mitochondria interacts with prohibitin 2 to regulate complex IV assembly and respiration. *The FASEB Journal* 25: 600-612.
150. Takabe, K., and S. Spiegel. 2014. Export of sphingosine-1-phosphate and cancer progression. *J Lipid Res* . 55(9):1839-1846.
151. Brindley, D. N. 2004. Lipid phosphate phosphatases and related proteins: Signaling functions in development, cell division, and cancer. *Journal of Cellular Biochemistry* 92: 900-912.
152. Giussani, P., M. Maceyka, H. Le Stunff, A. Mikami, S. Lépine, E. Wang, S. Kelly, H. Merrill Alfred, S. Milstien, and S. Spiegel. 2006. Sphingosine-1-Phosphate Phosphohydrolase Regulates Endoplasmic Reticulum-to-Golgi Trafficking of Ceramide. *Molecular and Cellular Biology* 26: 5055-5069.
153. Huang, W.-C., J. Liang, M. Nagahashi, D. Avni, A. Yamada, M. Maceyka, A. R. Wolen, T. Kordula, S. Milstien, K. Takabe, T. Oravecz, and S. Spiegel. 2016. Sphingosine-1-phosphate phosphatase 2 promotes disruption of mucosal integrity, and contributes to ulcerative colitis in mice and humans. *The FASEB Journal* 30: 2945-2958.
154. Mechtcheriakova, D., A. Wlachos, J. Sobanov, T. Kopp, R. Reuschel, F. Bornancin, R. Cai, B. Zemann, N. Urtz, G. Stingl, G. Zlabinger, M. Woisetschläger, T. Baumruker, and A. Billich. 2007. Sphingosine 1-phosphate phosphatase 2 is induced during inflammatory responses. *Cellular Signalling* 19: 748-760.
155. Gottlieb, D., W. Heideman, and J. D. Saba. 1999. TheDPL1Gene Is Involved in Mediating the Response to Nutrient Deprivation inSaccharomyces cerevisiae. *Molecular Cell Biology Research Communications* 1: 66-71.
156. Birchwood, C. J., R. C. Saba Jd Fau - Dickson, K. W. Dickson Rc Fau - Cunningham, and K. W. Cunningham. 2001. Calcium influx and signaling in yeast stimulated by intracellular sphingosine 1-phosphate accumulation. *J Biol Chem* . 276(15):11712-11718.
157. Bektas, M., M. L. Allende, B. G. Lee, W. Chen, M. J. Amar, A. T. Remaley, J. D. Saba, and R. L. Proia. 2010. Sphingosine 1-phosphate lyase deficiency disrupts lipid homeostasis in liver. *The Journal of biological chemistry* 285: 10880-10889.
158. Weber, C., A. Krueger A Fau - Münk, C. Münk A Fau - Bode, P. P. Bode C Fau - Van Veldhoven, M. H. Van Veldhoven Pp Fau - Gräler, and M. H. Gräler. 2009. Discontinued postnatal thymocyte development in sphingosine 1-phosphate-lyase-deficient mice. *J Immunol* . 183(7):4292-4301.
159. Allende, M. L., B. G. Bektas M Fau - Lee, E. Lee Bg Fau - Bonifacino, J. Bonifacino E Fau - Kang, G. Kang J Fau - Tuymetova, W. Tuymetova G Fau - Chen, J. D. Chen W Fau - Saba, R. L. Saba Jd Fau - Proia, and R. L. Proia. 2011. Sphingosine-1-phosphate lyase

deficiency produces a pro-inflammatory response while impairing neutrophil trafficking. *J Biol Chem* . 286(9):7348-7358.
160. -, D. E., P. A. -, B. P. -, K. A. -, E. A. -, Z. M. -, Y. Y. -, N. M. -, d. J. P. J. -, F. L. G. -, Y. S. G. -, B. R. -, A. Y. -, and J. D. Saba. 2014. Sphingosine-1-phosphate lyase downregulation promotes colon carcinogenesis through STAT3-activated microRNAs. *J Clin Invest* . 124(12):5368-5384.
161. Mitroi, D. N., A. U. Deutschmann, M. Raucamp, I. Karunakaran, K. Glebov, M. Hans, J. Walter, J. Saba, M. Gräler, D. Ehninger, E. Sopova, O. Shupliakov, D. Swandulla, and G. van Echten-Deckert. 2016. Sphingosine 1-phosphate lyase ablation disrupts presynaptic architecture and function via an ubiquitin- proteasome mediated mechanism. *Scientific Reports* 6: 37064.
162. Serra, M., and J. D. Saba. 2010. Sphingosine 1-phosphate lyase, a key regulator of sphingosine 1-phosphate signaling and function. *Advances in enzyme regulation* 50: 349-362.
163. Van Veldhoven, P. P., and G. P. Mannaerts. 1991. Subcellular localization and membrane topology of sphingosine-1-phosphate lyase in rat liver. *J Biol Chem* . 266(19):12502-12507.
164. Van Veldhoven, P. P. 2000. Sphingosine-1-phosphate lyase. *In* Methods in Enzymology. Academic Press. 244-254.
165. Dawoody Nejad, L., M. Stumpe, M. Rauch, A. Hemphill, R. Schneiter, P. Bütikofer, and M. Serricchio. 2020. Mitochondrial sphingosine-1-phosphate lyase is essential for phosphatidylethanolamine synthesis and survival of Trypanosoma brucei. *Scientific Reports* 10: 8268.
166. Degtyar, E., T. Zusman, M. Ehrlich, and G. Segal. 2009. A Legionella effector acquired from protozoa is involved in sphingolipids metabolism and is targeted to the host cell mitochondria. *Cellular Microbiology* 11: 1219-1235.
167. Ebenezer, D. L., R. Ramchandran, P. Fu, L. A. Mangio, V. Suryadevara, A. W. Ha, E. Berdyshev, P. P. Van Veldhoven, S. J. Kron, F. Schumacher, B. Kleuser, and V. Natarajan. 2021. Nuclear Sphingosine-1-phosphate Lyase Generated Δ2-hexadecenal is A Regulator of HDAC Activity and Chromatin Remodeling in Lung Epithelial Cells. *Cell Biochemistry and Biophysics* 79: 575-592.
168. Wallington-Beddoe, C. T., M. K. Bennett, K. Vandyke, L. Davies, J. R. Zebol, P. A. B. Moretti, M. R. Pitman, D. R. Hewett, A. C. W. Zannettino, and S. M. Pitson. 2017. Sphingosine kinase 2 inhibition synergises with bortezomib to target myeloma by enhancing endoplasmic reticulum stress. *Oncotarget; Vol 8, No 27*.
169. Li, L., H. Wang, J. Zhang, Y. Sha, F. Wu, S. Wen, L. He, L. Sheng, Q. You, M. Shi, L. Liu, and H. Zhou. 2020. SPHK1 deficiency protects mice from acetaminophen-induced ER stress and mitochondrial permeability transition. *Cell Death & Differentiation* 27: 1924-1937.
170. Taguchi, Y., M. L. Allende, H. Mizukami, E. K. Cook, O. Gavrilova, G. Tuymetova, B. A. Clarke, W. Chen, A. Olivera, and R. L. Proia. 2016. Sphingosine-1-phosphate Phosphatase 2 Regulates Pancreatic Islet β-Cell Endoplasmic Reticulum Stress and Proliferation. *J Biol Chem* . 291(23):12029-12038.
171. Epstein, S., C. L. Kirkpatrick, G. A. Castillon, M. Muñiz, I. Riezman, F. P. A. David, C. B. Wollheim, and H. Riezman. 2012. Activation of the unfolded protein response pathway causes ceramide accumulation in yeast and INS-1E insulinoma cells. *Journal of lipid research* 53: 412-420.
172. Park, K., H. Ikushiro, H. S. Seo, K.-O. Shin, Y. i. Kim, J. Y. Kim, Y.-M. Lee, T. Yano, W. M. Holleran, P. Elias, and Y. Uchida. 2016. ER stress stimulates production of the key antimicrobial peptide, cathelicidin, by forming a previously unidentified intracellular S1P signaling complex. *Proceedings of the National Academy of Sciences* 113: E1334.
173. Lee, S.-Y., I.-K. Hong, B.-R. Kim, S.-M. Shim, J. Sung Lee, H.-Y. Lee, C. Soo Choi, B.-K. Kim, and T.-S. Park. 2015. Activation of sphingosine kinase 2 by endoplasmic reticulum stress ameliorates hepatic steatosis and insulin resistance in mice. *Hepatology* 62: 135-146.
174. Ali, T., X. Lei, S. E. Barbour, A. Koizumi, C. E. Chalfant, and S. Ramanadham. 2021. Alterations in β-Cell Sphingolipid Profile Associated with ER Stress and iPLA2β: Another Contributor to β-Cell Apoptosis in Type 1 Diabetes. *Molecules* 26.

175. Sentelle, R. D., C. E. Senkal, W. Jiang, S. Ponnusamy, S. Gencer, S. Panneer Selvam, V. K. Ramshesh, Y. K. Peterson, J. J. Lemasters, Z. M. Szulc, J. Bielawski, and B. Ogretmen. 2012. Ceramide targets autophagosomes to mitochondria and induces lethal mitophagy. *Nature Chemical Biology* 8: 831-838.
176. Hong, S.-W., J. Lee, H. Kwon, S. E. Park, E.-J. Rhee, C.-Y. Park, K.-W. Oh, S.-W. Park, and W.-Y. Lee. 2018. Deficiency of Sphingosine-1-Phosphate Reduces the Expression of Prohibitin and Causes β-Cell Impairment via Mitochondrial Dysregulation. *Endocrinol Metab* 33: 403-412.
177. Kim, S., and D. Sieburth. 2018. Sphingosine Kinase Activates the Mitochondrial Unfolded Protein Response and Is Targeted to Mitochondria by Stress. *Cell Rep* 24: 2932-2945 e2934.
178. Schmitz, M. L., M. S. Shaban, B. V. Albert, A. Gökçen, and M. Kracht. 2018. The Crosstalk of Endoplasmic Reticulum (ER) Stress Pathways with NF-κB: Complex Mechanisms Relevant for Cancer, Inflammation and Infection. *Biomedicines* 6: 58.
179. Chen, G. Y., and G. Nuñez. 2010. Sterile inflammation: sensing and reacting to damage. *Nature Reviews Immunology* 10: 826-837.
180. Guo, H., J. B. Callaway, and J. P. Y. Ting. 2015. Inflammasomes: mechanism of action, role in disease, and therapeutics. *Nature Medicine* 21: 677-687.
181. Lerner, A. G., P. V. K. Upton Jp Fau - Praveen, R. Praveen Pv Fau - Ghosh, Y. Ghosh R Fau - Nakagawa, A. Nakagawa Y Fau - Igbaria, S. Igbaria A Fau - Shen, V. Shen S Fau - Nguyen, B. J. Nguyen V Fau - Backes, M. Backes Bj Fau - Heiman, N. Heiman M Fau - Heintz, P. Heintz N Fau - Greengard, S. Greengard P Fau - Hui, Q. Hui S Fau - Tang, A. Tang Q Fau - Trusina, S. A. Trusina A Fau - Oakes, F. R. Oakes Sa Fau - Papa, and F. R. Papa. 2012. IRE1α induces thioredoxin-interacting protein to activate the NLRP3 inflammasome and promote programmed cell death under irremediable ER stress. *Cell Metab* . ;16(2):250-264.
182. Chen, Y., J. J. Wang, J. Li, K. I. Hosoya, R. Ratan, T. Townes, and S. X. Zhang. 2012. Activating transcription factor 4 mediates hyperglycaemia-induced endothelial inflammation and retinal vascular leakage through activation of STAT3 in a mouse model of type 1 diabetes. *Diabetologia* 55: 2533-2545.
183. Soni, P. R., M. Noval Rivas, and M. Arditi. 2020. A Comprehensive Update on Kawasaki Disease Vasculitis and Myocarditis. *Current Rheumatology Reports* 22: 6.
184. McCrindle, B. W., A. H. Rowley, J. W. Newburger, J. C. Burns, A. F. Bolger, M. Gewitz, A. L. Baker, M. A. Jackson, M. Takahashi, P. B. Shah, T. Kobayashi, M.-H. Wu, T. T. Saji, E. Pahl, and n. null. 2017. Diagnosis, Treatment, and Long-Term Management of Kawasaki Disease: A Scientific Statement for Health Professionals From the American Heart Association. *Circulation* 135: e927-e999.
185. Newburger, J. W., M. Takahashi, and J. C. Burns. 2016. Kawasaki Disease. *Journal of the American College of Cardiology* 67: 1738-1749.
186. Burns, J. C. 2009. Kawasaki Disease update. *The Indian Journal of Pediatrics* 76: 71-76.
187. Skochko, S. M., S. Jain, X. Sun, N. Sivilay, J. T. Kanegaye, J. Pancheri, C. Shimizu, R. Sheets, A. H. Tremoulet, and J. C. Burns. 2018. Kawasaki Disease Outcomes and Response to Therapy in a Multiethnic Community: A 10-Year Experience. *J Pediatr* . 203:408-415.e3.
188. Lee, Y., D. J. Schulte, K. Shimada, S. Chen, T. R. Crother, N. Chiba, M. C. Fishbein, T. J. A. Lehman, and M. Arditi. 2012. Interleukin-1β Is Crucial for the Induction of Coronary Artery Inflammation in a Mouse Model of Kawasaki Disease. *Circulation* 125: 1542-1550.
189. Wakita, D., Y. Kurashima, T. R. Crother, M. Noval Rivas, Y. Lee, S. Chen, W. Fury, Y. Bai, S. Wagner, D. Li, T. Lehman, M. C. Fishbein, H. M. Hoffman, P. K. Shah, K. Shimada, and M. Arditi. 2016. Role of Interleukin-1 Signaling in a Mouse Model of Kawasaki Disease–Associated Abdominal Aortic Aneurysm. *Arteriosclerosis, Thrombosis, and Vascular Biology* 36: 886-897.
190. Porritt, R. A., D. Zemmour, M. Abe, Y. Lee, M. Narayanan, T. T. Carvalho, A. C. Gomez, D. Martinon, C. Santiskulvong, M. C. Fishbein, S. Chen, T. R. Crother, K. Shimada,

M. Arditi, and M. Noval Rivas. 2021. NLRP3 Inflammasome Mediates Immune-Stromal Interactions in Vasculitis. *Circulation Research* 129: e183-e200.
191. Xu, M., Q. Qi, L. Men, S. Wang, M. Li, M. Xiao, X. Chen, S. Wang, G. Wang, H. Jia, and C. Liu. 2020. Berberine protects Kawasaki disease-induced human coronary artery endothelial cells dysfunction by inhibiting of oxidative and endoplasmic reticulum stress. *Vascular Pharmacology* 127: 106660.
192. Shi, Z., Y. Yin, C. Li, H. Ding, N. Mu, Y. Wang, S. Jin, H. Ma, M. Liu, and J. Zhou. 2021. Lipocalin-2-induced proliferative endoplasmic reticulum stress participates in Kawasaki disease-related pulmonary arterial abnormalities. *Science China Life Sciences* 64: 1000-1012.
193. Iwawaki, T., R. Akai, S. Yamanaka, and K. Kohno. 2009. Function of IRE1 alpha in the placenta is essential for placental development and embryonic viability. *Proceedings of the National Academy of Sciences* 106: 16657.
194. Allen, J. J., M. Li, C. S. Brinkworth, J. L. Paulson, D. Wang, A. Hübner, W.-H. Chou, R. J. Davis, A. L. Burlingame, R. O. Messing, C. D. Katayama, S. M. Hedrick, and K. M. Shokat. 2007. A semisynthetic epitope for kinase substrates. *Nature Methods* 4: 511-516.
195. Bedia, C., L. Camacho, J. Casas, J. L. Abad, A. Delgado , P. P. Van Veldhoven, and G. Fabriàs. 2009. Synthesis of a Fluorogenic Analogue of Sphingosine-1-Phosphate and Its Use to Determine Sphingosine-1-Phosphate Lyase Activity. *ChemBioChem* 10: 820-822.
196. Zhang, D., and J. S. Armstrong. 2007. Bax and the mitochondrial permeability transition cooperate in the release of cytochrome c during endoplasmic reticulum-stress-induced apoptosis. *Cell Death Differ* 14, 703–715.
197. Lee, Y., D. Wakita, J. Dagvadorj, K. Shimada, S. Chen, G. Huang, T. J. A. Lehman, M. C. Fishbein, H. M. Hoffman, T. R. Crother, and M. Arditi. 2015. IL-1 Signaling Is Critically Required in Stromal Cells in Kawasaki Disease Vasculitis Mouse Model. *Arteriosclerosis, Thrombosis, and Vascular Biology* 35: 2605-2616.
198. Becht, E., L. McInnes, J. Healy, C.-A. Dutertre, I. W. H. Kwok, L. G. Ng, F. Ginhoux, and E. W. Newell. 2019. Dimensionality reduction for visualizing single-cell data using UMAP. *Nature Biotechnology* 37: 38-44.
199. Porritt, R. A., J. L. Markman, D. Maruyama, B. Kocaturk, S. Chen, T. J. A. Lehman, Y. Lee, M. C. Fishbein, M. Noval Rivas, and M. Arditi. 2020. Interleukin-1 Beta–Mediated Sex Differences in Kawasaki Disease Vasculitis Development and Response to Treatment. *Arteriosclerosis, Thrombosis, and Vascular Biology* 40: 802-818.
200. Jaggi, P. A.-O., A. Mejias, Z. Xu, H. Yin, M. Moore-Clingenpeel, B. Smith, J. C. Burns, A. H. Tremoulet, A. Jordan-Villegas, D. Chaussabel, K. Texter, V. Pascual, and O. Ramilo. 2018. Whole blood transcriptional profiles as a prognostic tool in complete and incomplete Kawasaki Disease. *PLoS One* . 13(5):e0197858.
201. Wright, V. J., J. A. Herberg, M. Kaforou, C. Shimizu, H. Eleftherohorinou, H. Shailes, A. M. Barendregt, S. Menikou, S. Gormley, M. Berk, L. T. Hoang, A. H. Tremoulet, J. T. Kanegaye, L. J. M. Coin, M. P. Glodé, M. Hibberd, T. W. Kuijpers, C. J. Hoggart, J. C. Burns, M. Levin, and I. a. I. D. S. C. a. t. P. E. M. K. D. R. G. for the Immunopathology of Respiratory. 2018. Diagnosis of Kawasaki Disease Using a Minimal Whole-Blood Gene Expression Signature. *JAMA Pediatrics* 172: e182293-e182293.
202. Hoang, L. T., C. Shimizu, L. Ling, A. N. M. Naim, C. C. Khor, A. H. Tremoulet, V. Wright, M. Levin, M. L. Hibberd, and J. C. Burns. 2014. Global gene expression profiling identifies new therapeutic targets in acute Kawasaki disease. *Genome Medicine* 6: 541.
203. Wu, R., Q.-H. Zhang, Y.-J. Lu, K. Ren, and G.-H. Yi. 2015. Involvement of the IRE1α-XBP1 pathway and XBP1s-dependent transcriptional reprogramming in metabolic diseases. *DNA and cell biology* 34: 6-18.
204. Di Pardo, A., E. Amico, A. Basit, A. Armirotti, P. Joshi, M. D. Neely, R. Vuono, S. Castaldo, A. F. Digilio, F. Scalabrì, G. Pepe, F. Elifani, M. Madonna, S. K. Jeong, B.-M. Park, M. D'Esposito, A. B. Bowman, R. A. Barker, and V. Maglione. 2017. Defective Sphingosine-1-phosphate metabolism is a druggable target in Huntington's disease. *Scientific Reports* 7: 5280.
205. Corazzari, M., P. E. Lovat, J. L. Armstrong, G. M. Fimia, D. S. Hill, M. Birch-Machin, C. P. F. Redfern, and M. Piacentini. 2007. Targeting homeostatic mechanisms of endoplasmic

reticulum stress to increase susceptibility of cancer cells to fenretinide-induced apoptosis: the role of stress proteins ERdj5 and ERp57. *British Journal of Cancer* 96: 1062-1071.
206. Parks, E. J., and M. K. Hellerstein. 2000. Carbohydrate-induced hypertriacylglycerolemia: historical perspective and review of biological mechanisms. *The American Journal of Clinical Nutrition* 71: 412-433.
207. Borradaile, N. M., X. Han, J. D. Harp, S. E. Gale, D. S. Ory, and J. E. Schaffer. 2006. Disruption of endoplasmic reticulum structure and integrity in lipotoxic cell death. *Journal of Lipid Research* 47: 2726-2737.
208. Feng, B., P. M. Yao, Y. Li, C. M. Devlin, D. Zhang, H. P. Harding, M. Sweeney, J. X. Rong, G. Kuriakose, E. A. Fisher, A. R. Marks, D. Ron, and I. Tabas. 2003. The endoplasmic reticulum is the site of cholesterol-induced cytotoxicity in macrophages. *Nature Cell Biology* 5: 781-792.
209. Chang, Y.-C., S.-W. Hee, M.-L. Hsieh, Y.-M. Jeng, and L.-M. Chuang. 2015. The Role of Organelle Stresses in Diabetes Mellitus and Obesity: Implication for Treatment. *Analytical Cellular Pathology* 2015: 972891.
210. Cortés Sanchón, A., H. Santhosh Kumar, M. Mantovani, I. Osinnii, J. M. Mateos, A. Kaech, D. Shcherbakov, R. Akbergenov, and E. C. Böttger. 2021. ER-misfolded proteins become sequestered with mitochondria and impair mitochondrial function. *Communications biology* 4: 1350-1350.
211. Cartier, A., and T. Hla. 2019. Sphingosine 1-phosphate: Lipid signaling in pathology and therapy. *Science* 366.
212. Huang, Y. L., C. L. Chang, C. H. Tang, Y. C. Lin, T. K. Ju, W. P. Huang, and H. Lee. 2014. Extrinsic sphingosine 1-phosphate activates S1P5 and induces autophagy through generating endoplasmic reticulum stress in human prostate cancer PC-3 cells. *Cell Signal.* (3):611-8.
213. Taylor, Rebecca C., and A. Dillin. 2013. XBP-1 Is a Cell-Nonautonomous Regulator of Stress Resistance and Longevity. *Cell* 153: 1435-1447.
214. Özbey, N. P., S. Imanikia, C. Krueger, I. Hardege, J. Morud, M. Sheng, W. R. Schafer, M. O. Casanueva, and R. C. Taylor. 2020. Tyramine Acts Downstream of Neuronal XBP-1s to Coordinate Inter-tissue UPRER Activation and Behavior in C. elegans. *Developmental Cell* 55: 754-770.e756.
215. Shen, Z., C. Liu, P. Liu, J. Zhao, and W. Xu. 2014. Sphingosine 1-phosphate (S1P) promotes mitochondrial biogenesis in Hep G2 cells by activating Peroxisome proliferator-activated receptor γ coactivator 1α (PGC-1α). *Cell stress & chaperones* 19: 541-548.
216. Mielke, M. M., P. Vemuri, and W. A. Rocca. 2014. Clinical epidemiology of Alzheimer's disease: assessing sex and gender differences. *Clinical epidemiology* 6: 37-48.
217. Ciccone, M. M., E. Bilianou, A. Balbarini, M. Gesualdo, L. Ghiadoni, M. Metra, P. Palmiero, R. Pedrinelli, M. Salvetti, P. Scicchitano, A. Zito, S. Novo, and A. V. Mattioli. 2013. Task force on: 'Early markers of atherosclerosis: influence of age and sex'. *Journal of Cardiovascular Medicine* 14.
218. Cao, A. T., M. Mackova, D. Kerage, D. N. Brindley, and D. G. Hemmings. 2017. Sexual dimorphism of metabolic and vascular dysfunction in aged mice and those lacking the sphingosine 1-phosphate receptor 3. *Experimental Gerontology* 99: 87-97.
219. Kumar, A., and J. D. Saba. 2015. Regulation of Immune Cell Migration by Sphingosine-1-Phosphate. *Cellular and molecular biology (OMICS)* 61: 121.
220. Ye, D., Y. Zhao, R. B. Hildebrand, R. R. Singaraja, M. R. Hayden, T. J. C. Van Berkel, and M. Van Eck. 2011. The dynamics of macrophage infiltration into the arterial wall during atherosclerotic lesion development in low-density lipoprotein receptor knockout mice. *The American journal of pathology* 178: 413-422.
221. Takahashi, K., T. Oharaseki, and Y. Yokouchi. 2011. Pathogenesis of Kawasaki disease. *Clinical and experimental immunology* 164 Suppl 1: 20-22.
222. Levkau, B. 2015. HDL-S1P: cardiovascular functions, disease-associated alterations, and therapeutic applications. *Frontiers in pharmacology* 6: 243-243.

223. Hansen, K. G., N. Aviram, J. Laborenz, C. Bibi, M. Meyer, A. Spang, M. Schuldiner, and J. M. Herrmann. 2018. An ER surface retrieval pathway safeguards the import of mitochondrial membrane proteins in yeast. *Science* 361: 1118.
224. Li, H., V. Korennykh Alexei, L. Behrman Shannon, and P. Walter. 2010. Mammalian endoplasmic reticulum stress sensor IRE1 signals by dynamic clustering. *Proceedings of the National Academy of Sciences* 107: 16113-16118.
225. Cao, H., K. Gerhold, J. R. Mayers, M. M. Wiest, S. M. Watkins, and G. S. Hotamisligil. 2008. Identification of a lipokine, a lipid hormone linking adipose tissue to systemic metabolism. *Cell* 134: 933-944.
226. Stefan, N., K. Kantartzis, N. Celebi, H. Staiger, J. Machann, F. Schick, A. Cegan, M. Elcnerova, E. Schleicher, A. Fritsche, and H.-U. Häring. 2010. Circulating palmitoleate strongly and independently predicts insulin sensitivity in humans. *Diabetes care* 33: 405-407.
227. Mozaffarian, D., H. Cao, I. B. King, R. N. Lemaitre, X. Song, D. S. Siscovick, and G. S. Hotamisligil. 2010. Circulating palmitoleic acid and risk of metabolic abnormalities and new-onset diabetes. *The American journal of clinical nutrition* 92: 1350-1358.
228. Wu, J., and R. J. Kaufman. 2006. From acute ER stress to physiological roles of the Unfolded Protein Response. *Cell Death & Differentiation* 13: 374-384.
229. Hait, N. C., J. Allegood, M. Maceyka, G. M. Strub, K. B. Harikumar, S. K. Singh, C. Luo, R. Marmorstein, T. Kordula, S. Milstien, and S. Spiegel. 2009. Regulation of histone acetylation in the nucleus by sphingosine-1-phosphate. *Science (New York, N.Y.)* 325: 1254-1257.
230. Maceyka, M., and S. Spiegel. 2014. Sphingolipid metabolites in inflammatory disease. *Nature* 510: 58-67.
231. Venkatesh, S., M. Li, T. Saito, M. Tong, E. Rashed, S. Mareedu, P. Zhai, C. Bárcena, C. López-Otín, G. Yehia, J. Sadoshima, and C. K. Suzuki. 2019. Mitochondrial LonP1 protects cardiomyocytes from ischemia/reperfusion injury in vivo. *Journal of Molecular and Cellular Cardiology* 128: 38-50.
232. Smyrnias, I., S. P. Gray, D. O. Okonko, G. Sawyer, A. Zoccarato, N. Catibog, B. López, A. González, S. Ravassa, J. Díez, and A. M. Shah. 2019. Cardioprotective Effect of the Mitochondrial Unfolded Protein Response During Chronic Pressure Overload. *Journal of the American College of Cardiology* 73: 1795-1806.
233. Wai, T., J. García-Prieto, J. Baker Michael, C. Merkwirth, P. Benit, P. Rustin, J. Rupérez Francisco, C. Barbas, B. Ibañez, and T. Langer. 2015. Imbalanced OPA1 processing and mitochondrial fragmentation cause heart failure in mice. *Science* 350: aad0116.
234. Marek-Iannucci, S., A. B. Ozdemir, D. Moreira, A. C. Gomez, M. Lane, R. A. Porritt, Y. Lee, K. Shimada, M. Abe, A. Stotland, D. Zemmour, S. Parker, E. Sanchez-Lopez, J. Van Eyk, R. A. Gottlieb, M. C. Fishbein, M. Karin, T. R. Crother, M. N. Rivas, and M. Arditi. 2021. Autophagy-mitophagy induction attenuates cardiovascular inflammation in a murine model of Kawasaki disease vasculitis. *JCI insight* 6: e151981.
235. Fury, W., A. H. Tremoulet, V. E. Watson, B. M. Best, C. Shimizu, J. Hamilton, J. T. Kanegaye, Y. Wei, C. Kao, S. Mellis, C. Lin, and J. C. Burns. 2010. Transcript abundance patterns in Kawasaki disease patients with intravenous immunoglobulin resistance. *Human immunology* 71: 865-873.
236. Chakravarthy, M. V., I. J. Lodhi, L. Yin, R. R. V. Malapaka, H. E. Xu, J. Turk, and C. F. Semenkovich. 2009. Identification of a physiologically relevant endogenous ligand for PPARalpha in liver. *Cell* 138: 476-488.

JOHN WILEY AND SONS LICENSE
TERMS AND CONDITIONS

May 25, 2022

This Agreement between Bilkent University -- Asli Yildirim ("You") and John Wiley and Sons ("John Wiley and Sons") consists of your license details and the terms and conditions provided by John Wiley and Sons and Copyright Clearance Center.

License Number	5310390659916
License date	May 15, 2022
Licensed Content Publisher	John Wiley and Sons
Licensed Content Publication	EMBO Reports
Licensed Content Title	The integrated stress response
Licensed Content Author	Adrienne M Gorman, Afshin Samali, Mila Ljujic, et al
Licensed Content Date	Sep 14, 2016
Licensed Content Volume	17
Licensed Content Issue	10

Licensed Content Pages	22
Type of use	Dissertation/Thesis
Requestor type	University/Academic
Format	Print and electronic
Portion	Figure/table
Number of figures/tables	1
Will you be translating?	No
Title	INVESTIGATING THE TARGETS AND BIOLOGICAL ROLES OF IRE1'S TWO ENZYMATIC ACTIVITIES
Institution name	Bilkent University
Expected presentation date	Jun 2022
Portions	Figure 1
Requestor Location	Bilkent University BIlkent Universtiy Cankaya Ankara, 06800 Turkey Attn: Bilkent University

SPRINGER NATURE LICENSE
TERMS AND CONDITIONS

May 25, 2022

This Agreement between Bilkent University -- Asli Yildirim ("You") and Springer Nature ("Springer Nature") consists of your license details and the terms and conditions provided by Springer Nature and Copyright Clearance Center.

License Number	5310390930527
License date	May 15, 2022
Licensed Content Publisher	Springer Nature
Licensed Content Publication	Nature Reviews Molecular Cell Biology
Licensed Content Title	Mitochondrial protein import: from proteomics to functional mechanisms
Licensed Content Author	Oliver Schmidt et al
Licensed Content Date	Dec 31, 1969
Type of Use	Thesis/Dissertation
Requestor type	academic/university or research institute
Format	print and electronic

Portion	figures/tables/illustrations
Number of figures/tables/illustrations	1
Will you be translating?	no
Circulation/distribution	1 - 29
Author of this Springer Nature content	no
Title	INVESTIGATING THE TARGETS AND BIOLOGICAL ROLES OF IRE1'S TWO ENZYMATIC ACTIVITIES
Institution name	Bilkent University
Expected presentation date	Jun 2022
Portions	Figure 1
Requestor Location	Bilkent University BIlkent Universtiy Cankaya Ankara, 06800 Turkey Attn: Bilkent University
Total	0.00 USD

Terms and Conditions

SPRINGER NATURE LICENSE
TERMS AND CONDITIONS

May 25, 2022

This Agreement between Bilkent University -- Asli Yildirim ("You") and Springer Nature ("Springer Nature") consists of your license details and the terms and conditions provided by Springer Nature and Copyright Clearance Center.

License Number	5310391100711
License date	May 15, 2022
Licensed Content Publisher	Springer Nature
Licensed Content Publication	Nature Reviews Molecular Cell Biology
Licensed Content Title	Quality control of the mitochondrial proteome
Licensed Content Author	Jiyao Song et al
Licensed Content Date	Oct 22, 2020
Type of Use	Thesis/Dissertation
Requestor type	academic/university or research institute
Format	print and electronic

Portion	figures/tables/illustrations
Number of figures/tables/illustrations	1
High-res required	no
Will you be translating?	no
Circulation/distribution	1 - 29
Author of this Springer Nature content	no
Title	INVESTIGATING THE TARGETS AND BIOLOGICAL ROLES OF IRE1'S TWO ENZYMATIC ACTIVITIES
Institution name	Bilkent University
Expected presentation date	Jun 2022
Portions	Figure 5
Requestor Location	Bilkent University BIlkent Universtiy Cankaya Ankara, 06800 Turkey Attn: Bilkent University
Total	0.00 USD

Terms and Conditions

SPRINGER NATURE LICENSE
TERMS AND CONDITIONS

May 25, 2022

This Agreement between Bilkent University -- Asli Yildirim ("You") and Springer Nature ("Springer Nature") consists of your license details and the terms and conditions provided by Springer Nature and Copyright Clearance Center.

License Number	5310391185934
License date	May 15, 2022
Licensed Content Publisher	Springer Nature
Licensed Content Publication	Nature Reviews Molecular Cell Biology
Licensed Content Title	The mitochondrial UPR: mechanisms, physiological functions and implications in ageing
Licensed Content Author	Tomer Shpilka et al
Licensed Content Date	Nov 22, 2017
Type of Use	Thesis/Dissertation
Requestor type	academic/university or research institute
Format	print and electronic

Portion	figures/tables/illustrations
Number of figures/tables/illustrations	1
High-res required	no
Will you be translating?	no
Circulation/distribution	1 - 29
Author of this Springer Nature content	no
Title	INVESTIGATING THE TARGETS AND BIOLOGICAL ROLES OF IRE1'S TWO ENZYMATIC ACTIVITIES
Institution name	Bilkent University
Expected presentation date	Jun 2022
Portions	Figure 2
Requestor Location	Bilkent University BIlkent Universtiy Cankaya Ankara, 06800 Turkey Attn: Bilkent University
Total	0.00 USD